



Diese Dissertation haben begutachtet:

Prof. Ulrich SCHUBERT

Prof. Nicola HÜSING

Dissertation

Synthesis and Characterization of Iron(III)- Oxo Clusters and Their Use as Building Blocks for Cluster-Reinforced Polymers

ausgeführt zum Zwecke der Erlangung des akademischen Grades eines
Doktors der technischen Wissenschaften

unter der Leitung von

o.Univ.Prof. Dr.rer.nat. Ulrich SCHUBERT

eingereicht an der Technischen Universität Wien
Fakultät für Technische Chemie

von

Dipl. Ing. Robert POTZMANN

Mat.Nr. 0125593

Dommesgasse 9–15/8/11

1110 Wien

Wien, 21.12.2010

„Hello darkness my old friend, I've come to talk with you again...“

Simon and Garfunkel

Zum Ende der schlimmsten Zeit meines Lebens!
Gewidmet meiner verstorbenen Mutter Eva-Maria Potzmann.
Ich vermisse dich!

Ich danke...

...meinem Betreuer Prof. Schubert, von dem ich in den vergangenen dreieinhalb Jahren über mich und andere Menschen sicher mehr gelernt habe als über Chemie. Insbesondere danke ich ihm, dass er es ermöglichte die letzte Zeit mit meiner Mutter zu verbringen.

...Prof Nicola Hüsing, die sich die Mühe gemacht und die Zeit genommen hat, meine Zweit-Begutachterin/Prüferin zu sein.

...Robert und Alexandra für die langen Gespräche und die Gewissheit immer verstanden zu werden. Jonas dafür, dass er ein Kind ist und mich gern hOAT - mehr kann man als Kind nicht richtig machen - und Elias dafür, dass er sabbert wie ein Weltmeister - er weiß, warum hier Stroh liegt.

...Stefan O. und Tanja (the taliban girl) für die Umarmungen und den Rückhalt. Dafür, dass Ihr immer wusstet, was ich nicht sagen konnte. Stefan O. danke ich weiters, dass er meine Kristalle auch beim 10. Versuch noch immer nicht aufgegeben hat und beim Lösen fluchte wie ein Bauarbeiter - da fühlt man sich verstanden.

...Karl und Monika, die man immer anrufen kann, wenn man was braucht, wenn man nichts braucht, wenn man noch nicht weiß, dass man was braucht, wenn man weiß, dass man was braucht, aber man weiß nicht was... und vor allem: es macht einfach Spaß mit euch zusammen zu sein.

...allen FeministInnen, die mir verzeihen, dass ich die Männer zuerst genannt habe.

...Jasmin, die es schafft einen grauen Tag mit Sonne zu füllen und ein soziales Verständnis aufweist, das einfach nur beeindruckend ist und wahrscheinlich mit dem exzessiven Gebrauch (Missbrauch) von 1 € Liebesromanen zusammenhängt.

...dem alten Mann dafür, dass er sich meine Spinnereien angehört hat und dann in einem Satz sagen konnte, warum das niiiiiee funktioniert, dafür dass er schadenfroh ist wie kein Zweiter, aber auch sagt, wie man´s nächstes Mal besser macht und dafür, dass er gerne Kaffee trinkt und redet.

...meinen Wahlpraktikanten Karl, Peter, Stefan, Martin und Armin, die trotz Temperaturen von bis zu 39,4 °C (gefühlte 100) allesamt toll gearbeitet haben und mit denen ich viel Spaß hatte.

...Majka, die in ihrer Arbeitsweise und in ihrem Sein das genaue Gegenteil zu mir darstellt, aber genau so unpünktlich ist wie ich.

...meinen beiden Abzugsnachbarn: Christian M., als Spiegel meiner Selbst: mit Explosionen und Feuern ein warnendes Beispiel und Christian M., die genaue Antithese dazu - aber er war glücklicher!

...meinen KollegInnen Angelika, Bernhard, Christoph R., Christoph L., Claudia, Denisa, Denise, Doris, Elmar, Fatmir, Giedrius, Guido, Harald, Hongzhi, Jakob, Jingxia, Maia, Marco, Marina, Matthias, Melitta, Mirka, Mohsin, Nele, Ofer, Philipp, Ralf, Rene, Rupali, Rupert, Simas, Sorin, Stefan E., Stefan R. und Stefan K.

...Rodney dafür, dass er der einzige Lichtblick in der Hölle von Saragossa war und dafür, dass er den anderen Teil der Seite (nicht) verstanden hat.

...Silvia Pabisch für Ihre Zeit und den Versuch, sich in chemische Inhalte hineinzudenken.

...Ewa Partyka für Ihre unermüdlichen Versuche aus den Müll, den ich Ihr brachte etwas Wertvolles zu erschaffen.

...Thomas Koch, der es mit seiner freundlichen und aufbauenden Art nicht nur schaffte mich aus dem Sumpf der Motivationslosigkeit zu befreien, sondern mir auch erklärte, worauf es beim Schreiben ankommt.

...dem FWF für die Finanzierung des Projektes.

...dem ÖAD für die Finanzierung des unvergesslichen Aufenthaltes in Saragossa.

...meiner Familie, die trotz der vielen Schicksalsschläge noch Zeit gefunden hat mich zu unterstützen und mit mir zu reden. Der lange Winter ist nun hoffentlich vorbei und vielleicht können wir bald neue grüne Sprosse an den Zweigen erkennen - es kann eigentlich nur besser werden!

...meiner Schwester Simone für das Zusammenrücken in schlimmsten Zeiten.

...meiner Freundin Nicole für die schöne Zeit zwischen dem hektischen und traurigen Alltag.

Kurzfassung

Anorganisch-organische Hybridmaterialien erweckten in den letzten Jahren reges wissenschaftliches Interesse, da sie nicht nur die Eigenschaften der anorganischen und organische Komponente in sich vereinigen, sondern gleichzeitig auch synergetische Eigenschaften aufweisen können. Eine wichtige Unterklasse dieser Materialien sind clusterverstärkte Polymere. In diesem speziellen Fall werden anorganische Cluster, welche polymerisierbare Oberflächengruppen tragen, mit organischen Monomeren reagiert und auf diese Weise ein molekulares Netzwerk aus den beiden Bausteinen geschaffen. Die erhaltenen Hybridmaterialien zeigen in der Regel verbesserte thermische und mechanische Eigenschaften.

Im ersten Teil der Arbeit wird die Herstellung Methacrylat-modifizierter Eisen(III)-Oxocluster beschrieben. Diese Verbindungen mit der generellen Formel $[\text{Fe}_3\text{O}(\text{MA})_6(\text{L})_3]\text{X}$, wobei L in der folgenden Untersuchung ein koordiniertes Lösungsmittelmolekül (Wasser, Methanol, Ethanol oder Pyridin) und X ein Anion (Nitrat, Chlorid, Bromid, Methacrylat oder Tetrafluoroborat) war, sind leicht herzustellen und luftstabil. Besonderes Augenmerk lag auf der Untersuchung der Lösungsstabilität der erhaltenen Verbindungen, da diese für die folgende Umsetzung zum Hybridmaterial von entscheidender Bedeutung war. Mittels Lösungs-IR- und NMR-Spektroskopie wurden systematisch die Auswirkungen der Substituenten und der Anionen auf die Stabilität der Cluster untersucht und durch stetige Optimierung auf Basis der erhaltenen Ergebnisse schlussendlich der lösungsstabile Cluster $[\text{Fe}_3\text{O}(\text{MA})_6(\text{py})_3]\text{BF}_4$ erhalten, welcher in weiteren Synthesen zu clusterverstärkten Polymeren eingesetzt wurde.

Aufgrund der schlechten Löslichkeit von $[\text{Fe}_3\text{O}(\text{MA})_6(\text{py})_3]\text{BF}_4$ in organischen Monomeren wurde eine Lösungspolymerisation in Pyridin mit Styrol und Methylmethacrylat (MMA) als organische Komponente durchgeführt. Hierbei stellte sich heraus, dass sowohl das Lösungsmittel, aber vor allem der Cluster selbst, als Radikalübertragungsgagens wirksam waren, was sowohl die Reaktionsdauer, Kettenlänge der erhaltenen Polymere als auch die Ausbeute negativ beeinflusste. Daher musste eine Optimierung der Reaktionsbedingungen und der Initiatormenge durchgeführt werden. Von den erhaltenen Hybridpolymeren wurden die thermischen Eigenschaften bestimmt, sowie die Polymerkettenlänge detailliert untersucht.

Um Polymerisation in Masse durchführen zu können, wurden der Cluster und das organische Monomer variiert, wobei auf die Resultate der Stabilitätsoptimierung zurückgegriffen werden konnte. Einerseits wurden $[\text{Fe}_3\text{O}(\text{MA})_6(4\text{-vpy})_3]\text{NO}_3$ als anorganische Komponente und andererseits 4-Vinylpyridin, ein potentiell koordinierendes Monomer, als organischer Netzwerkbilder verwendet. Die erhaltenen Hybridmaterialien zeigten neben stark erhöhter Härte auch ein verbessertes E-Modul, waren aber auch entsprechend spröder. Die thermischen Eigenschaften wurden indes kaum beeinflusst.

Abstract

Inorganic-organic hybrid materials are an emerging field in materials science during the last decades. Apart from the combination of the properties of the inorganic and organic building units, they may even reinforce the materials properties by synergetic effects. One important sub-class is cluster-reinforced polymers. In this case, an inorganic cluster, bearing polymerizable surface groups, is reacted with an organic monomer to obtain a molecular network of the two building blocks. These hybrid materials show improved thermal stability and mechanical properties.

The first part of this work is focused on the synthesis of methacrylate-modified iron(III) oxo clusters. These compounds with the general formula $[\text{Fe}_3\text{O}(\text{MA})_6(\text{L})_3]\text{X}$, where L is a coordinating solvent molecule (water, methanol, ethanol or pyridine), X an anion (nitrate, chloride, bromide, methacrylate or tetrafluoroborate) and MA = methacrylate, are easily prepared and stable to air and moisture. The solution stability of the synthesized clusters was of special interest, because it determines the further use in the synthesis of hybrid materials. Therefore, detailed systematic investigations by solution FT-IR and NMR spectroscopy were performed to evaluate the influence of the different substituents and anions. On the basis of these results, the clusters were optimized, and the solution-stable cluster $[\text{Fe}_3\text{O}(\text{MA})_6(\text{py})_3]\text{BF}_4$ was eventually obtained and used in the further syntheses to cluster-reinforced polymers.

Due to the bad solubility of $[\text{Fe}_3\text{O}(\text{MA})_6(\text{py})_3]\text{BF}_4$ in organic monomers, solution polymerization in pyridine with styrene and MMA as organic part was performed. Initial results made clear that the solvent as well as the clusters themselves acted as transfer agent and had a negative influence on the reaction rate, the obtained chain length and the yield. Therefore, the reaction conditions as well as the initiator proportion were optimized and detailed investigations on the chain length of the reinforced polymers were done. The obtained hybrid materials showed improved thermal stability as expected.

The inorganic and organic building blocks had to be adjusted to perform bulk polymerization. The substituents and anions of the clusters were varied on the basis of the stabilization optimization results. Whereas $[\text{Fe}_3\text{O}(\text{MA})_6(4\text{-vpy})_3]\text{NO}_3$ was used as inorganic building block, the coordinating monomer 4-vinylpyridine was used as organic moiety. The obtained hybrid materials showed improved hardness and Young's modulus, accompanying with an increase of brittleness. The thermal properties of the materials were hardly influenced.

Index of Abbreviations

A	Peak Area
Ac	Acetate
AIBN	Azo-bis-(isobutyronitril)
ATR-IR	Attenuated Total Reflection Infrared Spectroscopy
ATRP	Atom Transfer Radical Polymerization
COSY	Correlated Spectroscopy
CS	Quadrupole Splittings
D	Isomer Shifts
DSC	Differential Scanning Calorometry
EtOH	Ethanol
FT-IR	Fourier Transform Infrared Spectroscopy
GPC	Gel Permeation Chromatography
H	Magnetic Field Strength
HMQC	Heteronuclear Multiple Quantum Coherence
IR	Infrared Spectroscopy
M	Magnetization
MA	Methacrylate
MAH	Methacrylic Acid
MeOH	Methanol
MMA	Methyl Methacrylate
M_n	Number Average Molar Weight
M_w	Weight Average Molar Weight
NMR	Nuclear Magnetic Resonance
P_d	Polydispersity
POSS	Polyhedral Oligomeric Silsesquioxanes
PMMA	Polymethylmethacrylate
PS	Polystyrene
py	Pyridine

Re	Residual Mass
S	Spin Number
SAXS	Small Angle X-Ray Scattering
SOMO	Single Occupied Molecular Orbital
SQUID	Superconducting Quantum Indifference
T _g	Glass Transition Temperature
TGA	Thermogravimetric Analysis
THF	Tetrahydrofuran
4-vpy	4-Vinylpyridine
w	Peak Area Ratio
wt	Weight
χ	Magnetic Susceptibility
XRD	X-Ray Diffraction

Table of Contents

1	Introduction	1
1.1	Reinforced Polymers	1
1.1.1	Ion and Metal Complex Reinforced Polymers	1
1.1.2	Nanoparticle-, Nanorod- and Nanodisc-Reinforced Polymers	3
1.1.3	Cluster-Reinforced Polymers	4
1.2	Trinuclear Oxo-Bridged Iron Clusters	9
2	Results and Discussion	15
2.1	Evolution of Methacrylate-Modified Fe ₃ O-Clusters	15
2.1.1	Clusters of General Formula [Fe ₃ O(MA) ₆ (H ₂ O) ₃]X	15
2.1.2	IR Investigations	27
2.1.3	Discussion and Conclusion	30
2.1.4	Clusters of General Formula [Fe ₃ O(MA) ₆ (HOR) ₃]X	36
2.1.5	IR Investigations	45
2.1.6	Discussion and Conclusion	46
2.1.7	Clusters of General Formula [Fe ₃ O(MA) ₆ (py) ₃]X	51
2.1.8	IR Investigations	55
2.1.9	NMR Investigations	58
2.1.10	Discussion and Conclusion	63
2.2	Cluster-Reinforced Polymers	65
2.2.1	Solution Co-Polymerization of [Fe ₃ O(MA) ₆ (py) ₃]BF ₄	65
2.2.2	Discussion and Conclusion	81
2.2.3	Bulk Co-Polymerization of [Fe ₃ O(MA) ₆ (4-vpy) ₃]NO ₃	81
2.2.4	Conclusion	94
3	Summary	96
4	Experimental Section	103
4.1	General Methods and Materials	103
4.2	Analytical Techniques	103
4.2.1	IR Spectroscopy	103
4.2.2	Single Crystal XRD	104

4.2.3	NMR Spectroscopy	104
4.2.4	Elemental Analysis	104
4.2.5	Gel Permeation Chromatography	104
4.2.6	Small Angle X-ray Scattering	105
4.2.7	Thermo Gravimetric Analysis	105
4.2.8	Magnetic Measurements	105
4.2.9	Nano-Indentation	105
4.2.10	Differential Scanning Calorimetry	105
4.3	Methacrylate-Modified Iron(III) Oxo Clusters	106
4.3.1	Water-Substituted Clusters	106
4.3.2	Alcohol-Modified Clusters	108
4.3.3	Pyridine-Modified Clusters	110
4.3.4	4-Vinylpyridine-Modified Clusters	112
4.4	Cluster-Co-Polymers	113
4.4.1	Solution Polymerization of Styrene and MMA in Pyridine	113
4.4.2	Solution Styrene-Co-Polymerization of $[\text{Fe}_3\text{O}(\text{MA})_6(\text{py})_3]\text{BF}_4$	113
4.4.3	Solution MMA-Co-Polymerization of $[\text{Fe}_3\text{O}(\text{MA})_6(\text{py})_3]\text{BF}_4$	114
4.4.4	Bulk Co-Polymerization of $[\text{Fe}_3\text{O}(\text{MA})_6(\text{vpy})_3]\text{NO}_3$	114
4.5	Crystallographic Data	115
5	References	120

1 Introduction

The fast development of today's technology is mainly mediated by the availability of new materials with tailored chemical, physical and mechanical properties. On the other hand, the synthesis and tailoring of these materials is more and more a question of using sophisticated high tech methods. The accelerating competition of scientist all over the world has led to fascinating new developments in this research field during the last years. To enhance materials properties, a detailed fundamental understanding of the molecular interactions in the materials and the mechanisms leading to the different characteristics are elementarily necessary. This identifies a hierarchical design of the materials from the precursors, over the nano-scale-structure to the micrometer-scale as an absolute must.

The combination of organic and inorganic components in one material is a versatile method to enhance the properties of the resulting hybrid materials. This idea has gained much attention during the last decades, and different synthetic approaches and material classes have emerged. In general, these materials can be classified in two main groups: The inorganic and organic components of the class I hybrid materials show only weak interactions, while in class II of hybrid materials the two components are linked through covalent or coordinative interactions.

These materials combine the advantages of both classes of materials, namely hardness, mechanical and chemical stability of the inorganic components on the one hand and the well-developed, low temperature and cost efficient processing techniques of the organic polymers on the other. Additionally, synergetic properties can be found and therefore many applications have already been developed for such types of hybrid materials.

Nowadays efforts are done to further improve the properties of hybrid materials by designing the inorganic component. Preeminent are the developments in the field of polymer-based hybrid materials ranging from complex- over cluster- to nanoparticle-reinforced polymers. These multifunctional materials open a new horizon for technological developments. Many approaches have been followed towards materials which are reviewed in current literature.¹ In the following, the focus is on inorganic-organic class II of hybrid materials with small inorganic moieties in a continuous polymer matrix.

1.1 Reinforced Polymers

1.1.1 Ion and Metal Complex Reinforced Polymers

Early developments focused on materials to deionize water and organic liquids.^{2,3,4} Metal ions were thus incorporated in the polymers. Since the second generation of these materials, one of the scientific driving forces is the synthesis and further development of new heterogeneous catalysts. Compared to conventionally used homogenous metal catalysis, the

active center is immobilized on the inert polymer substrate, which allows easy separation and recycling. The evolution, advantages and disadvantages of such catalysts are summarized in a recent review.⁵

As presented in Figure 1.1, two different synthetic pathways were followed. In the first process, the organic monomer is polymerized first and then the metal salt or complex is added in order to react with the functional group of the polymer. In the second approach, a polymerizable complex is prepared first, which is subsequently copolymerized. The big advantage of the second route is that the catalytic activity as well as the thermal and other physical properties of the salt or complex can be tested prior to the reaction. In addition, the changes due to the incorporation into the polymer can be monitored.⁶ First, the complexes and salts were varied to a large extent, while mostly polyvinylpyridine was used as polymer or as copolymer with polystyrene, due to its potential to coordinate to the metal ions via the pyridine group. Later on, the set of used polymers was extended to coordinating polymers such as polyacrylamide or polypyrrolidine.⁷

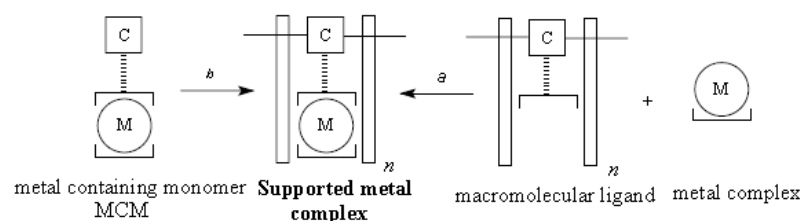


Figure 1.1: Synthesis of supported metal complexes (C = polymerizable group, M = metal center of a complex).⁵

Although ion- and complex-containing polymers were investigated and used in widespread applications for some decades, the influence of the metal ions on the mechanical and thermal properties remained more or less unexplored for a long time. In the late 1980s, the enhancement of the glass transition temperature (T_g) by ruthenium and osmium complexes was reported.^{8,9} In the following, some investigations focused on the influence on the decomposition temperature, but did not result in a uniform trend. Many publications described an improved thermal stability, while others reported a decrease.¹⁰ A systematic study that compares the thermal properties with the coordination environment in the polymer, is still missing, mainly due to the lack of proper analytical tools for the determination of coordination modes.¹¹ In addition, no detailed studies concerning the influence of the metal ions or complexes on the mechanical properties of the hybrid materials have been published.

In recent years, the applications were extended to corrosion protection, polymers with paramagnetic properties or semiconducting films. Although good results were obtained, ion and metal complexes containing polymers are still a marginally investigated research field.

1.1.2 Nanoparticle-, Nanorod- and Nanodisc-Reinforced Polymers

If somebody is asked which development has mostly influenced material science during the last years, he will definitely answer that it is nanotechnology. The discovery that, at the border between bulk materials and molecular compounds, the size of a particle influences the physical properties and that it can even create new characteristics like superparamagnetism or quantum dot properties led to enormous scientific efforts to synthesize new materials based on nano-sized compounds.

Nanoparticles always show some size distribution that manifests in disparate physical properties. Additionally, they are not soluble but only dispersible in organic solvents and monomers. The first experiments to incorporate unmodified inorganic particles into polymer matrices were done by dispersing the preformed particles in the respective monomer followed by a polymerization. This led to partial phase separation and therefore the formation of large agglomerates of the particles in the material. These agglomerates weakened the mechanical, optical and electrical properties of the hybrid materials compared to homogeneously dispersed systems. To avoid this problem, synthetic methods like the use of functional polymers that interact with the particle surface or in situ growth of inorganic particles in preformed polymers were developed.^{12,13} Another very general route is the surface modification of preformed nanoparticles. Organic groups improve the dispersibility and open the possibility to introduce functional groups that can crosslink the polymers.

The incorporation of particles provides several benefits to the polymers. The hardness and thermal stability of the hybrid materials is improved compared to the parent polymers, whereas physical properties can be introduced, additionally. The mechanical reinforcement can rather be traced back to a nano filler effect than to the crosslinking of the polymer by the particles. The more particles are introduced the better are the mechanical properties, up to a certain threshold. Due to the fact that the particles are just dispersed, the viscosity of the precursor monomer solution increases drastically. Therefore, only particle loadings up to 10 wt% are applicable in industry.

Anisotropy can be introduced into the hybrid material by using anisotropic building units (structure 1 in Figure 1.2). Nanorods or platelets are widely used in scientific applications, because they are easy to synthesize and functionalize.¹⁴ Another quite common method is the intercalation of monomers into layered inorganic material followed by a polymerization reaction, here presented in Figure 1.2.¹⁵ These inorganic layers can be natural layered structures like molybdenum trioxide or artificially designed for example by sol-gel methods.¹⁶

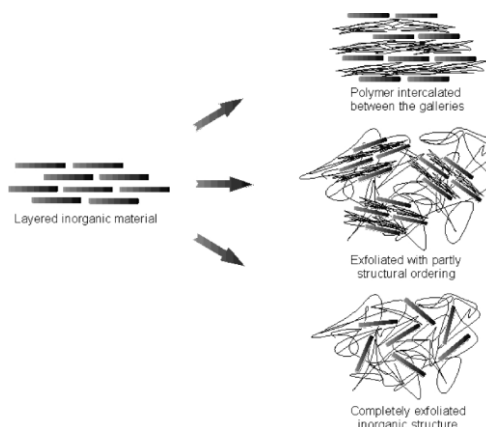


Figure 1.2: Three examples of differently structured materials derived by intercalation of monomers into layered inorganic compounds followed by polymerization.¹

1.1.3 Cluster-Reinforced Polymers

According to the strict definition, a cluster is an assembly of metal atoms with predominant metal-metal bonds in the core and an organic shell that saturates the coordination sphere of the metal atoms.¹⁷ Nowadays this definition is not used in this rigorous way, which means that all kind of polynuclear compounds with defined size and shape can be called cluster.

Parallel to the emerging and impressive success of nanoparticle-based hybrid materials, cluster-reinforced polymers get closer in the spotlight of scientific interest. This is reflected in numerous publications and reviews during the last years. In contrast to nanoparticles, where the distribution of the particle size leads to a distribution of the properties, clusters are molecular compounds with uniform size and shape and, therefore, uniform physical, chemical, thermal and mechanical properties. They can be crystallized and their structure can be determined by single crystal X-ray diffraction. As molecular compounds, they are soluble and hence standard analysis methods such as solution NMR spectroscopy can be performed. Solubility is also the reason why, compared to nanoparticles dispersed in monomers, the viscosity is not that much depending on the cluster proportion in the monomer mixture, which allows the use and manufacture of highly loaded hybrid materials.

1.1.3.1 The Nano Building Block Approach

The nano building block approach is a general route for the synthesis of hybrid materials, but it has special relevance for cluster-reinforced polymers. As presented in Figure 1.3, the main idea is that two independent monomers, one inorganic and one organic, are copolymerized to form a homogenous network. Thereby, the organic monomers build up the polymer backbone that is crosslinked by the inorganic clusters. The two building blocks can be prepared and designed separately to tailor their physical and chemical properties before they are introduced into the final material. Additionally, the separate synthesis of the building

blocks allows studying the properties of the individual compounds prior to the network formation. Therefore, synergetic or depressing effects can easily be determined.

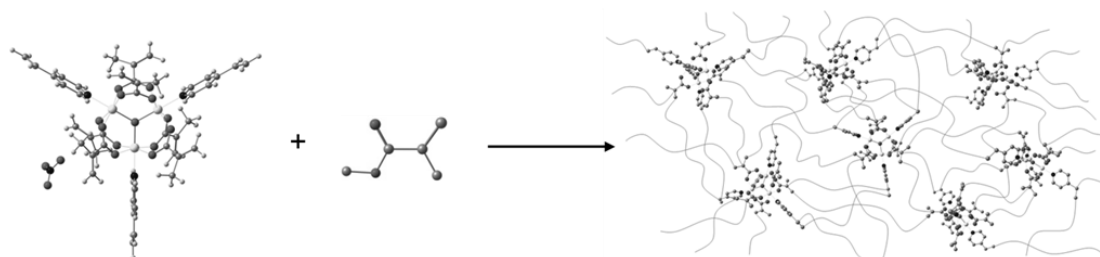


Figure 1.3: The inorganic cluster $[\text{Fe}_3\text{O}(\text{MA})_6(4\text{-VP})_3]\text{NO}_3$ reacts with methylmethacrylate (MMA) to form an inorganic-organic hybrid material.

As mentioned above, a cluster consists of an inorganic core surrounded by an organic shell. The composition, size and geometry of the core are responsible for the major physical properties. The organic coordination sphere around the core bears the functional groups for the network formation. Depending on the number of functional groups per cluster, on their symmetry as well as on their relative reactivity different crosslinking densities can be achieved.¹⁸ On the other hand, the organic monomer has to be a good solvent for the cluster and bears a functional group for the network formation. Monomers like styrene, vinylacetate or MMA are widely used.

1.1.3.2 Polymerizable Cluster and Cluster-Reinforced Polymers

In principle, there are two possibilities to attach a functional group to a cluster: i) post-synthesis modification of preformed non-functionalized clusters or ii) direct introduction as reactant during the synthesis. The first approach opens the possibility to use the full range of synthesis methods to obtain exactly the desired cluster shape and properties. In a second step the non-functional organic ligands need to be substituted with functional ones. The disadvantage is the lacking control of the second step. Furthermore, no good methods to purify and separate functionalized clusters with partially exchanged ligands are available. This can be overcome by the second synthetic route. Here, the disadvantage is the limited synthetic methods. All redox or radical reactions have to be avoided and therefore only a reduced number of different cluster motives can be achieved.

The most popular group of polymerizable clusters is based on POSS (Polyhedral Oligomeric Silsesquioxanes) cages. Their synthesis and applications are reported in many publications and reviews. In the last two decades, easy synthesis routes for cages with different size and tunable substitution motives were established.^{19,20} Due to the covalent Si-C bonds, all kind of functional groups could be introduced. Their incorporation into polymers and their influence on the thermal and mechanical properties has been studied intensively.

Hence, POSS-based hybrid materials serve as model systems for the incorporation of metal oxo clusters into polymer matrices.

The synthesis, solution behavior and finally the incorporation into polymers were mainly investigated for titanium oxo and zirconium oxo clusters. The standard synthesis is based on a non-aqueous sol-gel route that includes the reaction of metal alkoxides with carboxylic acids. By varying the alkoxides, acids and the alkoxide : acid ratio, many different cluster core structures and derivatives were obtained.²¹ In addition to free radical polymerization, other techniques were performed using functional acids like 5-norbornene-2-carboxylic acid for ring opening metathesis reactions and 2-bromoisobutyric acid for atom transfer radical polymerization (ATRP) or 5-hexynoic acid for click reactions.^{22,23,24}

Crosslinking of polymers by inorganic clusters provides benefits for the hybrid materials. For instance, they show advanced chemical resistance and are insoluble, but swellable, in organic solvents. The swelling rate provides information about the hybrid network. Four quite similar tetranuclear clusters with different metals in the core were polymerized and their solvent uptake was investigated. As shown in Figure 1.4, the swelling depended on the cluster and did not correlate with the number of polymerizable groups per cluster unit.²⁵

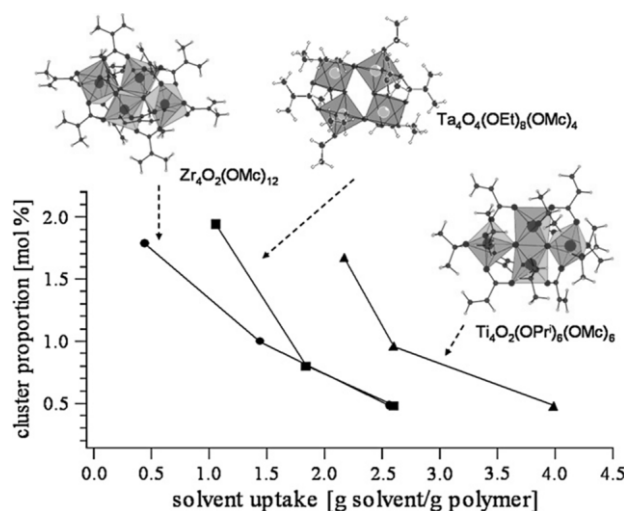


Figure 1.4: Swelling of PMMA crosslinked by several tetranuclear clusters (OMc = methacrylate).

In other words, all parts of the cluster, the organic shell with different number and reactivity of functional groups, as well as the inorganic core that determines the structure of the organic shell and affects the reactivity of the functional groups, have an influence on the hybrid network. More detailed investigations on that topic were accomplished by SAXS measurements. A constant shift of the maximum by varying the cluster proportion indicated a homogenous distribution of the clusters in the polymer matrices in most cases.²⁶ In some other cases, for example Zr₆(OH)₄O₄(MA)₁₂ incorporated in polystyrene, constant maxima at small distances independent from the cluster proportion were shown. That effect was assigned to a

clustering of clusters during the polymerization, which could be verified by TEM measurements.²⁷

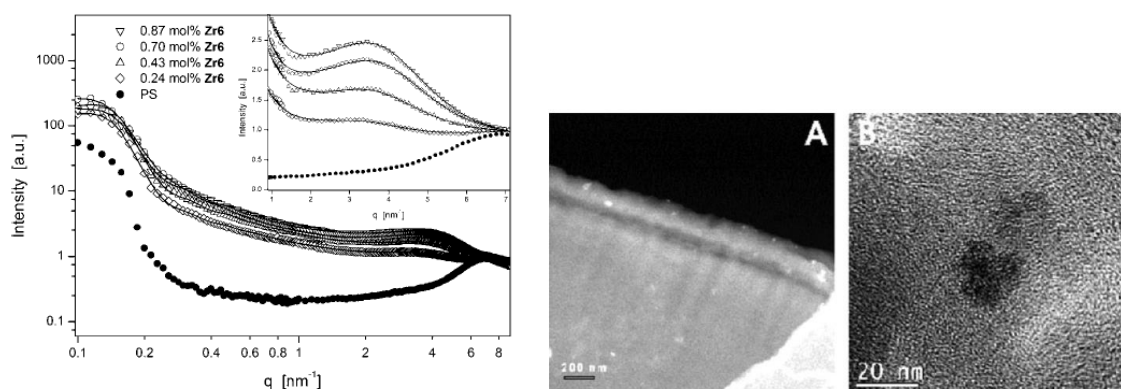


Figure 1.5: (l) SAXS measurements of the hybrid material derived by copolymerization of $\text{Zr}_6(\text{OH})_4\text{O}_4(\text{MA})_{12}$ with styrene; (r) TEM images of the inorganic islands in the material.²⁷

Indentation techniques were used to investigate changes in hardness, stiffness and scratch resistance.²⁸ The indentation hardness H_{IT} as well as the indentation modulus was found to increase slightly by about 10 % relative to the undoped polymers.

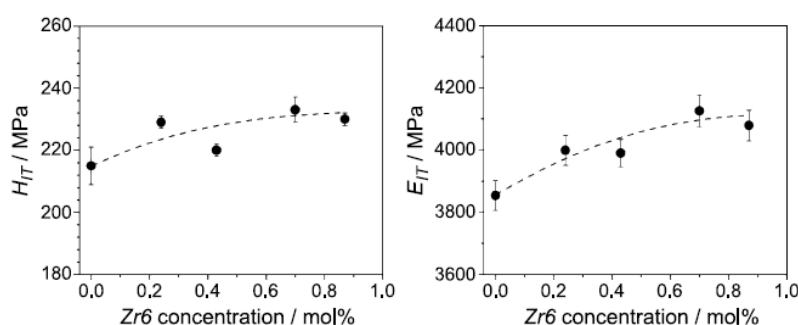


Figure 1.6: Indentation hardness H_{IT} and indentation modulus E_{IT} of $\text{Zr}_6\text{O}_4(\text{OH})_4(\text{MA})_{12}$ incorporated in polystyrene as a function of cluster proportion.²⁷

One of the most important synergetic features of cluster-reinforced polymers is the improved thermal stability. For small cluster proportions, the decomposition temperature improves rapidly, while higher cluster proportions do not lead to significant higher thermal stability. Enhancement up to another 50 °C, was obtained by a stepwise polymerization of $\text{Zr}_6\text{O}_4(\text{OH})_4(\text{MA})_{12}$ incorporated in PMMA and polystyrene.²⁹ In contrast to bulk polymerized of cluster-reinforced polymers, no residual monomers were detected after a stepwise polymerization. The decomposition of cluster-reinforced hybrid materials always leads to the formation of char. It was shown that a higher crosslinking density results in increased char formation during the thermal decomposition.³⁰

Closely related to the results for the thermal decomposition, studies on the glass transition temperature showed the increase of T_g with increasing cluster proportion. No detailed dependence between the crosslinking, the used metal oxide cluster and the value of T_g change were found. Polymeric materials are normally not used above T_g and therefore cluster-reinforced polymers open the possibility to extend the range of applications to slightly higher temperatures.

One first approach for a systematic structure-property study was the incorporation of different Zr_6 and Zr_{12} clusters into polystyrene.³¹ Different groups were attached to the clusters ranging from non-functional acetates to highly reactive acrylates. The results of the TGA analyses are shown in Figure 1.7. Improved thermal stability, glass transition temperature and char formation were detected for every sample, not clearly dependent on the crosslinking ability of the functional group. The authors concluded a nanofiller effect. An active role of the cluster in the polymerization reaction that transforms the network or acts as transfer agent was not discussed.

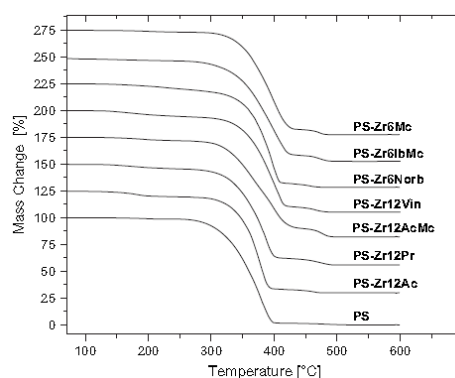


Figure 1.7: Comparison of TGA measurements of hybrid materials prepared from differently substituted functional (Mc = methacrylate, Norb = 3-norbornenate, Vin = acrylate) and non-functional (Ac = acetate, Pr = pivalate, Ib = proanate) clusters with neat polystyrene (PS).

In another publication, the chain length after the polymerization was determined.³² Therefore, $Zr_4O_2(MA)_{12}$ was copolymerized with MMA and styrene with different initiator proportions in step and bulk polymerization. Afterwards, the cluster was degraded in acetylacetone / ethyl acetate and the chain length of the crosslinked polymers was determined. In general, the chain lengths were in the range of the expected value and showed large polydispersity. With increasing initiator proportion, the chain length decreased, but was in all cases higher for step-polymerization.

1.1.3.3 Multifunctional Cluster-Reinforced Materials

During the last years, multifunctional materials were synthesized on the basis of cluster-reinforced polymers. The used clusters bear inherent physical properties, like magnetism,

quantum dot properties or luminescence, additional to their functional groups that are responsible for the mechanical and thermal reinforcing properties.

One of the first examples was the incorporation of the single molecular magnet $\text{Mn}_{12}\text{O}_{12}(\text{OAc})_{16}$ (OAc = acrylate) into a polyethylacrylate matrix.³³ It was shown that the magnetic properties of the cluster are basically retained after copolymerization. No clustering of clusters was detected by SAXS investigations. Therefore, from a physical point of view, the cluster can be seen as a magnetic moiety in an indefinite diamagnetic surrounding, only influenced by its neighboring cluster. Ac SQUID measurements showed weak antiferromagnetic coupling between neighbored clusters and therefore increased blocking temperatures for samples with lower cluster content.

Cadmium sulfide clusters show quantum dot properties and were tested as inorganic nano building blocks.³⁴ In contrast to the oxygen-based ligands mentioned above, thiolate ligands must be used to stabilize the cluster core. These groups react rapidly with double bonds and thus different approaches for the network formation had to be found. Additional, the investigated clusters were not stable in solution and tend to form nanoparticles.

1.2 Trinuclear Oxo-Bridged Iron Clusters

From the beginning of research, scientists investigated magnetic materials and tried to understand the basic principles of this phenomenon. Nanotechnology brought new aspects such as superparamagnetism, single domain particles etc. The available model systems boost scientific efforts. Detailed knowledge about the supermolecular interactions leading to different magnetic behavior is now accessible. Current developments try to achieve chiral magnetic fields or magnetic monopoles, which could start a revolution in the development of tomorrow's technology.

The element mostly associated with magnetism is iron, and therefore it was no big surprise that one of the first single molecular magnets was based on this element. The crystal structure of $[\text{Fe}_8\text{O}_2(\text{OH})_{12}(\text{C}_6\text{H}_{15}\text{N}_3)_6]\text{Br}_8$ was described by Wieghardt and his group and magnetic measurements resulted in a $S = 10$ ground state with a large anisotropy.³⁵ The cluster became a predominant model system for single molecular magnets, but further investigations showed its instability in solution.³⁶ Hence, during recent years a large variety of different iron-based molecular and bulk components were synthesized and tested for their magnetic properties.

The investigations on iron oxo clusters started at the beginning of the 20th century, when scientists began to understand that seemingly normal salts can consist of complex cations. Weinland and his group investigated the reaction of iron(III) chloride with acetic acid and found the $[\text{Fe}_3\text{O}(\text{OOCCH}_3)_6(\text{H}_2\text{O})_3]\text{Cl}$ cluster.³⁷ They concluded that the reaction of monocarboxylic acids with iron(III) salts always leads to the formation of analogous structures, and proved their theory by using different salts like iron(III) chloride or iron(III) nitrate and a large variety of acids such as formic acid, benzoic acid or malonic acid.^{38,39,40}

Additionally, they performed the first anion exchange reactions with hexachloroplatinate and showed that it is possible to substitute the water ligands for pyridine.⁴¹

60 years later, the postulated composition was confirmed by single crystal X-ray diffraction of $[\text{Fe}_3\text{O}(\text{OOCCH}_3)_6(\text{H}_2\text{O})_3]\text{ClO}_4$.⁴² As shown in Figure 1.8, the cluster core consists of three iron(III) ions lying in one plane with a bridging μ_3 -oxygen. Each of the iron(III) ions is connected to each of its neighbors by two μ_2 -acetates. A coordinated water molecule completes the octahedral coordination sphere. During the years, numerous variations of the $[\text{Fe}_3\text{O}(\text{OOCR})_6(\text{L})_3]\text{X}$ cluster motive were described in the literature. The most widely used acids (H-OOCR) were acetic acid, benzoic acid and pivalic acid.⁴³ Bond and his group investigated the electrochemical reduction properties of triiron clusters and synthesized an ensemble of different molecules.⁴⁴ Even though many variations of this cluster can be found in literature, with more or less the same shape, current literature still deals with the exact determination of the molecular and crystal structure to explain the magnetic properties of the molecules.⁴⁵

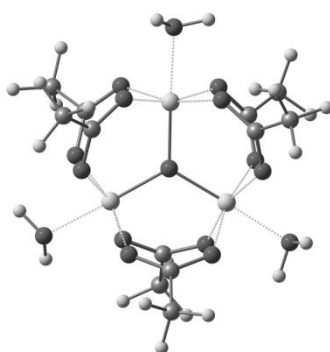


Figure 1.8: Structure of the $[\text{Fe}_3\text{O}(\text{OOCCH}_3)_6(\text{H}_2\text{O})_3]^+$ cluster cation.

Parallel to the availability of the first crystal structures, scientists started to investigate the magnetic properties of trinuclear oxo-bridged iron clusters. In 1966, the first systematic study on iron and analogous chromium compounds with different anions and ligands in a temperature range between 80 and 300 K was published.⁴⁶ All trinuclear clusters were strongly antiferromagnetic coupled resulting in a ground state spin of $S = 1/2$. Earnshaw and his group concluded that the antiferromagnetic exchange within the cluster core is caused by the interaction of three equal iron(III) ions over the Fe–O–Fe bonds. However, only three years later Duncan and his group claimed that the iron(III) ions within the core cannot be equal.⁴⁷ These results started a long scientific discussion about the origin of the asymmetry in the cluster core. Long and his group extended the measurement region down to 20 K and found that in fact two different groups of clusters exist, each exhibiting one of the two expected exchange mechanism.⁴⁸ Two groups claimed that a Jahn Teller distortion of the iron(III) ions is responsible, while others blame dynamic dangling of the central oxygen.^{49,50,51} The second suggestion led to a dynamic spin exchange model that currently appears most

probable. The main idea is that a cluster with equal Fe–O distances can show different iron(III) sites and therefore differences in the magnetic interaction. In other words, the symmetry of the crystal lattice and the magnetic lattice are independent from one another, but the symmetry of each lattice influences the other. A good example was given by Overgaard and his group who investigated changes in the crystal structure and the electronic and magnetic exchange in $\text{Fe}_3\text{O}(\text{OOCH})_6(\text{NC}_5\text{H}_4\text{CH}_3)_3$ depending on the temperature.⁵² Below 100 K, the iron(II) and iron(III) show typical distances to the central oxygen atom. Above this temperature electron transfer takes place and, as presented in Figure 1.9, this exchange shortens the distances for the Fe^{II} and elongates that of Fe^{III} . At the same time, the Mössbauer signals converge more and more, and at room temperature the iron(II) signal disappeared and the signal corresponds to just one iron(III) species, which is different to the starting ones. While in this case the valence state changes continuously, investigations on $[\text{Fe}_3\text{O}(\text{OOCCH}_2\text{CN})_6(\text{H}_2\text{O})_3]$ showed that this transition can proceed abruptly and can feature the characteristics of a phase transition.⁵³ The same results were obtained by Seung and his group, who investigated $[\text{Fe}_3\text{O}(\text{OOCCH}_3)_6(\text{L})](\text{L})$ with $\text{L} = \text{pyridine}$ or 4-ethylpyridine. This small difference in the ligand led to a change of the transition from continuous to abrupt.^{54,55} They furthermore found out that changes of the solvate molecules incorporated in the crystal structure led to differences in the exchange properties.⁵⁶

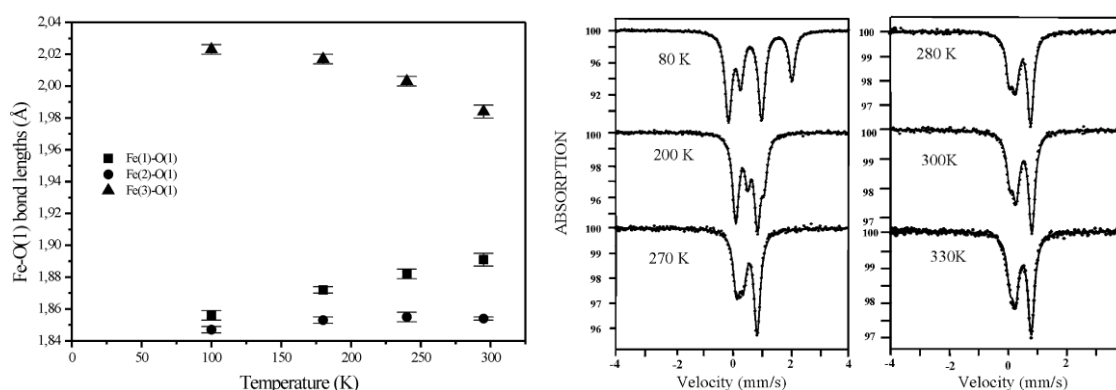


Figure 1.9: (l) changes of the three Fe–O bond lengths in $\text{Fe}_3\text{O}(\text{OOCH})_6(\text{NC}_5\text{H}_4\text{CH}_3)_3$ by increasing the temperature; (r) comparison of Mössbauer spectra at different temperatures.

As mentioned above, the dynamic spin exchange model was first proposed for $\text{Fe}^{\text{II}}\text{Fe}^{\text{III}}_2$ clusters and afterwards extended to trinuclear Fe^{III} clusters. Sowrey et al. studied $[\text{Fe}_3\text{O}(\text{OOCPh})_6(\text{py})_3]\text{ClO}_4$, which crystallizes in space group $\text{P6}_3/\text{m}$ and containing two D_3 symmetric clusters in the unit cell at $T = 233 \text{ K}$.⁵⁷ IINS investigations of this crystalline cluster at $T = 1.5 \text{ K}$ showed two different sets of energy transfer signals, which could be assigned to the two different clusters. This means that the same cluster with the same structure shows different electron transfer properties depending on the localization in the crystal lattice. On the other hand, the data clearly showed that at 1.5 K a cluster with a D_3 symmetry shows asymmetric magnetic interaction between the iron(III) ions. This was assigned to spin

frustration that drives a distortion of the molecular symmetry. At higher temperatures, the asymmetry is masked by electron transfer and the motion of the atoms. Filoti et al. followed this hypothesis and studied the magnetic properties of $[\text{Fe}_3\text{O}(\text{OOCCH}_3)_6(\text{py})_3]\text{NO}_3$.⁵⁸ As presented in Figure 1.10, they proved that the system was indeed spin-frustrated and showed that antiferromagnetic coupling was so strong that the spin did not align parallel even at 14 T.

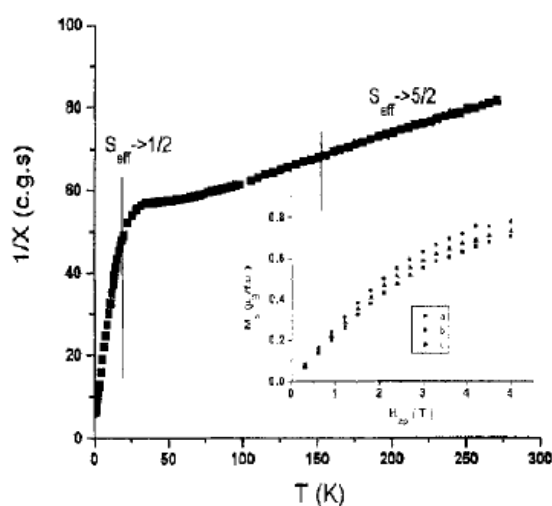


Figure 1.10: Reciprocal susceptibility versus temperature plot of $[\text{Fe}_3\text{O}(\text{OOCCH}_3)_6(\text{py})_3]\text{NO}_3$.

A completely different approach of electron transfer was established by Cannon et al. After some experiments on intramolecular spin exchange they investigated intermolecular electron self exchange in solution. To this end, they performed solution NMR investigations on mixtures of $[\text{Fe}_3\text{O}(\text{OOCCH}_3)_6(\text{py})_3]\text{Cl}$ and mixed valence $[\text{Fe}_3\text{O}(\text{OOCCH}_3)_6(\text{py})_3]$ compounds.⁵⁹ From the line broadening in the NMR spectra, they concluded that outer sphere electron transfer occurs and were even able to calculate a rate constant. They could show that the energy barrier for the electron transfer is related to the intramolecular reorganization energy. This raised the question whether this electron transfer can be used to perform catalytic oxidation. Nagl et al. systematically tested mixed valence iron(II,III,III) and pure iron(III) clusters with different acids and ligands for their catalytic activity towards oxidation of alkanes. The iron nitrobenzoate $[\text{Fe}_3\text{O}(4\text{-OOC}_6\text{H}_4\text{NO}_2)_6(\text{H}_2\text{O})_3](4\text{-OOC}_6\text{H}_4\text{NO}_2)$ was quite successful in these tests and inspired further investigations with bigger clusters derived by condensation of the triiron core.^{60,61}

After the emergence of single molecular magnets, the synthesis of bigger clusters with large ground state spins and anisotropies became one major goal of synthetic chemists. Due to the easy synthesis and the possibility to tune the composition, trinuclear oxo-bridged iron clusters became a prominent precursor and countless examples for further syntheses could be given. For instance, the controlled pyrolysis of nitrate and chloride, pivalate and benzoate clusters led to the formation of $[\text{Fe}_6\text{O}_2(\text{OH})_2]^{12+}$ and $[\text{Fe}_{11}\text{O}_6(\text{OH})_6]^{15+}$ cluster cores.⁶² Some

examples were reported, where the size of different coordinated carboxylates influence further reactions. The reaction of $[\text{Fe}_3\text{O}(\text{OOCR})_6(\text{H}_2\text{O})_3]\text{Cl}$ ($\text{R} = \text{CH}_3, \text{C}_6\text{H}_5$) with cyclohexenephosphonic acid led in the first case to the formation of a cluster with a $[\text{Fe}_4\text{OCl}]^{10+}$ core, while in the other case a $[\text{Fe}_7\text{O}_2]^{19+}$ core was obtained.^{63,64} Methanolysis of $[\text{Fe}_3\text{O}(\text{OOCR})_6(\text{H}_2\text{O})_3]\text{NO}_3$ in the presence of additional iron(III) nitrate yielded in the big family of ferric wheel compounds.^{65,66} These compounds with the general formula $[\text{Fe}(\text{OCH}_3)_2(\text{OOCR})]_{10}$ are perfect antiferromagnets with a $S = 0$ ground state, but, due to the low-lying excited spin states, exhibit different spin ground states $S = 1, 2, 3, \dots$ depending on the strength of the applied external magnetic field. It was even possible to obtain single molecular magnet properties in the trinuclear oxo-bridged iron cluster $[\text{Fe}_3\text{O}(\text{OCH}_3)_2(\text{OOCH}_3)_2(\text{phen})_2\text{Cl}_3]$.⁶⁷ As presented in Figure 1.11, the cluster core is distorted showing a short $\text{Fe1}-\text{Fe2}$ distance and a long $\text{Fe2}-\text{Fe2}'$ one. The iron(III) ions are bridged by an acetato and a methanolato ligands and a coordinated chloride ion completes the octahedral coordination sphere. Nevertheless, due to the angle of about 90° between Fe1 and Fe2 , the antiferromagnetic coupling is relatively weak, while being enhanced for the interaction Fe2 and $\text{Fe2}'$. This results in an enhanced ground state $S = 5/2$ located at Fe1 and an easy plane perpendicular to that of the cluster core and including Fe1 and O1 .

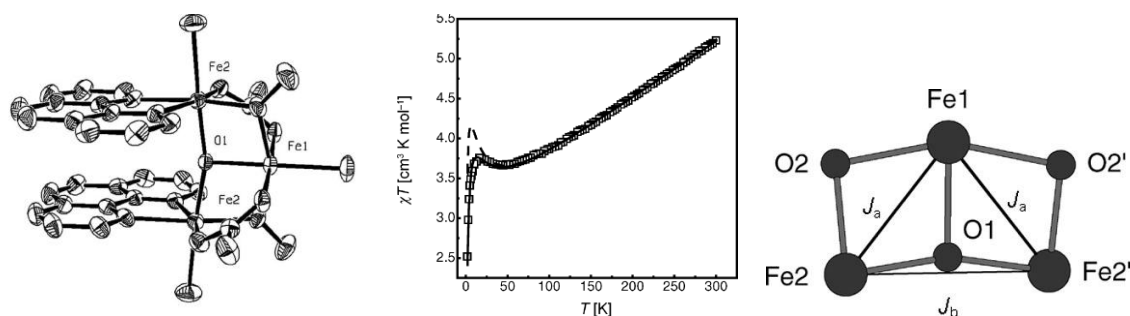


Figure 1.11: (l) crystal structure of $[\text{Fe}_3\text{O}(\text{OCH}_3)_2(\text{OOCH}_3)_2(\text{phen})_2]\text{Cl}_3$; (m) χT versus T plot at 1 T of a powdered sample, squares indicate the measurement, dashed line the fitting; (n) spin interactions within the cluster core showing the pairwise interaction.⁶⁷

In a current publication, Trif et al. investigated a trinuclear copper compound exposed to an external electric field.^{68,69} Due to the field the ground state split in two chiral energy levels. They proposed to use a STM-tip to selectively store and read out the information from the molecular magnets. This is theoretically also possible with $[\text{Fe}_3\text{O}(\text{OOCR})_6(\text{L})_3]\text{X}$ clusters, however, five different chiral states have to be considered in this case.⁷⁰

Materials scientists currently recover trinuclear oxo-bridged iron clusters as building blocks in their materials. During recent years they were intensively investigated concerning their use as secondary building units in the synthesis of new multifunctional MOF systems.^{71,72} Some polymerizable trinuclear iron(III) clusters were also reported. Zhang et al. investigated the reaction of trans-2-butenoic acid with FeSO_4 .⁷³ Within the crystal structure of the product they obtained two differently charged clusters, one mixed valence $\text{Fe}^{\text{II}}\text{Fe}^{\text{III}}_2$ and

one with only Fe^{III} ions in the core. No evidence of polymerization due to the redox reaction during the formation process was reported. Losada et al. reported a series of acrylate-modified mono-metal- and mixed metal-oxo clusters.⁷⁴ They investigated the electrochemical properties and did not find any evidence of polymerization reactions during the electric cycles either. Ten years later Long et al. reported the first crystal structures of this acrylate cluster [Fe₃O(OOCCHCH₂)₆(H₂O)₃]Cl.⁷⁵

2 Results and Discussion

2.1 Optimization of Methacrylate-Modified Fe₃O-Clusters

As elucidated before, the synthesis of class II cluster-reinforced hybrid materials requires the application of the nano building block approach. While the organic monomers in most cases were commercially available, the functionalized inorganic clusters have to be prepared in the laboratory. From the synthetic point of view, the clusters have to fulfill two main requirements: i) easy and upscale-able synthesis in quantitative yields and starting from cheap precursors, and ii) good solubility in organic monomers without condensation, decomposition or exchange reactions. Especially the second point, the behavior of clusters in solution, had recently been investigated for Zr₄, Zr₆ and Zr₁₂ clusters.^{76,77} Temperature dependent ¹H, as well as EXSY liquid NMR measurements showed a continuous exchange of the attached carboxylato ligands on the cluster surface.

Therefore, first and foremost a solution stable paramagnetic compound with polymerizable groups has to be prepared. Fe₃O-clusters are an excellent model system to study the behavior of paramagnetic late transition metal clusters in the synthesis of cluster-reinforced polymers. The Fe₃O core structure can be found as basic building unit in the majority of larger iron clusters. The results of the investigations could therefore provide a basis to explain the behavior of such molecules in polymerization reactions. Furthermore, this family of clusters was reported to be stable to air and moisture and was thus expected to be stable in solution as well. The synthesis allowed designing the cluster properties by introducing different coordinated carboxylates and monodentate ligands.

2.1.1 Clusters of General Formula [Fe₃O(MA)₆(H₂O)₃]X

Two different synthetic strategies were reported for the synthesis of [Fe₃O(MA)₆(H₂O)₃]X compounds: i) starting from an Fe^{II} salt, followed by the oxidation to Fe^{III} by refluxing the solution in air^{43,73}, or ii) starting from an Fe^{III} precursor salt and use sodium carboxylates.⁴⁴ The second strategy was chosen to avoid redox reactions during the synthesis. The clusters were prepared by a simple one-pot synthesis according to the preparation procedure reported for acrylate clusters.⁷⁴ As described in equation 1, the iron(III) salt was dissolved in water and two equivalents of sodium methacrylate were added followed by the precipitation of the clusters.



In the literature, the synthesis was exclusively described starting from common, commercially available, cheap iron(III) salts, such as iron(III) chloride, iron(III) perchlorate or iron(III) nitrate. Sometimes differently coordinated products were reported, but a detailed investigation of the anion influence on the cluster formation process is still missing.⁷⁸ A strong acid (HX) is formed during the reaction, which protonates an unreacted methacrylate in a second step and therefore leads to overall low yields. Although this synthesis is reported to result in clusters of the general formula $[\text{Fe}_3\text{O}(\text{MA})_6(\text{H}_2\text{O})_3]\text{X}$, first analysis of the precipitated powders by ATR-IR (see chapter 2.1.2), showed that different products were obtained depending on the anion. Further analysis clarified that also the behavior of the clusters differed from one another. Therefore, clusters with different anions will be discussed separately.

2.1.1.1 Nitrate

Iron(III) nitrate nonahydrate was dissolved in water and 2 eq. of sodium methacrylate were added accompanied by the precipitation of an orange solid. The dried powder was dissolved in acetone and water was added to the solution. Single crystals were grown from this acetone/water mixture by slow evaporation of the acetone. The results from the single crystal X-ray structure analysis, the structure of $[\text{Fe}_3\text{O}(\text{MA})_6(\text{H}_2\text{O})_3]\text{NO}_3$ **1**, is presented in Figure 2.1. The unit cell contains two clusters **1a** and **1b**, which are structurally equal, but show different bond angles and distances.

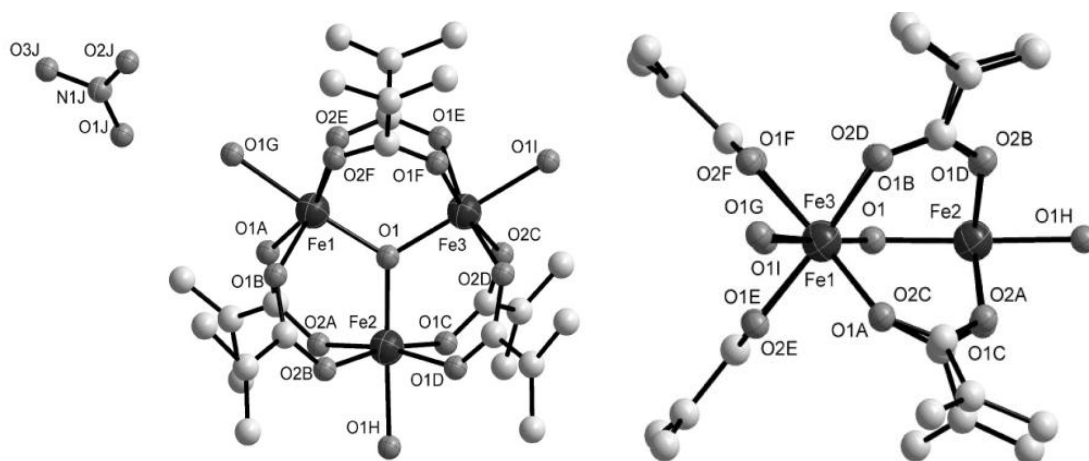


Figure 2.1: Crystal structure of $[\text{Fe}_3\text{O}(\text{MA})_6(\text{H}_2\text{O})_3]\text{NO}_3$ **1**; (l) view perpendicular to the core plane; (r) view along the core plane.

The numbering of the atoms is as follows: The iron ion that was somehow special, for example due to another ligand or a coordinated anion, was marked as Fe1 and the others are numbered clockwise. The μ_3 -oxygens in the center of the core have full numbers without any addendum. The methacrylate ligand connected to Fe1 and Fe2 and lying above the core plane was called A, while that beneath the plane B, and so on. The methacrylate oxygen that was coordinated to the iron ion with the lower number was signed O1X and the other O2X. All

methacrylates not coordinated to the cluster core were ranked after the ones at the cluster, followed by other solvents molecules.

A comparison of the most important distances and angles is presented in Table 2.1. The core of the clusters consists of three octahedrally coordinated iron(III) ions, which are connected by a central μ_3 -oxygen. The Fe– μ_3 O distances within the core range from 188.1(6) pm to 192.1(6) pm. The central oxygen is pulled 1.59 (0.56) pm for O1 and 0.38 (0.53) pm for O2 out of the core plane of the three iron(III) ions. This leads within the error limits to a C_{3v} symmetry of the first core and the highly symmetric group D_{3h} for the other.

Table 2.1: Selected bond distances [pm] and angles [°] in **1**.

Fe1–O1	190.0(6)	Fe4–O2O	201.5(6)	O1B–Fe1–O1G	85.4(4)
Fe1–O1A	198.4(8)	Fe4–O1K	201.7(6)	O1–Fe1–O5J	168.1(8)
Fe1–O2E	202.2(7)	Fe4–O1Q	208.2(6)	O1A–Fe1–O5J	70.9(8)
Fe1–O2F	202.4(12)	Fe5–O2	188.1(6)	O2E–Fe1–O5J	83.2(13)
Fe1–O1B	202.8(7)	Fe5–O2L	199.5(6)	O2F–Fe1–O5J	93.2(15)
Fe1–O5J	205.0(3)	Fe5–O1N	199.8(7)	O1B–Fe1–O5J	88.0(14)
Fe1–O1G	213.3(10)	Fe5–O2K	205.0(6)	O1–Fe1–O1G	174.8(4)
Fe2–O1	189.5(6)	Fe5–O1M	207.4(6)	O1A–Fe1–O1G	87.8(4)
Fe2–O1C	199.8(6)	Fe5–O1R	212.2(6)	O2E–Fe1–O1G	85.6(4)
Fe2–O2B	200.7(6)	Fe6–O2	191.6(6)	O2F–Fe1–O1G	76.2(13)
Fe2–O1D	202.3(6)	Fe6–O1O	199.2(6)	O5J–Fe1–O1G	17.1(8)
Fe2–O2A	202.4(7)	Fe6–O1P	199.8(6)	Fe2–O1–Fe1	120.2(3)
Fe2–O1H	209.3(7)	Fe4–O1L	201.2(6)	Fe2–O1–Fe3	120.2(3)
Fe3–O1	191.2(6)	Fe6–O2M	200.3(6)	Fe1–O1–Fe3	119.6(3)
Fe3–O2C	198.5(6)	Fe6–O2N	202.2(6)	O2J–N1J–O1J	125.0(10)
Fe3–O2D	198.5(7)	Fe6–O1T	207.2(7)	O2J–N1J–O3J	118.2(10)
Fe3–O1E	200.1(8)	N1U–O1U	123.6(13)	O1J–N1J–O3J	116.7(10)
Fe3–O1F	202.5(11)	N1U–O3U	124.5(13)	O5J–N4J–O6J	120.3(14)
Fe3–O1F2	203.0(13)	N1U–O2U	126.0(13)	O5J–N4J–O4J	120.1(14)
Fe3–O1I	210.5(7)	O1–Fe1–O1A	97.4(3)	O6J–N4J–O4J	119.5(14)
O1A–C1A	124.7(14)	O1–Fe1–O2E	94.6(3)	N4J–O5J–Fe1	132.0(2)
N1J–O2J	122.5(10)	O1A–Fe1–O2E	89.0(3)	Fe5–O2–Fe6	120.0(3)
N1J–O1J	126.0(10)	O1–Fe1–O2F	98.6(12)	Fe5–O2–Fe4	119.6(3)
N1J–O3J	126.5(11)	O1A–Fe1–O2F	163.7(11)	Fe6–O2–Fe4	120.3(3)
N4J–O5J	124.5(14)	O2E–Fe1–O2F	93(2)	O1U–N1U–O3U	120.5(14)
N4J–O6J	125.3(14)	O1–Fe1–O1B	94.4(3)	O1U–N1U–O2U	118.0(13)
N4J–O4J	125.8(14)	O1A–Fe1–O1B	89.9(3)	O3U–N1U–O2U	120.9(14)
Fe4–O2	192.1(6)	O2E–Fe1–O1B	171.0(3)		
Fe4–O2P	199.4(6)	O2F–Fe1–O1B	85.8(19)		

From an electronic point of view, the three iron(III) ions are formally identical. The distribution of the electrons is well described in a recent publication.⁷⁹ To fulfill the 18-electron rule, the trivalent iron ions need the donation of 13 electrons from the ligands.

Eight electrons originate from the methacrylate ligands and another two are donated by each water molecule. The missing three electrons should come from the central μ_3 -oxygen. However, the O^{2-} -ion is only able to donate 8 electrons, which leads to 8/3 electrons per iron(III) ion. Therefore the positive charge of the cluster is well distributed over the whole cluster core. It is noteworthy that spin exchange occurs through the central oxygen.

As presented in Figure 2.2, each of the iron(III) ions is coordinated by one oxygen of four bridging methacrylato ligands, forming a square around the metal center whose plane is perpendicular to the one of the cluster core. The distances between the iron(III) ions and the coordinated oxygens range from 198.7(6) pm to 207.2(6) pm. The O–Fe–O angles within the methacrylate oxygen square range from 87.2° to 92.5° . As shown in Figure 2.1 (r) the methacrylato ligands themselves enclose an about 45° angle with the plane of the iron(III) oxo core. The large differences in the distances between the iron(III) ions and the methacrylate oxygens were accompanied by a slight twist of the methacrylato ligand out of the 45° plane. A coordinated water molecule completes the octahedral coordination sphere of the iron(III) ion. The distances between the iron ions and the water molecules range from 207.2(7) pm to 213.3(1.0) pm. The reason for this are the hydrogen bridges to other clusters, solvent molecules and the anions. As shown in Figure 2.2, the iron(III) ions were not located in the center of the coordination octahedra, but are shifted towards the central μ_3 -oxygen, accompanied by the enlargement of the distance between the iron(III) ions and the coordinated water molecules. A detailed comparison and interpretation of the relationship between the Fe–O_l and the Fe–O_{water} distances are given in chapter 2.1.3.

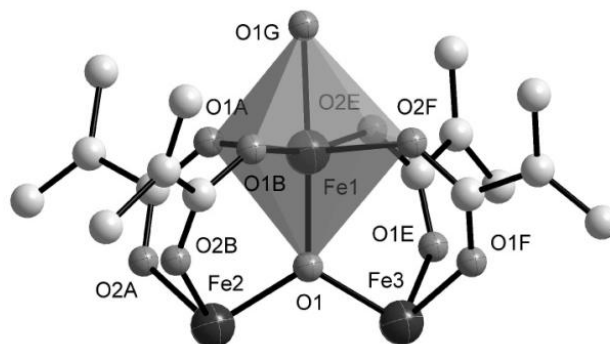


Figure 2.2: Octahedral coordination sphere around Fe1 in $[\text{Fe}_3\text{O}(\text{MA})_6(\text{H}_2\text{O})_3]\text{NO}_3$ **1**.

As shown in Figure 2.3, the clusters form a layered crystal structure with alternating inorganic cluster and solvent layers. The solvent layer is a highly disordered aggregation of water molecules, hold together by hydrogen bonds. Each inorganic cluster layer consists of two rows of clusters. One of the nitrate anions is located between the clusters and connects four of them by hydrogen bonds. Another nitrate is on the surface of these layers and forms intense hydrogen bonds to the water solvent molecules. The coordinated water molecules at the cluster are additionally incorporated in the solvent layer hydrogen bond network.

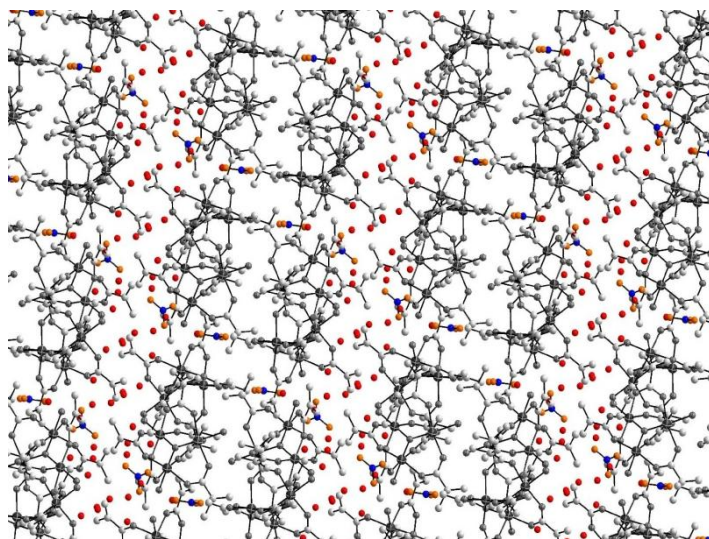


Figure 2.3: Crystal structure of $[\text{Fe}_3\text{O}(\text{MA})_6(\text{H}_2\text{O})_3]\text{NO}_3$ **1**.

The structure showed another remarkable feature of the nitrate anion in the center of the cluster layer. There were two disordered anion positions, one in the lattice, while the other was attached to the cluster core replacing a coordinated water molecule. The resulting cluster $\text{Fe}_3\text{O}(\text{MA})_6(\text{H}_2\text{O})_2\text{NO}_3$ was present in a proportion of about 20 %. The coordinated nitrate showed only little changes in the structural parameter. Compared to Fe1–O1G in Figure 2.1, the bond distance of Fe1–O5J decreased from 213.3(1.0) pm to 205.0(3) pm by coordination of the nitrate. No further effects could be found for the bonds and angles within the cluster.

Crystallization of the precipitated powder from a $\text{CH}_2\text{Cl}_2/n$ -hexane solution yielded $\text{Fe}_3\text{O}(\text{MA})_6(\text{H}_2\text{O})_2\text{NO}_3$ **2**. As shown in Figure 2.4, the cluster was isostructural to the disordered cluster in **1**. The anion was attached to the cluster core and replaces one coordinated water molecule. This results in an uncharged cluster.

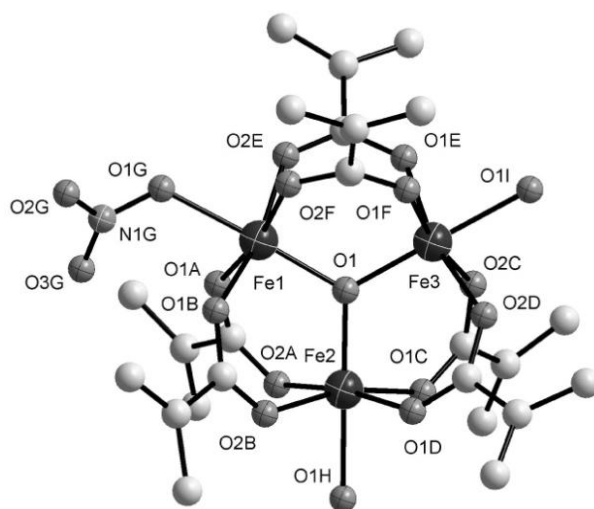


Figure 2.4: Crystal structure of $\text{Fe}_3\text{O}(\text{MA})_6(\text{H}_2\text{O})_2\text{NO}_3$ **2**.

The cluster core had the same structure as in the case of the disordered structure of compound **1**, but the distances of the different groups were much more uniform, due to the lack of hydrogen bonds to solvent molecules. The most important distances and angles are listed in Table 2.2.

Table 2.2: Selected bond distances [pm] and angles [°] in **2**.

Fe1–O1	189.6(4)	Fe3–O1F	201.9(4)
Fe1–O1A	198.3(4)	Fe3–O1I	208.0(4)
Fe1–O2E	199.8(4)	N1G–O3G	121.7(6)
Fe1–O1B	200.6(4)	N1G–O2G	123.4(6)
Fe1–O2F	203.5(4)	N1G–O1G	128.2(6)
Fe1–O1G	209.5(4)	O1–Fe1–O1A	92.41(17)
Fe2–O1	189.7(4)	O1–Fe1–O1B	95.24(17)
Fe2–O1C	199.2(5)	O1–Fe1–O2E	96.83(16)
Fe2–O2B	199.9(5)	O1–Fe1–O2F	96.62(17)
Fe2–O1D	200.9(4)	Fe3–O1–Fe1	120.52(19)
Fe2–O2A	201.0(5)	Fe3–O1–Fe2	119.7(2)
Fe2–O1H	209.4(5)	Fe1–O1–Fe2	119.7(2)
Fe3–O1	188.7(4)	O3G–N1G–O2G	121.5(5)
Fe3–O2D	200.1(4)	O3G–N1G–O1G	120.4(5)
Fe3–O1E	200.2(4)	O2G–N1G–O1G	118.1(5)
Fe3–O2C	201.9(4)		

The Fe–O1 distances were somewhat shorter and more uniform with 188.7(4) pm to 189.7(4) pm. The distances between the coordinated iron(III) ions and the water molecules were shorter as well with values of 208.0(4) pm and 209.4(5) pm. The oxygen of the coordinated nitrate anion had a Fe1–O1G distance of 209.5(4) pm. In contrast to **1**, the nitrate was slightly distorted with a long N1G–O1G distance of 128.2(6) pm and two short N1G–O2G and N1G–O3G distances of 123.4(6) pm and 121.7(6) pm, respectively. Compared to compound **1**, no effects of the anion coordination could be found on either the Fe1–O1 distance with a value 189.6(4) pm or on the distances between the iron(III) ions and the oxygens of the methacrylate ligands. This means that the cluster core is symmetric although the iron(III) ions are asymmetrically substituted.

2.1.1.2 Chloride

In analogy to the nitrate compounds, the cluster was prepared by the reaction of iron(III) chloride hexahydrate with sodium methacrylate in aqueous solution. Crystals grew from an acetone/water solution and were analyzed by single crystal XRD. Surprisingly the crystal structure of **3** contained two differently coordinated compounds, one $[\text{Fe}_3\text{O}(\text{MA})_6(\text{H}_2\text{O})_3]\text{Cl}$ **3b** as expected, and one $[\text{Fe}_3\text{O}(\text{MA})_6(\text{H}_2\text{O})_2(\text{MAH})]\text{Cl}$ **3a** with one water replaced by a

methacrylic acid. The overall composition is thus $[\text{Fe}_3\text{O}(\text{MA})_6(\text{H}_2\text{O})_{2.5}(\text{MAH})_{0.5}]\text{Cl}$ **3**. The structure of both compounds is shown in Figure 2.5.

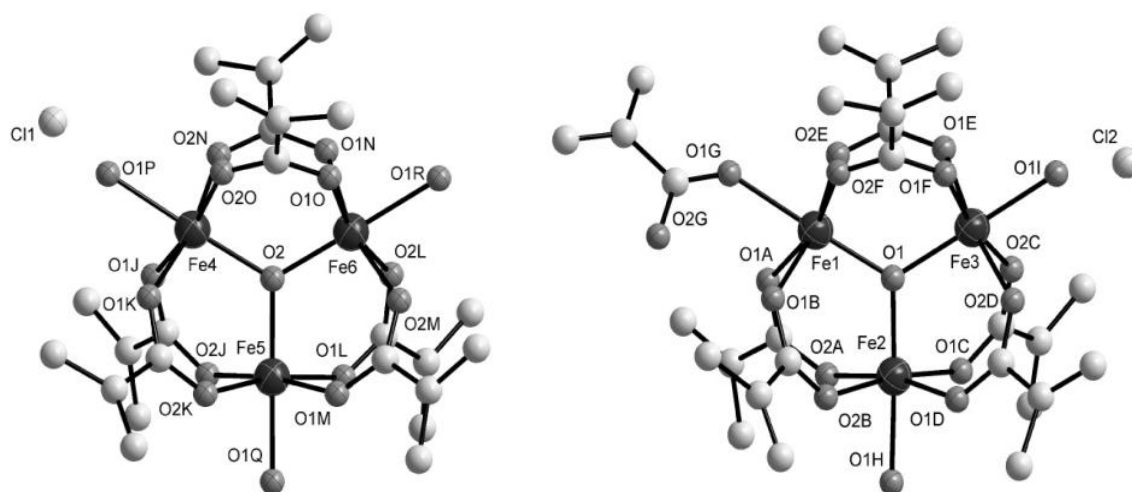


Figure 2.5: Molecular structure of $[\text{Fe}_3\text{O}(\text{MA})_6(\text{H}_2\text{O})_{2.5}(\text{MAH})_{0.5}]\text{Cl}$ **3** with the two subunits $[\text{Fe}_3\text{O}(\text{MA})_6(\text{H}_2\text{O})_3]\text{Cl}$ **3b** (l) and $[\text{Fe}_3\text{O}(\text{MA})_6(\text{H}_2\text{O})_2(\text{MAH})]\text{Cl}$ **3a** (r).

Many structural parallels could be found comparing the molecular structure of the nitrate compound **1** with the two chloride compounds **3a** and **3b**. The overall shape of the clusters, including the cluster core with three iron(III) ions surrounding a central μ_3 -oxygen and the six bridging methacrylate ligands, was identical, but the coordination of the methacrylic acid in **3a** led to a more distorted cluster core. The most important distances and angles are listed in Table 2.3.

Table 2.3: Selected bond distances [pm] and angles [$^\circ$] in **3**.

Fe1–O1	186.9(3)	Fe5–O2K	198.2(3)
Fe1–O2E	197.2(3)	Fe5–O2J	199.0(3)
Fe1–O2F	200.7(3)	Fe5–O1M	200.4(3)
Fe1–O1A	200.7(3)	Fe5–O1L	201.6(3)
Fe1–O1B	207.4(3)	Fe5–O1Q	205.0(3)
Fe1–O1G	211.2(3)	Fe6–O2	187.2(2)
Fe2–O1	190.9(3)	Fe6–O1O	198.2(3)
Fe2–O1D	198.3(3)	Fe6–O2M	199.0(3)
Fe2–O1C	198.6(3)	Fe6–O1N	206.6(3)
Fe2–O2A	201.5(3)	Fe6–O2L	207.6(3)
Fe2–O2B	202.6(3)	Fe6–O1R	210.9(3)
Fe2–O1H	207.0(3)	O1G–C1G	118.7(5)
Fe3–O1	193.0(3)	O2G–C1G	133.0(6)
Fe3–O1F	199.3(3)	O1–Fe1–O1A	98.28(11)
Fe3–O2C	199.7(3)	O1–Fe1–O1B	96.12(11)
Fe3–O2D	201.5(3)	O1–Fe1–O2E	96.12(12)

Fe3–O1E	201.9(3)	O1–Fe1–O2F	96.52(11)
Fe3–O1I	205.9(3)	Fe1–O1–Fe2	120.49(13)
Fe4–O2	192.2(2)	Fe1–O1–Fe3	120.12(13)
Fe4–O1K	199.4(3)	Fe2–O1–Fe3	119.34(13)
Fe4–O2O	200.8(3)	Fe6–O2–Fe4	120.88(13)
Fe4–O1J	201.0(3)	Fe6–O2–Fe5	119.38(13)
Fe4–O2N	202.5(3)	Fe4–O2–Fe5	119.74(13)
Fe4–O1P	207.8(3)	O1G–C1G–O2G	121.0(4)
Fe5–O2	192.9(3)		

The distances between the iron(III) ions and the central μ_3 -oxygen ranged from 186.9(3) pm to 193.0(3) pm. As in the case of **1**, different distances were found for the coordinated water molecules due to hydrogen bond network. The Fe–O distances between the iron ions and the coordinated water molecules were ranging from 205.0(3) pm to 210.9(3) pm. The acid was coordinated by the carbonyl functionality O1G with a C1G–O1G distance of 118.7(5) pm, while the OH group O2G, with a C1G–O2G distance of 133.0(6) pm, was twisted in direction of O1B forming a hydrogen bond. The distance between the iron(III) ion and the oxygen of the acid Fe1–O1G was, due to the sp^2 hybridisation of O1G, with 211.2(3) pm larger than the water-iron(III) distance.

In Figure 2.6, the crystal structure of $[\text{Fe}_3\text{O}(\text{MA})_6(\text{H}_2\text{O})_{2.5}(\text{MAH})_{0.5}]\text{Cl}\cdot 4.5\text{H}_2\text{O}$ is presented. The structure is closely related to **1**, but instead of the nitrate the coordinated methacrylic acid plays the role of the hydrogen bond acceptor and donor in the center of the four clusters. The clusters form layered structures, which were separated by solvent layers. The chloride anions were exclusively located on the surface of the cluster layers, forming a strong hydrogen bond network to the coordinated water molecules analogous to the nitrate in structure **1**.

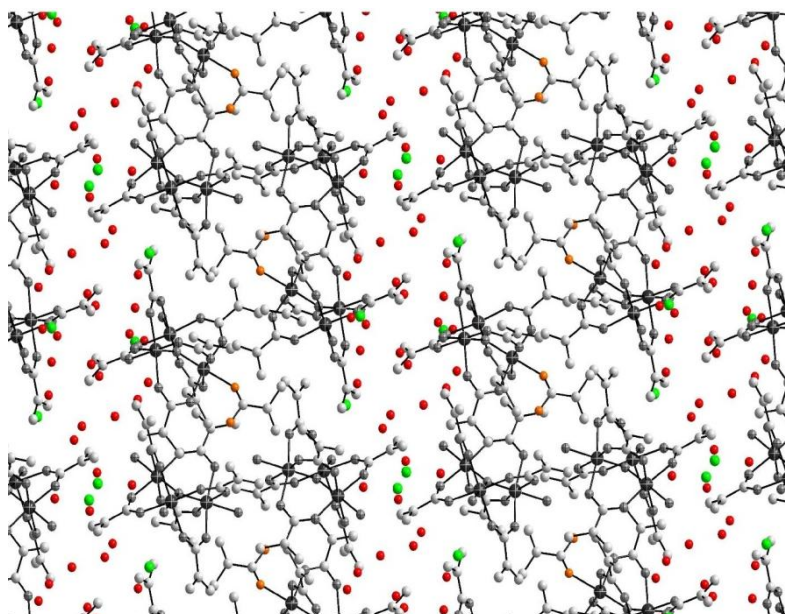


Figure 2.6: Crystal structure of $[\text{Fe}_3\text{O}(\text{MA})_6(\text{H}_2\text{O})_{2.5}(\text{MAH})_{0.5}]\text{Cl}\cdot 4.5\text{H}_2\text{O}$.

It was nevertheless possible to crystallize the single compound $[\text{Fe}_3\text{O}(\text{MA})_6(\text{H}_2\text{O})_3]\text{Cl}$ **4** by diffusion of ether into a chloroform solution of extensively dried $[\text{Fe}_3\text{O}(\text{MA})_6(\text{H}_2\text{O})_{2.5}(\text{MAH})_{0.5}]\text{Cl}$ **3**. The molecular structure is drawn in Figure 2.7. The cluster is identical to compound $[\text{Fe}_3\text{O}(\text{MA})_6(\text{H}_2\text{O})_3]\text{Cl}$ **3b**.

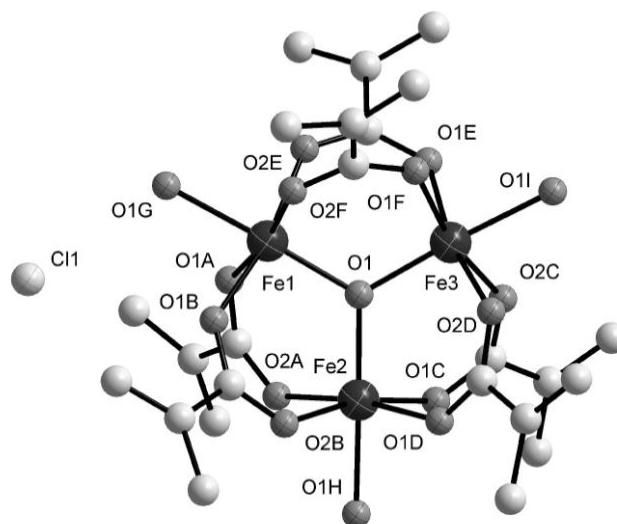


Figure 2.7: Molecular structure of $[\text{Fe}_3\text{O}(\text{MA})_6(\text{H}_2\text{O})_3]\text{Cl}$ **4**.

The cluster core is very symmetric. The most important angles and distances are listed in Table 2.4. The distances between the iron(III) ions and the central μ_3 -oxygen O1 in the center of the core were equidistant with values ranging from 190.1(3) pm to 190.5(3) pm. Likewise, the distances between the coordinated water molecules and the iron(III) ions were uniform ranging from 206.0(3) pm to 207.3(3) pm.

Table 2.4: Selected bond distances [pm] and angles [°] in **4**.

Fe1–O1	190.3(3)	Fe3–O2D	199.5(4)
Fe1–O1B	199.6(4)	Fe3–O2C	200.6(4)
Fe1–O1A	200.4(4)	Fe3–O1E	201.8(4)
Fe1–O2F	200.4(4)	Fe3–O1F	203.7(4)
Fe1–O2E	203.1(3)	Fe3–O1I	206.0(3)
Fe1–O1G	207.0(3)	O1–Fe1–O1A	94.03(14)
Fe2–O1	190.5(3)	O1–Fe1–O1B	95.04(14)
Fe2–O1C	199.8(3)	O1–Fe1–O2E	95.61(14)
Fe2–O2B	201.4(3)	O1–Fe1–O2F	94.64(14)
Fe2–O1D	202.0(4)	Fe3–O1–Fe1	119.60(16)
Fe2–O2A	203.5(4)	Fe3–O1–Fe2	120.21(16)
Fe2–O1H	207.3(3)	Fe1–O1–Fe2	120.19(16)
Fe3–O1	190.1(3)		

2.1.1.3 Bromide

The precipitated powder from the reaction of anhydrous iron(III) bromide with sodium methacrylate in water was dissolved in acetone, whereas water was subsequently added to the solution. Crystals of $[\text{Fe}_3\text{O}(\text{MA})_6(\text{H}_2\text{O})_{2.5}(\text{MAH})_{0.5}]\text{Br}$ **5** grew within one week by evaporation of the acetone. Their structure was closely related to **3**, consisting of two different clusters. In $[\text{Fe}_3\text{O}(\text{MA})_6(\text{H}_2\text{O})_2(\text{MAH})]\text{Br}$ **5a**, two water molecules as well as one methacrylic acid were coordinated to the iron(III) ions, while in $[\text{Fe}_3\text{O}(\text{MA})_6(\text{H}_2\text{O})_3]\text{Br}$ **5b** three water molecules were coordinated. The structure is drawn in Figure 2.8. The most important angles and distances are presented in Table 2.5.

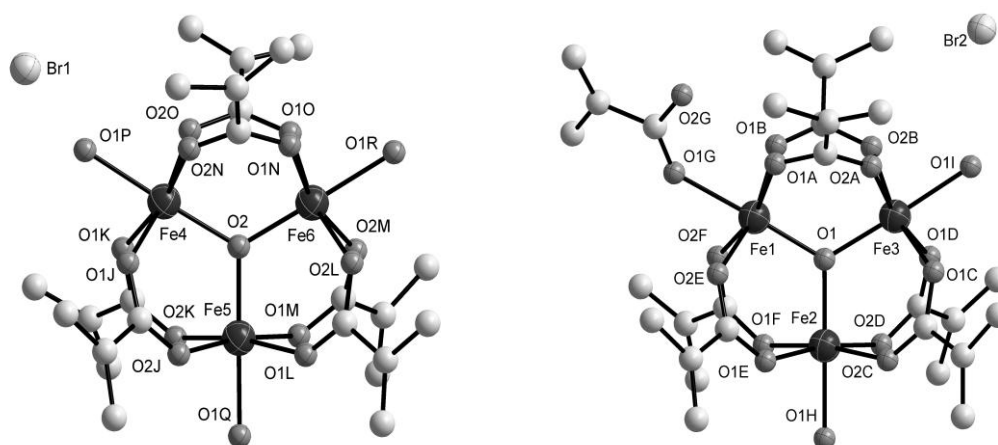


Figure 2.8: Molecular structure of the two subunits in $[\text{Fe}_3\text{O}(\text{MA})_6(\text{H}_2\text{O})_{2.5}(\text{MAH})_{0.5}]\text{Br}$ **5**; $[\text{Fe}_3\text{O}(\text{MA})_6(\text{H}_2\text{O})_3]\text{Br}$ **5b** (l) and $[\text{Fe}_3\text{O}(\text{MA})_6(\text{H}_2\text{O})_2(\text{MAH})]\text{Br}$ **5a** (r).

Table 2.5: Selected bond distances [pm] and angles [°] in **5**.

Fe1–O1	188.1(4)	Fe4–O1P	206.6(4)
Fe1–O2F	197.4(4)	Fe5–O2	192.9(4)
Fe1–O2E	200.7(4)	Fe5–O2J	198.6(4)
Fe1–O1B	201.3(4)	Fe5–O2K	199.5(4)
Fe1–O1A	208.6(4)	Fe5–O1M	199.9(4)
Fe1–O1G	211.1(4)	Fe5–O1L	201.5(4)
Fe2–O1	192.8(4)	Fe5–O1Q	205.5(5)
Fe2–O1E	199.1(4)	Fe6–O2	187.6(4)
Fe2–O2D	199.3(4)	Fe6–O1O	198.5(4)
Fe2–O1F	201.6(4)	Fe6–O2M	199.1(4)
Fe2–O2C	201.8(4)	Fe6–O1N	207.1(4)
Fe2–O1H	205.8(4)	Fe6–O2L	208.5(4)
Fe3–O1	189.9(4)	Fe6–O1R	211.2(4)
Fe3–O1D	198.3(4)	O1G–C1G	121.4(7)
Fe3–O1C	198.7(4)	O2G–C1G	131.5(7)
Fe3–O2B	202.0(4)	O1–Fe1–O1A	97.00(16)
Fe3–O2A	202.4(4)	O1–Fe1–O1B	97.61(17)
Fe3–O1I	208.0(4)	O1–Fe1–O2E	96.11(16)
Fe4–O2	191.4(4)	O1–Fe1–O2F	96.51(17)
Fe4–O1K	199.9(4)	Fe1–O1–Fe3	120.4(2)
Fe4–O2O	201.0(4)	Fe1–O1–Fe2	119.78(19)
Fe4–O1J	201.3(4)	Fe3–O1–Fe2	119.77(19)
Fe4–O2N	202.7(4)	O1G–C1G–O2G	123.0(6)

The distance between the methacrylic acid-substituted iron(III) ion Fe1 and the central μ_3 -oxygen O1 was 188.9(4) pm. The iron(III)–oxygen distances within the core of the water-substituted sites of the clusters **5a** and **5b** ranged from 187.6(4) pm to 192.9(4) pm. The Fe1–O1G distance was 211.1(4) pm. The distances between the iron(III) ions and the coordinated water molecules range from 205.5(5) pm to 211.2(4) pm. The acid is coordinated by the C=O group of the acid with a C1G–O1G distance of 121.4(7) pm, while the OH group shows a C1G–O2G distance of 131.5(7) pm.

2.1.1.4 Methacrylate

It was described in the literature that the use of iron(II) sulfate as precursor for the cluster synthesis leads to an iron(III,III,II) cluster and no sulfate anion could be observed.⁴³ Therefore, the synthesis was performed by reaction of iron(III) sulfate with sodium methacrylate in aqueous solution. The ATR-IR spectrum of the precipitated powder showed many bands in the region of coordinated methacrylates. Single crystals were grown from an acetone/water solution in extremely low yield resulting in the structure of $\text{Fe}_3\text{O}(\text{MA})_6(\text{H}_2\text{O})_2(\text{MA})$ **6** presented in Figure 2.9.

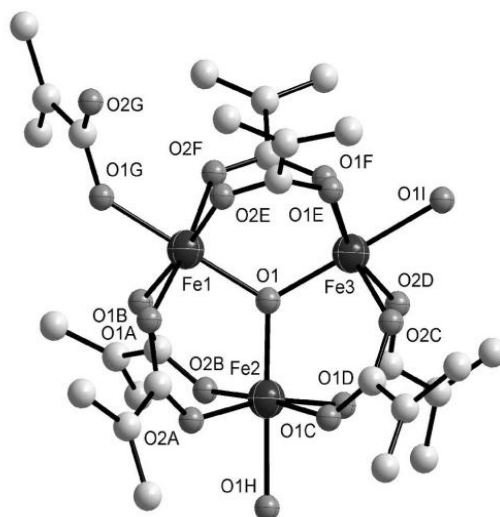


Figure 2.9: Molecular structure of $\text{Fe}_3\text{O}(\text{MA})_6(\text{H}_2\text{O})_2(\text{MA})$ **6**.

No sulfate was found in the crystal structure. Instead methacrylate ions were present, which were coordinated to the cluster core, leading to an uncharged cluster analogous to the coordinated nitrate in structure **2**. The most important angles and distances are presented in Table 2.6. The iron(III) ions form an irregular triangle with an Fe1–O1 distance of 194.0(2) pm, while the Fe2–O1 and Fe3–O1 were equal with values of 189.1(2) pm and 189.6(2) pm. The distance between the coordinated water molecules and the iron(III) ions were 209.7(3) pm and 209.5(3) pm, respectively. The Fe1–O1G distance was found to be 197.3(3) pm, remarkable longer than the distances found in **3a** with 186.9(3) pm and **5a** with 188.4(4) pm, which evidenced that in this case no acid, but a carboxylate is coordinated.

Table 2.6: Selected bond distances [pm] and angles [°] in **6**.

Fe1–O1	194.0(2)	Fe3–O2D	202.1(4)
Fe1–O1G	197.3(3)	Fe3–O1I	209.5(3)
Fe1–O2E	200.9(3)	O1G–C1G	127.8(5)
Fe1–O1B	202.3(3)	O2G–C1G	123.0(5)
Fe1–O1A	202.6(3)	O1J–C1J	133.4(11)
Fe1–O2F	207.4(3)	O2J–C1J	135.0(13)
Fe2–O1	189.1(2)	O1–Fe1–O1A	91.61(11)
Fe2–O2A	199.9(3)	O1–Fe1–O1B	92.48(11)
Fe2–O2B	200.1(3)	O1–Fe1–O2E	92.24(11)
Fe2–O1D	201.5(4)	O1–Fe1–O2F	94.28(11)
Fe2–O1C	201.9(3)	Fe2–O1–Fe3	118.99(12)
Fe2–O1H	209.7(3)	Fe2–O1–Fe1	121.14(12)
Fe3–O1	189.6(2)	Fe3–O1–Fe1	119.86(12)
Fe3–O1F	198.5(3)	O2G–C1G–O1G	123.1(4)
Fe3–O2C	200.3(3)	O1J–C1J–O2J	115.7(14)
Fe3–O1E	200.7(4)		

2.1.2 IR Investigations

2.1.2.1 Nitrate

The nitrate cluster **1** will be discussed in more detail to serve as model system for the other clusters. All presented and discussed IR data in this thesis are, except as noted otherwise, obtained only from crystalline compounds. The IR spectrum of **1** is presented in Figure 2.10. The spectrum is only shown from 550 cm^{-1} to 2000 cm^{-1} for two reasons. At first, the ATR-IR method is most applicable in this region, while absorption bands get less intensive at lower wavelength (higher wavenumbers). Secondly, the most important bands, which indicated the coordination of the different ligands to the cluster core, are located in this region.

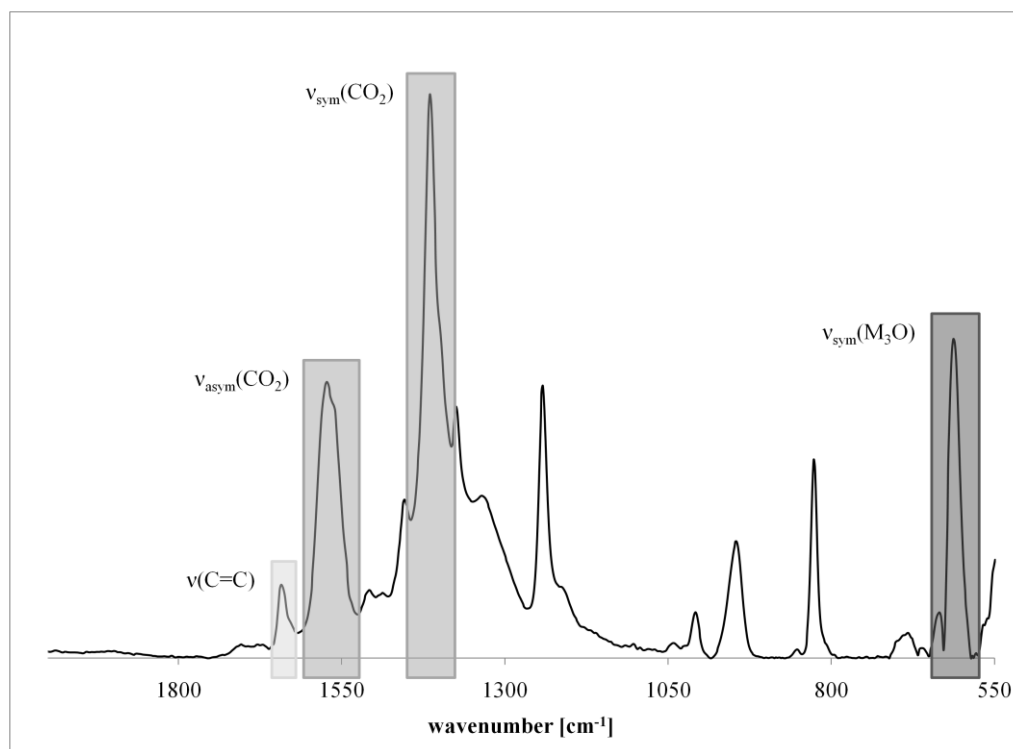


Figure 2.10: IR spectra of compound **1** in the region between 550 cm^{-1} and 2000 cm^{-1} .

Numerous publications report IR investigations of trinuclear basic carboxylates, especially acetates.^{80,81} The four most important bands in Figure 2.10 are marked with grey bars. A comparison of these signals for crystalline samples of all water-substituted compounds **1–6** is presented in Table 2.7. At 1642 cm^{-1} , the vibration of the C=C double bond was visible indicating the presence of the polymerizable group. The spectrum is dominated by two bands, which were assigned to the coordinated carboxyl groups of the methacrylato ligand. At 1573 cm^{-1} , the band of the asymmetric stretching vibration of the bridging methacrylato ligand is visible, while at 1415 cm^{-1} the most intense band indicates the

symmetric stretching vibration. The typical signal for the asymmetric stretching of the central μ_3 -oxygen within the iron(III) ion triangle was detected at 612 cm^{-1} . In this region, the transmittance of the ATR cell was decreasing rapidly due to interferences of the ZnSe crystal.

Table 2.7: Comparison of selected bands in **1–6**.

Compound	$\nu(\text{C}=\text{C})$	$\nu_{\text{asym}}(\text{CO}_2)$	$\nu_{\text{sym}}(\text{CO}_2)$	$\nu_{\text{sym}}(\text{Fe}_3\text{O})$
1	1642	1573	1415	612
2	1641	1570	1413	611
3	1642	1569	1414	612
4	1642	1573	1415	612
5	1641	1570	1414	613
6	1644	1579	1414	613

According to Cannon et al., coordinated water of basic chromium acetate has three very weak bands at 700 , 570 and 491 cm^{-1} , which could only be detected at liquid nitrogen temperatures.⁸⁰ Indeed, no bands for coordinated or free water could be detected in the IR spectra with exception of a broad band from 2700 to 3300 cm^{-1} , which increased with increasing water content.

For the nitrate anion in compound **1**, an additional broad band was visible with a maximum at 1336 cm^{-1} . The ATR-IR spectrum of compound **2** did not differ much from that of compound **1** mentioned above. The C=C stretching vibration was slightly shifted to 1641 cm^{-1} accompanied by the shift of the CO_2 bands to 1570 cm^{-1} and 1413 cm^{-1} . The most obvious shift was visible for the nitrate band, which was found at 1301 cm^{-1} . Therefore, the band of the nitrate anion is the best possibility to distinguish between coordinated and free species. The ATR-IR analysis of the crystals clarified that the methacrylate bands of the precipitated powder before crystallization were equal to that found for compound **1**, but the nitrate signal was much sharper for the crystalline compound. The next step, the investigation of the cluster solution by IR, faced the problem that the precipitated powder as well as the crystalline compounds **1** and **2** were badly soluble. An extraction experiment was performed, where the precipitated powder was suspended in CHCl_3 . Thereby, the solution as well as the residue were investigated. The IR spectra clarified that there were two different compounds **1** and **2** present in the precipitated powder. Compound **2** was better soluble and predominant in solution, while the residue showed the same bands as found in compound **1**.

2.1.2.2 Chloride

ATR-IR investigations showed the coordination of the methacrylate ligands with the typical bands at 1643 cm^{-1} for the C=C double bond as well as 1573 cm^{-1} and 1414 cm^{-1} for the asymmetric and symmetric CO_2 vibration. The coordinated methacrylic acid with the band for the double bond at 1678 cm^{-1} and for the C–O at 1518 cm^{-1} is visible in the spectrum. Furthermore, the cluster was soluble in organic solvents after excessive drying over P_4O_{10} ,

solution IR spectroscopy of the compound could thus be performed. Comparison of the two spectra in the solid state and in CHCl_3 solution is presented in Figure 2.11. Additional to the signals described above, the solution spectrum showed bands indicating free methacrylic acid as well as methacrylates bridging a Fe–OH–Fe structure. Especially the presence of free methacrylic acid indicated condensation of the clusters, which could be verified by dynamic light scattering.

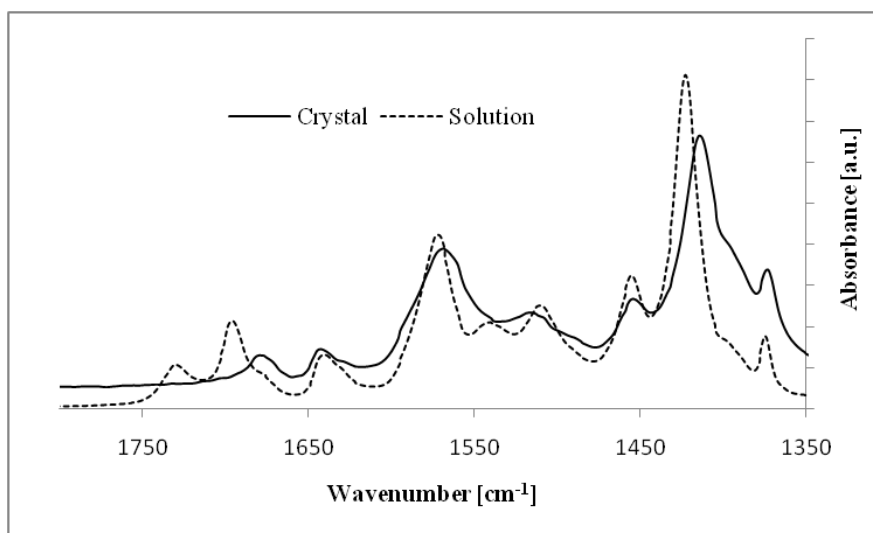


Figure 2.11: Comparison the ATR-IR spectrum of a crystalline sample (solid line) of $[\text{Fe}_3\text{O}(\text{MA})_6(\text{H}_2\text{O})_{2.5}(\text{MAH})_{0.5}]\text{Cl}$ **3** with the CHCl_3 solution (dotted line).

DLS measurements were carried out for compound **3** in ethanol, toluene, water, acetone and THF solution. The solutions were measured during one week. In aqueous and acetone solutions, large aggregates were observed at first, though they got smaller with time. The concentration of dissolved cluster did not cause a change in the size of the aggregates. The evolution of the aggregates in aqueous solution with time is presented in Figure 2.12. In acetone and water solutions the aggregates completely disappeared and in the end only individual clusters were observed. For ethanol, toluene and THF solutions the clusters did not dissolve completely, but the aggregate size remained constant after some time.

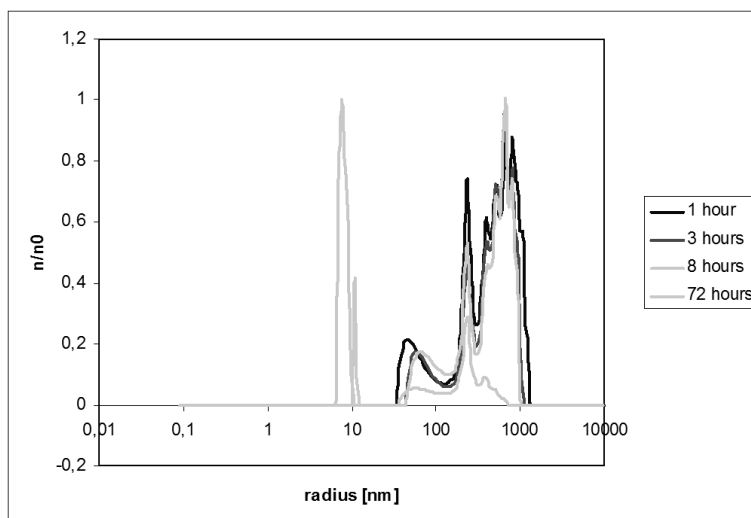


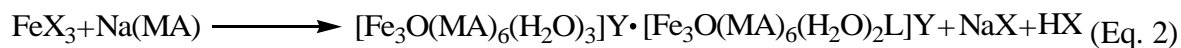
Figure 2.12: DLS measurements of **3** in aqueous solution after 1, 3, 8 and 72 hours.

2.1.2.3 Methacrylate

The IR spectra of **6** showed many not assignable signals in the region for differently coordinated methacrylate ligands after precipitation. For crystals of the methacrylate compound **6**, three signals were found in the region above 1600 cm^{-1} . The signal at 1644 cm^{-1} indicated the C=C stretching vibration, typical for these clusters, but at 1629 cm^{-1} a shoulder, which is assigned to the coordinated methacrylate, was detected. The compound was well soluble by heating in chloroform, but the solution IR spectrum differed markedly from the crystalline sample.

2.1.3 Discussion and Conclusion

A complete overview about methacrylate-substituted trinuclear iron oxo clusters with a variety of anions was given in this chapter. The synthesis was performed according to literature procedure, but in contrast to the predicted structure $[\text{Fe}_3\text{O}(\text{MA})_6(\text{H}_2\text{O})_3]\text{X}$, a variety of different compounds **1–6** were obtained. Compared to the expected synthesis (equation 1), the synthesis of the resulting clusters can better be described by equation 2 for compounds **1**, **3** and **5** and equation 3 for compounds **2**, **4** and **6**.



	X	Y	L
1	NO ₃	H ₂ O	0.8 H ₂ O/0.2 NO ₃
2	NO ₃	-	NO ₃
3	Cl	Cl	HMA
4	Cl	Cl	H ₂ O
5	Br	Br	HMA
6	SO ₄	-	MA

Compounds **3** and **5** consisted of two different clusters. In any case, one was the expected $[\text{Fe}_3\text{O}(\text{MA})_6(\text{H}_2\text{O})_3]\text{Y}$ (**3b**, **5b**), while at the other, $[\text{Fe}_3\text{O}(\text{MA})_6(\text{H}_2\text{O})_2(\text{MAH})]\text{Y}$ (**3a**, **5a**), a methacrylic acid was coordinated. The pure compound $[\text{Fe}_3\text{O}(\text{MA})_6(\text{H}_2\text{O})_3]\text{Cl}$ **4** was obtained by crystallization from $\text{CHCl}_3/\text{ether}$. A quite related molecular structure was found for compound $[\text{Fe}_3\text{O}(\text{MA})_6(\text{H}_2\text{O})_3]\text{NO}_3$ **1**. In the crystal structure of **1** a minority component with coordinated nitrate anion was present. This cluster $\text{Fe}_3\text{O}(\text{MA})_6(\text{H}_2\text{O})_2\text{NO}_3$ **2** could be obtained as individual component by recrystallization. It is noteworthy that the pure compounds **2** and **4** could be found in the mixed compounds **1** and **3**.

ATR-IR studies of the precipitated powders compared with the obtained single crystals showed that the powders were no single compounds, but mostly consisted of, at least, two different clusters. Starting from iron(III) nitrate, crystalline compounds **1** and **2** were obtained. Extraction experiments of the precipitated powder showed that both clusters were already present in the first precipitation. In the case of chloride, the compounds **3** and **4** were obtained and were therefore present in the powder. The situation was different for compound **6**. The IR spectra showed that the structure was not the predominant compound in the precipitated powder. From a synthetic point of view, this means that all clusters have to be crystallized first to have defined compounds for further reactions.

The use of the non-coordinating sulfate anion in the synthesis of trinuclear iron(III) clusters led to $\text{Fe}_3\text{O}(\text{MA})_6(\text{H}_2\text{O})_2(\text{MA})$ **6**. No sulfate was found in the crystal structure. Instead a methacrylate ligand had substituted one of the water molecules.

The role of the anion in the synthesis of the iron(III) oxo clusters was investigated in further experiments. Therefore, iron(III) chloride was reacted with silver tetrafluoroborate to give $\text{Fe}(\text{BF}_4)_3$, a precursor salt with a non-coordinating anion. Surprisingly, after the precipitation of silver chloride the solution was colorless, which means in other words the solvated iron(III) ions were colorless. The presence of iron(III) ions was tested by addition of NaOH , which resulted in the precipitation of $\text{FeO}(\text{OH})$. The reaction of $\text{Fe}(\text{BF}_4)_3$ with two equivalents sodium methacrylate in aqueous solution led to an orange precipitate that was not soluble in any common organic solvent. ATR-IR investigations showed the presence of many differently coordinated methacrylate species and the absence of the Fe_3O band at around

600 cm^{-1} . This could be interpreted in such way that no iron trimer with any ligand, but an undefined new compound, was formed.

Obviously, the formation of the cluster is dependent on the presence of a coordinating anion that take an active part of the reaction. In the literature, the deprotonation followed by dimerisation of the hexaquo iron(III) complex was reported as well as the incorporation of the anion in the resulting OH bridge.⁸² This leads to a prestructuring of the iron ions in solution and, by addition of methacrylate, the cluster can be formed. Sulfate is able to form these dimeric species indicated by the red-orange color of the aqueous iron(III) sulfate solution. Iron(III) tetrafluoroborate shows a different structure in solution and consequently by addition of methacrylate a different compound is formed.

Nevertheless this is not the only reaction where the anion plays an important role. After the addition of methacrylate the bridging OH group of the dimer has to condense with an OH group of a monomer to form the trinuclear oxo bridged cluster. The anion in cis position to the OH flips to trans and exchanges with a methacrylate anion that takes the bridging position. At last the anion is substituted by a water molecule. This last step requires large activation energy. The reaction mechanism explains why the compounds **1**, **2** and **6**, with coordinated anions, could be obtained although the reaction is done in an excess of coordinating solvent, namely water. It does not explain, why in the case of chloride or bromide, which have the biggest affinity to iron(III), no coordinated compound had been found. An explanation for this is given in chapter 2.1.10, but here it should be pointed out that for both compounds **3** and **5** the elemental analysis resulted in too high halogenide contents.

To further investigate the role of the anion in the cluster formation and at the same time verify the model established above, the reaction was also performed starting from iron(III) fluoride trihydrate. Fluoride is known to have a strong affinity to iron(III), which is manifested for instance in the crystal structure $\text{FeF}_3(\text{H}_2\text{O})_3$. Therefore, $\text{Fe}_3\text{O}(\text{MA})_6(\text{H}_2\text{O})_2\text{F}$, a related molecular structure to **2** or **6**, with coordinated anion, was expected. The ATR-IR spectrum of the precipitated powder showed many different signals in the region of the coordinated methacrylates, quite similar to the spectrum of compound **6**. The powder was not soluble in any common organic solvent, so it was reacted with pyridine as described in the next chapter. Crystals were obtained and found to be $\text{Fe}_6\text{O}_2(\text{OH})_2(\text{py})_2(\text{MA})_{12}$. For this purpose, it meant that the use of well-coordinating anions, as well as the use of non coordinating ones, lead to $\text{Fe}_3\text{O}(\text{MA})_6(\text{H}_2\text{O})_2(\text{MA})$ **6**, where only methacrylate, but no precursor anion is present. From further investigations on chloride and bromide in the next chapter, it could be concluded that the very stable FeF_4^- anion is formed during the substitution reaction and therefore the fluoride anion got lost.

The comparison of the methacrylate-substituted clusters with the acetate and acrylate derivatives known from the literature results in great similarities of the most important angles and distances. For an acetate derivative with a similar structure as $[\text{Fe}_3\text{O}(\text{MA})_6(\text{H}_2\text{O})_3]\text{Cl}$ **4**, Fe- $\mu_3\text{O}$ distances between 189.4(3) pm and 190.6(4) pm, compared with 190.1(3) pm to 190.5(3) pm in **4**, had been described.⁴⁵ The distances of the coordinating methacrylates and

water molecules also did not show significant differences. The kind of used carboxylates appeared to have a neglectable influence on the cluster structure, while the anion, as well as hydrogen bonds of the coordinated water molecules did have an impact. The formation of defined water clusters linked by hydrogen bonds with impact were already described in literature.^{83,84}

Two clusters similar to $\text{Fe}_3\text{O}(\text{MA})_6(\text{H}_2\text{O})_2(\text{MA})$ **6** were reported in the literature. In one case, the cluster $\text{Fe}_3\text{O}(\text{Ac})_6(\text{H}_2\text{O})_2(\text{Ac})$ showed an elongated $\text{Fe1}-\mu_3\text{O}$ distance of 195.1(1) pm compared to 194.0(2) pm for **6**.^{85,79} The bigger distance of the iron ion was due to the coordination of the anion. The $\text{Fe}-\text{O}$ distances of the two other water coordinated iron(III) ions were not much influenced. Only little changes of the $\text{Fe1}-\mu_3\text{O}$ distance with 190.9(3) pm and 191.1(3) pm were reported for the same cluster in a supramolecular hydrogen bond assembly.⁸⁵ The distances were comparable to that found for $\text{Fe}_3\text{O}(\text{MA})_6(\text{H}_2\text{O})_2\text{NO}_3$ **2**. Therefore, two types of clusters with coordinated anion can be distinguished: the ones with distortion of the cluster core and the ones without.

Magnetic exchange between single ions is mainly determined by their distance and the overlap of the orbitals. Therefore, the distances within the Fe_3O triangle were of major interest. A comparison of the $\text{Fe}-\mu_3\text{O}$ and $\text{Fe}-\text{O}_{\text{ligand}}$ distances is shown in Table 2.8.

Table 2.8: Comparison of the distances [pm] between the iron(III) ions and the μ_3 -oxygen and the iron(III) ion and the coordinated ligand in the compounds **1–6** determined by single crystal XRD

	1a (at 100 K)	$\text{Fe}-\mu_3\text{O} +$ $\text{Fe}-\text{O}_{\text{ligand}}$	1b (at 100 K)	$\text{Fe}-\mu_3\text{O} +$ $\text{Fe}-\text{O}_{\text{ligand}}$	2 (at 100 K)	$\text{Fe}-\mu_3\text{O} +$ $\text{Fe}-\text{O}_{\text{ligand}}$
Fe1–O1 (Fe4–O2)	190.0(6)	403.3	192.1(6)	400.3	189.6(4)	399.1
Fe1–O1G (Fe4–O1P)	213.3(10)		208.2(6)		209.5(4)	
Fe2–O1 (Fe5–O2)	189.5(6)	398.8	188.1(6)	400.3	189.7(4)	399.1
Fe2–O1H (Fe5–O1Q)	209.3(7)		212.2(6)		209.4(5)	
Fe3–O1 (Fe6–O2)	191.1(6)	401.6	191.6(6)	398.8	188.7(4)	396.7
Fe3–O1I (Fe6–O1R)	210.5(11)		207.2(6)		208.0(4)	
	3a (at 100 K)	$\text{Fe}-\mu_3\text{O} +$ $\text{Fe}-\text{O}_{\text{ligand}}$	3b (at 100 K)	$\text{Fe}-\mu_3\text{O} +$ $\text{Fe}-\text{O}_{\text{ligand}}$	4 (at 100 K)	$\text{Fe}-\mu_3\text{O} +$ $\text{Fe}-\text{O}_{\text{ligand}}$
Fe1–O1 (Fe4–O2)	186.9(3)	398.1	192.2(2)	400.0	190.3(3)	397.3
Fe1–O1G (Fe4–O1P)	211.2(3)		207.8(3)		207.0(3)	
Fe2–O1 (Fe5–O2)	190.9(3)	397.9	192.9(3)	397.9	190.5(3)	397.8
Fe2–O1H (Fe5–O1Q)	207.0(3)		205.0(3)		207.3(3)	
Fe3–O1 (Fe6–O2)	193.0(3)	398.9	187.2(2)	398.1	190.1(3)	396.1
Fe3–O1I (Fe6–O1R)	205.9(3)		210.9(3)		206.0(3)	
	5a (at 100 K)	$\text{Fe}-\mu_3\text{O} +$ $\text{Fe}-\text{O}_{\text{ligand}}$	5b (at 100 K)	$\text{Fe}-\mu_3\text{O} +$ $\text{Fe}-\text{O}_{\text{ligand}}$	6 (at 299 K)	$\text{Fe}-\mu_3\text{O} +$ $\text{Fe}-\text{O}_{\text{ligand}}$
Fe1–O1 (Fe4–O2)	188.1(4)	399.2	191.4(4)	398.0	194.0(2)	391.3
Fe1–O1G (Fe4–O1P)	211.1(4)		206.6(4)		197.3(3)	
Fe2–O1 (Fe5–O2)	192.8(4)	398.6	192.9(4)	398.4	189.1(2)	398.8
Fe2–O1H (Fe5–O1Q)	205.8(4)		205.5(4)		209.7(3)	
Fe3–O1 (Fe6–O2)	189.9(4)	397.9	187.6(4)	398.8	189.6(2)	399.1
Fe3–O1I (Fe6–O1R)	208.0(4)		211.2(4)		209.5(3)	

As elucidated before, the individual values differ over a wide range due to the hydrogen bonds. The measurements of the respective distances at different temperatures resulted in quite similar values. This means that the bond distances are independent from the temperature. Thus, for the water-substituted iron(III) sites, the Fe–O_{ligand} distances vary over 7.2 pm and range from 205.0(3) pm to 212.2(6) pm, while the Fe–μ₃O distances show values between 187.2(3) pm and 193.0(3) pm with a variation of 5.8 pm. The values for Fe1 in the molecular structure **1a** have, due to the disorder, not been taken into consideration. Nevertheless, comparing the dependency of the magnitude of Fe–μ₃O and Fe–O_{ligand} distances among one another, it becomes clear that long Fe–O_{ligand} distances cause short Fe–μ₃O distances and *vice versa*. Therefore, the sum of the Fe–O_{ligand} and the Fe–μ₃O distance only vary 3.7 pm from 397.9 pm to 401.6 pm.

This behavior was as well observed for the methacrylate, nitrate and methacrylic acid-substituted iron(III) ions. The shortest Fe–O_{ligand} distance was detected for the methacrylato-*O* ligand in compound **6** with 197.3(3) pm. This resulted in the biggest Fe–μ₃O value of 194.0(2) pm. The coordination of the nitrate resulted in no remarkable distortion, while the coordination of the methacrylic acid led to long Fe–O_{ligand} distances with 211.2(3) pm (**3a**) and 211.1(4) pm (**5a**) and short Fe–μ₃O distances of 186.9(3) pm (**3a**) and 188.1(4) pm (**5a**).

The coordinated μ-methacrylato-*O,O'* showed similar compensating effects in their bond distances compared to Fe–μ₃O and Fe–O_{ligand}. A long Fe–O distance resulted in a short Fe–O' distance and *vice versa*. Generally, the Fe–O_{methacrylate} distances show greater variations for more distorted cluster cores. Therefore, for symmetric clusters the four methacrylato ligands coordinating to one iron(III) ion have two similar bond distances, whose values are in between of the other two distances.

Two different types of clusters can be distinguished, the ones with a symmetric core and the ones with a distorted cluster core. Even though the hydrogen bonds of the coordinated water molecules have an overall impact on the distances within the cluster, the comparison of the Fe–μ₃O showed that in asymmetric clusters always two equal and one different distance were detected. This effect originates from the location of the positive charge at one iron(III) ion due to the hydrogen bond distorted cluster cores.

The compounds **1–7** can be distinguished by their crystal structure. The biggest differences were found for compounds **1**, **3** and **5**. They all had two different types of molecules in their unit cells and were arranged in layered structures. The layers alternate between solvent molecules and a double layer of clusters. Four clusters were connected by hydrogen bonds to a central anion or acid. The anions are located on the surface of the cluster layer and form hydrogen bonds to the solvent layer and the coordinated water molecules of the clusters. This assembly resulted in non-uniform angles and distances within the clusters. The solvent layer can reversibly be removed. This was shown by an experiment where single crystals of compound **3** were intensively dried over P₄O₁₀ and subsequently the mass was

determined. Afterwards, the crystals were stored over a water bath for one day and the mass change was calculated. The results of the cycles are shown in Figure 2.13.

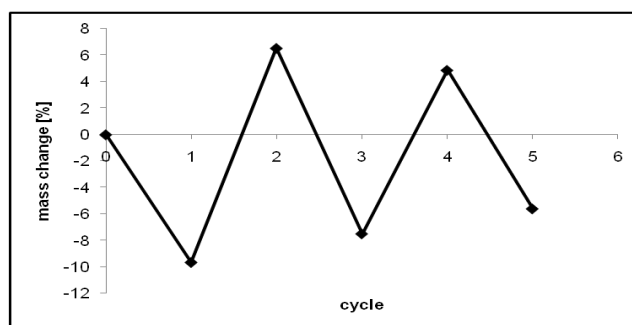


Figure 2.13: Percentage of mass change for loading and deloading of the solvent layer in **3**.

In the other structures **2**, **4**, **6** and **7**, the solvent molecules and hydrogen bonds were not that predominant. The cluster cores were all located in one plane. The anion, independent from a potential coordination to the cluster core, built a hydrogen bond assembly with the coordinated methacrylic acids and the coordinated water molecules within the plane. When a dichloromethane or chloroform molecule was present in the structure, it was located above and below the center of the core in a sandwich of two clusters. The clusters build cluster columns, in which they are arranged exactly on top of each other. The hydrogen bonds within the cluster plane might cause the insolubility.

As well as the distances of the iron ions to the ligands, the IR bands of the methacrylate-substituted compounds were comparable to those of the acetate-substituted derivatives. This was also visible in the small differences between the spectra of the acetate and acrylate substituted clusters.⁸⁰ This means that the strength of the coordination of the carboxylates is hardly influenced by the variation of the acid.

The clusters **2**, **4** and **7** were not soluble in common organic solvents, in contrast to the clusters **1**, **3** and **5**, which were soluble after intense drying over P_4O_{10} . Solution IR showed that the cluster decomposed in solution, and DLS measurements clarified that big aggregates were formed.

In conclusion, no stable clusters in solution, suitable for the potential use in the nano building block approach, could be obtained. Compounds **1**, **3** and **5** had two different clusters in the crystal structure and showed decomposition in solution. The pure compounds **2**, **4** and **7** were not soluble due to the intense hydrogen bond network in their crystal structures. Thus, the idea was developed to exchange the coordinated water molecules for more hydrophobic molecules in order to avoid the hydrogen bonds.

2.1.4 Clusters of General Formula $[\text{Fe}_3\text{O}(\text{MA})_6(\text{HOR})_3]\text{X}$

The great disadvantage of water-substituted iron(III) oxo clusters, which prevented the application in the nano building block approach, was their insolubility in organic solvents. This problem was traced back to the intense hydrogen bond system between the coordinated water molecules. It was therefore attempted to substitute the water ligands for more hydrophobic ones, such as methanol and ethanol. Three different synthetic routes were tested. The first one was started from the water-substituted clusters followed by the substitution of the ligands. Alternatively, the overall cluster preparation was carried out in the coordinating solvent. The third possibility was to dissolve preprepared water-substituted clusters in the respective alcohol. Surprisingly, the resulting clusters differed depending on the anion of the precursor salt and the synthesis method. For the latter strategy, no crystalline products, but a yellow precipitate, was obtained. The results will be discussed separately in 2.1.6.

2.1.4.1 Methanol-Nitrate

For the nitrate precursor, both approaches led to the trimethanol-substituted compound $[\text{Fe}_3\text{O}(\text{MA})_6(\text{HOCH}_3)_3]\text{NO}_3$ **7**. As presented in Figure 2.14, the structure consisted of the well-known iron(III) triangle with a centered μ_3 -oxygen and coordinated bridging methacrylate-*O,O'* ligands. Additionally, a methanol molecule was coordinated at every iron(III) ion.

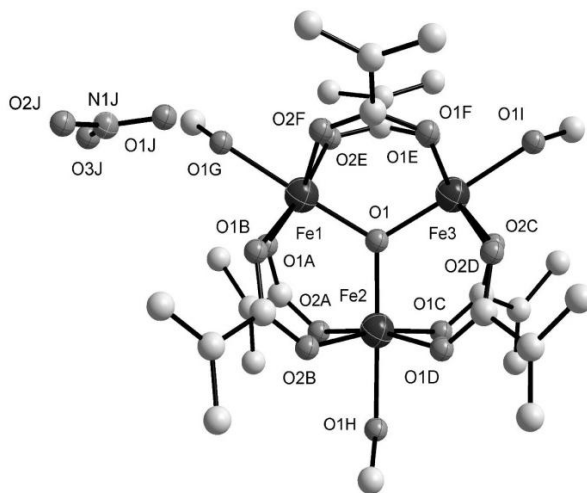


Figure 2.14: Molecular structure of $[\text{Fe}_3\text{O}(\text{MA})_6(\text{HOCH}_3)_3]\text{NO}_3$ **7**.

The most important distances and angles are listed in Table 2.9. Compared to the water-substituted compound **1**, the cluster is very symmetric. Only little differences in the $\text{Fe}-\mu_3\text{O}$ distances between 189.4(5) pm and 191.0(5) pm were detected. The distances between the iron(III) ions and the coordinated methanol, with magnitudes of 210.1(6) pm to 206.4(6) pm,

were in the range of that found for the distances between the iron(III) ions and coordinated water molecules for water-substituted clusters **1–6**.

Table 2.9: Selected bond distances [pm] and angles [°] in **7**.

Fe1–O1	189.9(5)	Fe3–O2C	200.1(6)
Fe1–O2E	200.1(6)	Fe3–O1F	200.1(6)
Fe1–O1B	200.6(6)	Fe3–O2D	201.2(6)
Fe1–O2F	201.2(6)	Fe3–O1E	201.9(6)
Fe1–O1A	203.1(6)	Fe3–O1I	206.4(6)
Fe1–O1G	207.3(6)	O1–Fe1–O1A	95.4(2)
Fe2–O1	189.4(5)	O1–Fe1–O1B	95.6(2)
Fe2–O1D	200.5(6)	O1–Fe1–O2E	93.9(2)
Fe2–O2B	201.4(6)	O1–Fe1–O2F	97.1(2)
Fe2–O2A	202.0(6)	Fe2–O1–Fe1	120.5(3)
Fe2–O1C	202.6(6)	Fe2–O1–Fe3	120.3(3)
Fe2–O1H	210.1(6)	Fe1–O1–Fe3	119.2(3)
Fe3–O1	191.0(5)		

2.1.4.2 Methanol-Chloride

Although starting from iron(III) chloride, and using the same synthetic methods as in the case of nitrate, two different clusters $[\text{Fe}_3\text{O}(\text{MA})_6(\text{HOCH}_3)_3]\text{Cl}$ **8** and $[\text{Fe}_3\text{O}(\text{MA})_6(\text{HOCH}_3)_2(\text{H}_2\text{O})]\text{FeCl}_4$ **9** were obtained. By addition of methanol to a chloroform solution of dry $[\text{Fe}_3\text{O}(\text{MA})_6(\text{H}_2\text{O})_{2.5}(\text{MAH})_{0.5}]\text{Cl}$ **3**, followed by the diffusion of n-pentane, crystals of $[\text{Fe}_3\text{O}(\text{MA})_6(\text{HOCH}_3)_3]\text{Cl}$ **8** were obtained. The structure is drawn in Figure 2.15.

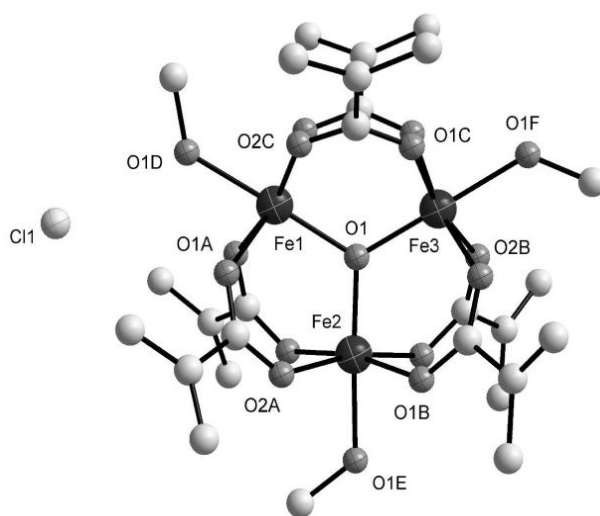


Figure 2.15: Molecular structure of $[\text{Fe}_3\text{O}(\text{MA})_6(\text{HOCH}_3)_3]\text{Cl}$ **8**.

As in the case of the nitrate compound **7**, one methanol was coordinated to each iron(III) ion. The most important angles and distances are reported in Table 2.10. For compound **8**, a mirror plane through the iron(III) ions and the central oxygen of the core was found. The methanol ligands were located within the core plane. Although the iron(III) ions were homogeneously-substituted, the distances within the core differ over a wide range. The Fe1–O1 distance was found to be 193.2(14) pm, while the other two have similar values with 188.7(13) pm and 188.8(14) pm. This distortion of the cluster core is bigger than the one caused by the coordination of the methacrylate anion in the case of compound **6**. In this case, neither the coordination of an anion, nor the hydrogen bonds could be a reasonable explanation for this effect, because in contrast to the water-substituted clusters discussed above, the chloride anion is centered in a cage of OH from all three ethanol ligands and should therefore have the same influence on every Fe–O bond.

Table 2.10: Selected bond distances [pm] and angles [°] in **8**.

Fe1–O1	193.2(14)	Fe3–O1C	200.3(11)
Fe1–O2C	200.3(12)	Fe3–O2B	200.9(11)
Fe1–O1A	202.9(12)	Fe3–O1F	208.1(15)
Fe1–O1D	204.0(15)	O1–Fe1–O1A	95.0(4)
Fe2–O1	188.7(13)	O1–Fe1–O2C	95.5(4)
Fe2–O1B	198.8(12)	Fe2–O1–Fe3	121.3(7)
Fe2–O2A	199.2(12)	Fe2–O1–Fe1	119.3(7)
Fe2–O1E	206.6(15)	Fe3–O1–Fe1	119.4(7)
Fe3–O1	188.8(14)		

2.1.4.3 Methanol-Tetrachloroferrate

Direct reaction of iron(III)chloride hexahydrate with sodium methacrylate in methanol led to the formation of $[\text{Fe}_3\text{O}(\text{MA})_6(\text{HOCH}_3)_2(\text{H}_2\text{O})]\text{FeCl}_4$ **9**. The molecular structure is drawn in Figure 2.16. Compared to the chloride compound **8**, only two coordination sites were coordinated by methanol molecules, while water was coordinated to the third.

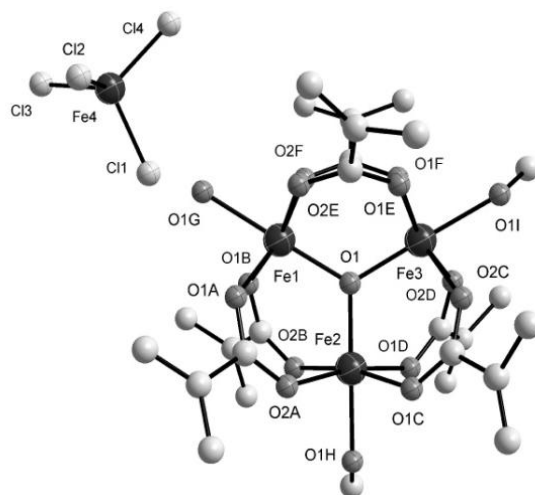


Figure 2.16: Molecular structure of $[\text{Fe}_3\text{O}(\text{MA})_6(\text{HOCH}_3)_2(\text{H}_2\text{O})]\text{FeCl}_4$ **9**.

The core was slightly distorted due to the different coordinated sites. The most important distances and angles are listed in Table 2.11. The water-substituted iron(III) ion includes a Fe1–O1 distance of 189.0(3) pm and is therefore somewhat shorter compared with the methanol-substituted ones with 190.3(3) pm and 190.4(3) pm. No characteristic differences were found for the iron-ligand distance with values of 208.6(3) pm for the Fe1–O1G distance as well as 208.9(3) pm and 208.2(3) pm for the Fe2–O1H and Fe3–O1I, respectively.

Table 2.11: Selected bond distances [pm] and angles [°] in **9**.

Fe1–O1	189.0(3)	Fe3–O1C	201.4(3)
Fe1–O2B	199.6(3)	Fe3–O2F	205.9(3)
Fe1–O1F	199.7(3)	Fe3–O1I	208.2(3)
Fe1–O2A	200.3(3)	Fe1J–Cl4J	217.2(15)
Fe1–O1E	201.4(3)	Fe1J–Cl2J	218.8(14)
Fe1–O1G	208.6(3)	Fe1J–Cl3J	220.7(14)
Fe2–O1	190.3(3)	Fe1J–Cl1J	221.3(18)
Fe2–O2C	199.3(3)	O1–Fe1–O2A	96.29(13)
Fe2–O1A	200.4(3)	O1–Fe1–O2B	94.60(13)
Fe2–O2D	201.6(3)	O1–Fe1–O1E	97.60(13)
Fe2–O1B	205.0(3)	O1–Fe1–O1F	94.44(13)
Fe2–O1H	208.9(4)	Fe1–O1–Fe2	119.45(15)
Fe3–O1	190.4(3)	Fe1–O1–Fe3	119.86(16)
Fe3–O2E	199.1(3)	Fe2–O1–Fe3	120.69(15)
Fe3–O1D	200.7(3)		

2.1.4.4 Ethanol-Nitrate

Analogous to methanol, the use of ethanol leads in both synthetic approaches to the formation of $[\text{Fe}_3\text{O}(\text{MA})_6(\text{HOEt})_3]\text{NO}_3$ **10**, by starting from iron (III) nitrate. The structure determined by single crystal X-ray diffraction is drawn in Figure 2.17.

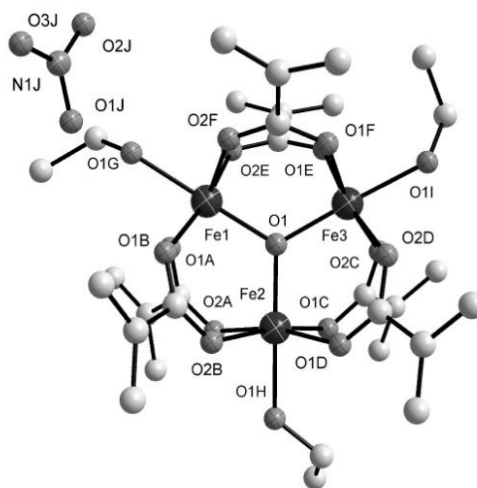


Figure 2.17: Molecular structure of $[\text{Fe}_3\text{O}(\text{MA})_6(\text{HOEt})_3]\text{NO}_3$ **10**.

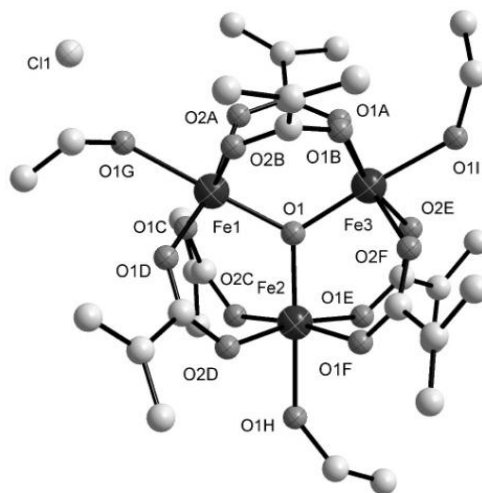
The structure consisted of an iron(III) triangle with a central μ_3 -oxygen complemented with six bridging methacrylate ligands and three coordinated ethanol molecules. The most important distances and angles are listed in Table 2.12. As in the case of the methanol-coordinated clusters, the core as well as the ligands were arranged very symmetrically around the Fe_3O core. The distances between the iron(III) ions and the μ_3 -oxygen ranged from 190.4(3) pm to 192.1(3) pm, somewhat elongated compared to the methanol- and the water-substituted clusters. The distances between the ethanol ligands and the iron(III) ions were with 206.9(4) pm to 209.2(3) pm in the range of the methanol ligands and therefore a little bit shorter than that of the water ligands.

Table 2.12: Selected bond distances [pm] and angles [°] in **10**.

Fe1–O1	190.9(3)	Fe3–O1F	200.0(4)
Fe1–O2F	200.4(3)	Fe3–O2C	200.2(4)
Fe1–O1B	200.7(8)	Fe3–O2D	200.3(4)
Fe1–O2E	202.5(3)	Fe3–O1E	201.4(4)
Fe1–O1A	203.0(3)	Fe3–O1I	209.2(3)
Fe1–O1G	208.3(4)	O1–Fe1–O1A	97.23(14)
Fe2–O1	190.4(3)	O1–Fe1–O1B	95.3(5)
Fe2–O1D	199.9(4)	O1–Fe1–O2E	93.94(14)
Fe2–O2A	201.4(4)	O1–Fe1–O2F	96.25(14)
Fe2–O1C	202.8(4)	Fe2–O1–Fe1	120.12(16)
Fe2–O2B	203.1(8)	Fe2–O1–Fe3	119.63(17)
Fe2–O1H	206.9(4)	Fe1–O1–Fe3	120.24(17)
Fe3–O1	192.1(3)		

2.1.4.5 Ethanol-Chloride

The addition of ethanol to a chloroform solution of $[\text{Fe}_3\text{O}(\text{MA})_6(\text{H}_2\text{O})_{2.5}(\text{MAH})_{0.5}]\text{Cl}$ **3** resulted, after the diffusion of n-pentane, in crystals of $[\text{Fe}_3\text{O}(\text{MA})_6(\text{HOEt})_3]\text{Cl}$ **11**. The structure determined by single crystal X-ray diffraction is shown in Figure 2.18.

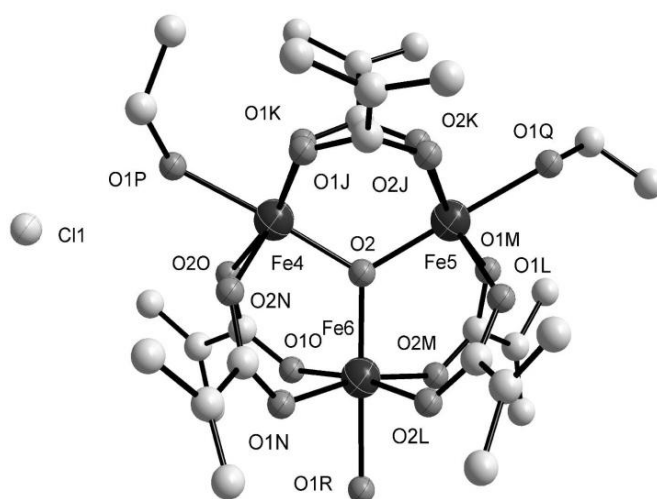
**Figure 2.18** Molecular structure of $[\text{Fe}_3\text{O}(\text{MA})_6(\text{HOEt})_3]\text{Cl}$ **11**.

The most important distances and angles are listed in Table 2.13. The cluster showed, compared to the water-substituted cluster **3**, an elongated distance between the iron(III) ions and the μ_3 -oxygen, with distances between 190.1(6) pm and 191.8(6) pm and a shorter iron(III) to ethanol ligand distance of 207.3(7) pm to 209.6(7) pm.

Table 2.13: Selected bond distances [pm] and angles [°] in **11**.

Fe1–O1	190.5(6)	Fe3–O1E	200.0(9)
Fe1–O2E	199.0(7)	Fe3–O2C	200.1(8)
Fe1–O1A	199.5(8)	Fe3–O1F	201.0(8)
Fe1–O1B	200.4(7)	Fe3–O2D	201.6(10)
Fe1–O2F	201.7(8)	Fe3–O1I	208.9(7)
Fe1–O1G	209.6(7)	O1–Fe1–O1A	91.5(3)
Fe2–O1	190.1(6)	O1–Fe1–O1B	96.3(3)
Fe2–O2A	197.6(8)	O1–Fe1–O2E	96.3(3)
Fe2–O1C	200.5(7)	O1–Fe1–O2F	93.2(3)
Fe2–O2B	200.8(8)	Fe2–O1–Fe1	120.8(3)
Fe2–O1D	201.1(8)	Fe2–O1–Fe3	120.0(3)
Fe2–O1H	207.3(7)	Fe1–O1–Fe3	119.2(3)
Fe3–O1	191.8(6)		

Another cluster with chloride as counter-ion was obtained by reacting iron(III) chloride hexahydrate with sodium methacrylate in ethanol solution. Crystals grew from a chloroform solution, resulting in $[\text{Fe}_3\text{O}(\text{MA})_6(\text{HOEt})_{2.5}(\text{H}_2\text{O})_{0.5}]\text{Cl}$ **12**. The structure consists of two different clusters, one $[\text{Fe}_3\text{O}(\text{MA})_6(\text{HOEt})_3]\text{Cl}$ **12a** isostructural to **11** with three coordinated ethanol molecules and another, $[\text{Fe}_3\text{O}(\text{MA})_6(\text{HOEt})_2(\text{H}_2\text{O})]\text{Cl}$ **12b**, where one of the three ethanol molecules was substituted by water. The structure of the mixed-ligand cluster $[\text{Fe}_3\text{O}(\text{MA})_6(\text{HOEt})_2(\text{H}_2\text{O})]\text{Cl}$ is shown in Figure 2.19.

**Figure 2.19:** Molecular structure of the subunit $[\text{Fe}_3\text{O}(\text{MA})_6(\text{HOEt})_2(\text{H}_2\text{O})]\text{Cl}$ **12b** in compound **12**.

The different coordination had no influence on the distances within the cluster core. The most important angles and distances are listed in Table 2.14. For the iron(III) ion with the water ligand, the distance of Fe6–O2 was found to be 191.2(2) pm. The other Fe–O1

distances were with 189.5(2) pm to 191.3(2) pm in the range of the exclusively ethanol coordinated clusters **10** and **11**.

Table 2.14: Selected bond distances [pm] and angles [°] in **12**.

Fe1–O1	189.5(2)	Fe5–O2J	199.3(3)
Fe1–O1B	199.3(3)	Fe5–O1M	200.6(3)
Fe1–O2F	199.9(3)	Fe5–O1L	200.8(7)
Fe1–O1A	200.8(10)	Fe5–O2K	202.0(3)
Fe1–O2E	201.3(3)	Fe5–O1Q	208.6(3)
Fe1–O1G	209.2(3)	Fe6–O2	191.2(2)
Fe2–O1	190.6(2)	Fe6–O1N	199.5(3)
Fe2–O1C	199.5(3)	Fe6–O1O	199.6(3)
Fe2–O2A	200.2(10)	Fe6–O2M	201.1(3)
Fe2–O2B	201.0(3)	Fe6–O2L	203.1(6)
Fe2–O1D	201.4(3)	Fe6–O1R	206.8(3)
Fe2–O1H	207.6(3)	O1–Fe1–O1A	95.9(8)
Fe3–O1	191.3(2)	O1–Fe1–O1B	95.01(12)
Fe3–O2C	198.0(3)	O1–Fe1–O2E	95.85(12)
Fe3–O1F	199.9(3)	O1–Fe1–O2F	95.59(11)
Fe3–O1E	200.3(4)	Fe1–O1–Fe2	120.53(12)
Fe3–O2D	201.2(4)	Fe1–O1–Fe3	119.54(12)
Fe3–O1I	207.9(3)	Fe2–O1–Fe3	119.92(12)
Fe4–O2	190.0(2)	O2–Fe4–O1J	96.31(11)
Fe4–O2O	200.1(3)	O2–Fe4–O1K	94.78(12)
Fe4–O1K	201.1(3)	O2–Fe4–O2N	93.92(13)
Fe4–O1J	201.2(3)	O2–Fe4–O2O	95.09(10)
Fe4–O2N	201.7(4)	Fe4–O2–Fe5	119.91(13)
Fe4–O1P	209.8(3)	Fe4–O2–Fe6	119.95(12)
Fe5–O2	190.4(2)	Fe5–O2–Fe6	120.13(12)

The elemental analysis of this compound showed extremely high content of chlorine in the product. This leads to the conclusion that the product consists mainly of $[\text{Fe}_3\text{O}(\text{MA})_6(\text{HOEt})_2(\text{H}_2\text{O})]\text{FeCl}_4$ **13** (see 2.1.4.6) with only small amounts of **12**.

2.1.4.6 Ethanol-Tetrachloroferrate

The cluster was synthesized similar to compound **12**, but crystallized by a different method. Iron(III) chloride hexahydrate was reacted with sodium methacrylate in ethanol solution. Afterwards, the solvent was removed and the residue was dissolved in chloroform, followed by the addition of n-hexane. Crystals of $[\text{Fe}_3\text{O}(\text{MA})_6(\text{HOEt})_2(\text{H}_2\text{O})]\text{FeCl}_4$ **13** were obtained by slow evaporation of the chloroform from the solvent mixture. The structure determined by single crystal X-ray diffraction is drawn in Figure 2.20.

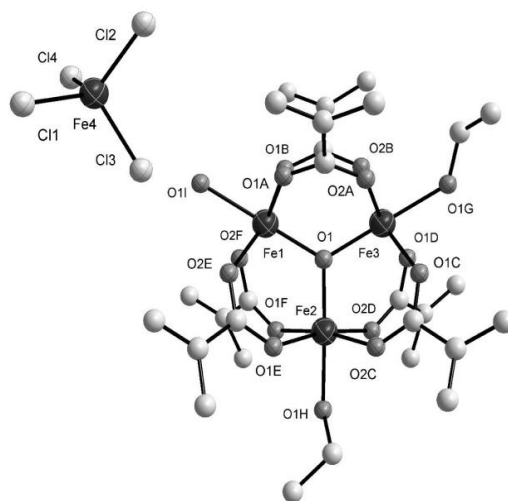


Figure 2.20: Molecular structure of $[\text{Fe}_3\text{O}(\text{MA})_6(\text{HOEt})_2(\text{H}_2\text{O})]\text{FeCl}_4$ **13**.

This cluster showed the same structural features caused by the substitution of water ligands with ethanol as the mixed ligand cluster in **12**. The most important angles and distances are listed in Table 2.15. The distance between the μ_3 -oxygen and the iron(III) ion with the coordinated water Fe3–O1 is the shortest with 188.4(2) pm. The ethanol-coordinated iron(III) ions included a Fe–O distance of 190.0(2)pm and 189.7(2) pm respectively, with the typical elongation of the bond distance. The coordinated water showed the largest Fe–O distance.

Table 2.15: Selected bond distances [pm] and angles [$^\circ$] in **13**.

Fe1–O1	190.0(2)	Fe3–O1C	203.0(3)
Fe1–O2A	199.6(3)	Fe3–O2E	203.9(3)
Fe1–O1F	199.8(3)	Fe3–O1I	209.9(3)
Fe1–O2B	200.1(3)	Fe1J–Cl1J	219.3(4)
Fe1–O1E	200.1(3)	Fe1J–Cl2J	219.9(4)
Fe1–O1G	209.6(3)	Fe1J–Cl3J	218.8(2)
Fe2–O1	189.7(2)	Fe1J–Cl4J	217.8(3)
Fe2–O1A	199.1(3)	O1–Fe1–O2A	94.33(12)
Fe2–O2C	199.9(3)	O1–Fe1–O2B	96.98(12)
Fe2–O1B	200.5(3)	O1–Fe1–O1E	93.50(11)
Fe2–O2D	200.7(3)	O1–Fe1–O1F	96.10(11)
Fe2–O1H	209.9(3)	Fe3–O1–Fe2	120.73(13)
Fe3–O1	188.4(2)	Fe3–O1–Fe1	120.20(13)
Fe3–O2F	200.3(3)	Fe2–O1–Fe1	119.07(13)
Fe3–O1D	200.9(3)		

2.1.5 IR Investigations

The IR spectra of the compounds **8–14** showed great similarities to the water-substituted clusters discussed in chapter 2.1.2. The most important bands are listed in Table 2.16. The spectrum of $[\text{Fe}_3\text{O}(\text{MA})_6(\text{EtOH})_3]\text{NO}_3$ **11** is presented in Figure 2.21 to illustrate the bands of a typical ethanol-modified cluster. The spectra were, like in the case of the water-substituted compounds, dominated by the asymmetric and symmetric CO_2 vibration.

Table 2.16: Comparison of the most important bands of crystalline compounds **7–13** [cm^{-1}].

Compound	$\nu(\text{C}=\text{C})$	$\nu_{\text{asym}}(\text{CO}_2)$	$\nu_{\text{sym}}(\text{CO}_2)$	$\nu_{\text{sym}}(\text{Fe}_3\text{O})$
7	1643	1575	1415	614
8	1644	1580	1413	610
9	1641	1561	1415	616
10	1644	1577	1415	614
11	1642	1570	1415	612
12	1642	1566	1412	613
13	1641	1564	1415	615

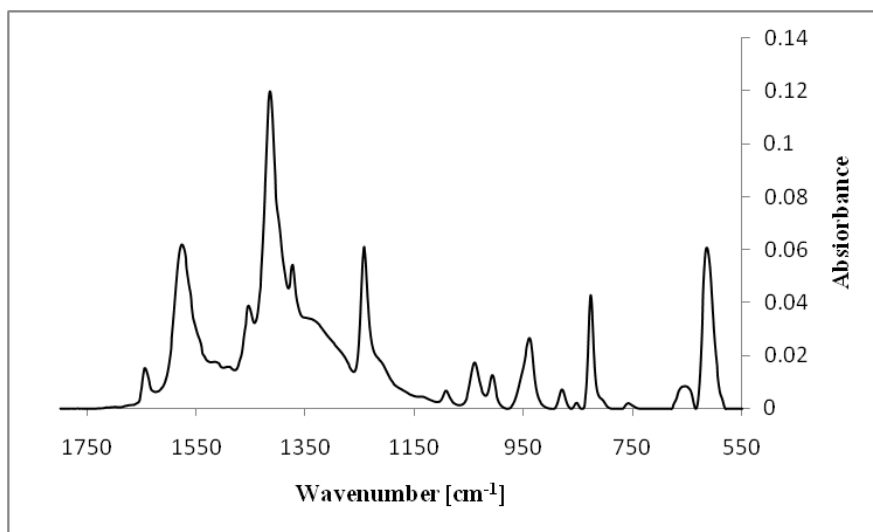


Figure 2.21: ATR-IR spectrum of crystalline $[\text{Fe}_3\text{O}(\text{MA})_6(\text{EtOH})_3]\text{NO}_3$ **11** in the region between 1800 cm^{-1} and 550 cm^{-1} .

For the tris-(m)ethanol coordinated compounds **7**, **8** and **10** the asymmetric CO_2 vibration was shifted from 1573 cm^{-1} for **1** and 1569 cm^{-1} for **3** to higher wavenumbers. The only exception was compound **11**, which is discussed separately below. The bands for the vibration of the central μ_3 -oxygen within the iron triangle ($\nu_{\text{sym}}\text{Fe}_3\text{O}$) were found for (m)ethanol-substituted clusters at higher wavenumbers compared with the water-substituted clusters **1–6**. The exception was compound **9** that showed a decrease of this band position, due to the remarkable shorter Fe–O distances in the core.

For the mixed-ligand compounds **9**, **12** and **13**, the $\nu_{\text{asym}}(\text{CO}_2)$ vibration was found at lower wavenumbers compared to the water-substituted clusters. The coordination of methanol was indicated by two bands at 1017 cm^{-1} and 962 cm^{-1} . The methanol-modified nitrate and chloride compounds **7** and **8** showed additional bands for differently coordinated methacrylate ligands and many bands in the region of the coordinated methanol, which indicated the co-crystallization of other species that could not be assigned to any of the known structure.

The bands for the coordinated ethanol were found at varying positions for the different compounds. A comparison of the band positions is given in

Table 2.17. The bands for the first CO vibration shifted from 1089 cm^{-1} to higher wavenumbers, while that of the other two bands decreased from 1048 cm^{-1} and 880 cm^{-1} .⁸⁶

Table 2.17: Comparison of the bands for the coordinated ethanol [cm^{-1}].

Compound	$\nu(\text{CO})$	$\nu(\text{CC}+\text{CO})$	$\nu(\text{CC}+\text{CO})$
10	1092	1040	879
12	1081	1029	876
13	1081	1030	877

No additional bands for coordinated ethanol were detected for compound **11**. This led to the conclusion that compound **11** was a minority compound in a batch of $[\text{Fe}_3\text{O}(\text{MA})_6(\text{H}_2\text{O})_3]\text{Cl}$ **4**, which was synthesized by a similar reaction. This is supported by the bands at 1570 cm^{-1} and 612 cm^{-1} , which showed great similarities to that of **4**.

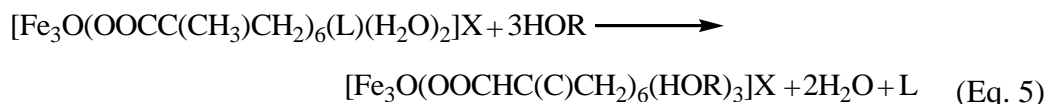
Liquid FT-IR investigations in chloroform were performed on all compounds to investigate the solution stability of the alcohol-substituted clusters **7–13**. As in the case of the water-substituted clusters broad signals in the region between 1650 cm^{-1} and 1750 cm^{-1} were obtained, which indicated the decomposition of the clusters in solution.

2.1.6 Discussion and Conclusion

Even though one of the first published structures of triiron oxo clusters was substituted by methanol, alcohol-coordinated triiron compounds were rarely described in the literature.⁸⁷ Some authors even claimed that it is impossible to synthesize alcohol derivatives of their compounds, so it was evident to closer investigate this reaction.

As elucidated before, three different synthesis strategies were followed to obtain alcohol-substituted clusters with the general formula $[\text{Fe}_3\text{O}(\text{MA})_6(\text{HOR})_3]\text{X}$. The reactions were exclusively performed with chloride and nitrate as anions.

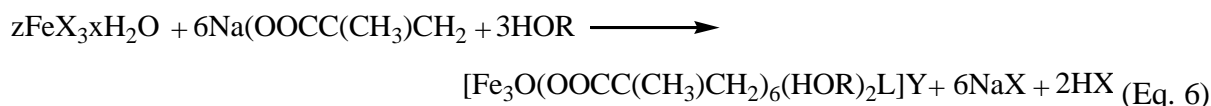
The first method was the substitution of the coordinated water molecules from the crystalline compounds **1** (NO_3^-) or **3** (Cl^-) against (m)ethanol by suspending the compound in non-coordinating chloroform, followed by the addition of 3 equivalents of alcohol. The reaction is presented in equation 5.



	X	R	L
7	NO ₃	CH ₃	H ₂ O
10	NO ₃	CH ₂ CH ₃	H ₂ O
8	Cl	CH ₃	0.5 HMA / 0.5 H ₂ O
11	Cl	CH ₂ CH ₃	0.5 HMA / 0.5 H ₂ O

As expected, the solids could now be dissolved in various organic solvents due to the exchange of the water molecules for the more hydrophobic alcohol ligands accompanied by the disappearance of the hydrogen bonds. Crystals could easily be obtained by diffusion of n-pentane. The structures were found to be exclusively trialcohol-substituted clusters with the general formula $[\text{Fe}_3\text{O}(\text{MA})_6(\text{HOR})_3]\text{X}$. No coordinated anion or methacrylic acid was found in the structures.

This first method includes a three step synthesis and is very time consuming. Therefore, the direct syntheses of (m)ethanol-modified clusters were researched. The corresponding iron(III) salt was dissolved in the corresponding alcohol and sodium methacrylate was added. The reaction is presented in equation 6. The conversion was indicated by the dissolution of the sodium methacrylate, a color change to dark red and the precipitation of sodium chloride.



	z	X	R	Y	L
7	3	NO ₃	CH ₃	NO ₃	HOCH ₃
10	3	NO ₃	CH ₂ CH ₃	NO ₃	HOCH ₂ CH ₃
9	4	Cl	CH ₃	FeCl ₄	H ₂ O
12	3	Cl	CH ₂ CH ₃	Cl	0.5 HOCH ₂ CH ₃ / 0.5 H ₂ O
13	4	Cl	CH ₂ CH ₃	FeCl ₄	H ₂ O

After the alcohol was removed, a red oil was obtained in all cases. Even small traces of alcohol inhibited the solidification and crystallization of the compounds. Therefore, it had to be removed by repeated dissolution of the product in dichloromethane, which was afterwards removed under reduced pressure. Crystals were obtained by different crystallization methods mentioned in the experimental section.

The nitrate compounds **9** and **10** were trialcohol-substituted triiron clusters and had the same crystal structure as found for the first synthetic method. For nitrate, it was unimportant, which synthetic route was taken. In contrast, for chloride compounds **9** and **13**, the high hydrochloric acid concentration, combined with the more hydrophobic media, led to the

formation of the tetrachloroferrate anion. The clusters showed two attached alcohol ligands and one attached water molecule. A mixture of homo-substituted and hetero-substituted clusters (see **8** and **11** and accordingly **9** and **13**) were both found in compound **12**. Although **12** was directly prepared in ethanol, the anion appeared to be chloride. Elemental analysis showed extremely high chlorine content, which led to the conclusion that this cluster was co-crystallized with compound **13**.

The third synthesis method was performed by dissolving the prepared clusters **1** or **3** in the corresponding alcohol. The original idea was to crystallize them directly from this solution to obtain $[\text{Fe}_3\text{O}(\text{MA})_6(\text{HOR})_3]\text{X}$, but instead an alcoholysis reaction took place and a yellow precipitate was formed, which turned red after drying. Further investigations evidenced that by addition of alcohol to the cluster the methacrylate ligands were cleaved and protonated, while the alcoholate is attached to the iron(III) ions. Although never described in the literature, this alcoholysis of the cluster did not only take place with methanol, but also with ethanol and isopropanol. The IR spectrum of the product obtained from methanolysis of **3** is presented in Figure 2.22.

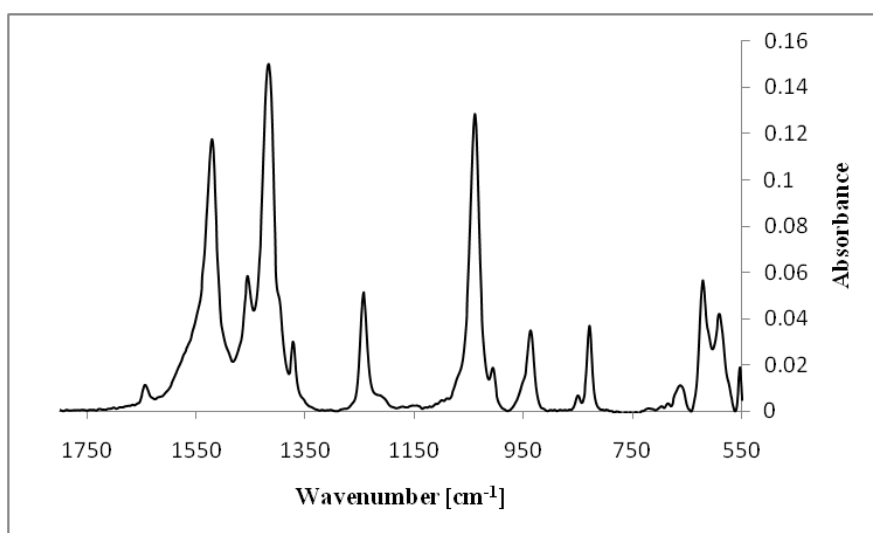


Figure 2.22: IR spectrum of the precipitated solid obtained by the methanolysis of **1** in the region between 1800 cm^{-1} and 550 cm^{-1} .

The bands showed great similarities to ferric wheel compounds, which were prepared by a comparable synthesis strategy.⁶⁵ As for the IR spectra discussed above, the spectrum was dominated by two bands at 1522 cm^{-1} and 1418 cm^{-1} , indicating the asymmetric and symmetric stretching vibration of the coordinated carboxylate. Compared to the oxygen-centered triiron clusters **7–13**, discussed above, the asymmetric vibration was significantly shifted by about 50 cm^{-1} to lower wavenumbers. The intense band of the μ_3 -oxygen at about 610 cm^{-1} disappeared and two bands at 622 cm^{-1} and 591 cm^{-1} were visible. The double bond at 1544 cm^{-1} was still visible and therefore not influenced by the reaction of the cluster.

Additional to the two carboxylate bands, a third intense band at 1040 cm^{-1} was visible that could be assigned to the bridging methoxy groups in ferric wheel compounds.

TGA investigations after solvent removal showed an increased iron content in the precipitated powder compared to the clusters. This fits quite well to the expected values of the hydrolyzed compound $[\text{Fe}(\text{OH})_2(\text{MA})]_x$. Further investigations were performed on the primary reaction mixture. After separation of the precipitate, the liquid was stored at -20°C . Instead of the desired product, white crystals were formed, which could be determined as methacrylic acid.

It is worth to note that this reaction is very general. It was as well tried for the solution-stable pyridine-substituted compound **14**, discussed in the next chapter. The experiments resulted in the same powder starting from the water-substituted compounds.

For all three synthetic methods yields were generally low. This was caused by the competition of the exchange reactions and the omnipresent alcoholysis reaction, which leads to the formation of larger undefined assemblies.

A comparison of the $\text{Fe}-\mu_3\text{O}$ and $\text{Fe}-\text{O}_{\text{ligand}}$ distances in the compounds **7–13** is presented in Table 2.18. For the methanol-substituted compounds **7–9**, $\text{Fe}-\text{O}_{\text{ligand}}$ distances between $204.0(15)\text{ pm}$ and $210.1(6)\text{ pm}$ were obtained. These values are shorter compared to that of the coordinated water ligands, but show similar distribution (6.1 pm). The distances within the core were found between $188.7(13)\text{ pm}$ and $193.2(14)\text{ pm}$. For the tris-methanol coordinated clusters **7** and **8**, one long $\text{Fe}-\mu_3\text{O}$ distance accompanied by two short distances were found. In contrast, the mixed ligand compound **9** showed one short $\text{Fe}-\mu_3\text{O}$ distance with $189.0(3)\text{ pm}$ for the water-substituted iron(III) ion, while the two methanol coordinated sites show similar $\text{Fe}-\mu_3\text{O}$ distances of $190.3(3)\text{ pm}$ and $190.4(3)\text{ pm}$. These data fit in quite well with the reported compound $[\text{Fe}_3\text{O}(\text{Ac})_6(\text{MeOH})_3]\text{Cl}$, which showed a $\text{Fe}-\mu_3\text{O}$ distance of $190.5(5)\text{ pm}$ and $\text{Fe}-\text{O}_{\text{ligand}}$ distance of $198(2)\text{ pm}$.⁸⁷ Although, as in the case of the water-substituted clusters **1–6**, the $\text{Fe}-\mu_3\text{O}$ and $\text{Fe}-\text{O}_{\text{ligand}}$ distances show a tendency to compensate the elongation/shortening of the one another, the distribution of the sum of the $\text{Fe}-\mu_3\text{O}$ and $\text{Fe}-\text{O}_{\text{ligand}}$ distances was higher than for the water-substituted clusters. This originated in the large distortion of the cluster cores. The sum of the $\text{Fe}-\mu_3\text{O}$ and $\text{Fe}-\text{O}_{\text{ligand}}$ distances were generally lower than for water-substituted compounds.

Table 2.18: Comparison of the distances [pm] between the iron(III) ions and the μ_3 -oxygen and the iron(III) ion and the coordinated ligand in the compounds **7–13** determined by single crystal XRD.

	7 (at 100 K)	Fe-μ_3O + Fe-O_{ligand}	8 (at 100 K)	Fe-μ_3O + Fe-O_{ligand}	9 (at 100 K)	Fe-μ_3O + Fe-O_{ligand}
Fe1–O1 (Fe4–O2)	189.9(5)	397.2	193.2(14)	397.2	189.0(3)	397.6
Fe1–O1G (Fe4–O1P)	207.3(6)		204.0(15)		208.6(3)	
Fe2–O1 (Fe5–O2)	189.4(5)	399.5	188.7(13)	395.3	190.3(3)	399.2
Fe2–O1H (Fe5–O1Q)	210.1(6)		206.6(15)		208.9(4)	
Fe3–O1 (Fe6–O2)	191.0(5)	397.4	188.8(14)	396.9	190.4(3)	398.6
Fe3–O1I (Fe6–O1R)	206.4(6)		208.1(15)		208.2(3)	
	10 (at 100 K)	Fe-μ_3O + Fe-O_{ligand}	11 (at 296 K)	Fe-μ_3O + Fe-O_{ligand}	12a (at 296 K)	Fe-μ_3O + Fe-O_{ligand}
Fe1–O1 (Fe4–O2)	190.9(3)	399.2	190.5(6)	400.1	189.5(2)	398.7
Fe1–O1G (Fe4–O1P)	208.3(4)		209.6(7)		209.2(3)	
Fe2–O1 (Fe5–O2)	190.4(3)	397.3	190.1(6)	397.4	190.6(2)	398.2
Fe2–O1H (Fe5–O1Q)	206.9(4)		207.3(7)		207.6(3)	
Fe3–O1 (Fe6–O2)	192.1(3)	401.3	191.8(6)	400.7	191.3(2)	399.2
Fe3–O1I (Fe6–O1R)	209.2(3)		208.9(7)		207.9(3)	
	12b (at 296 K)	Fe-μ_3O + Fe-O_{ligand}	13 (at 300 K)	Fe-μ_3O + Fe-O_{ligand}		
Fe1–O1 (Fe4–O2)	190.0(2)	399.8	190.0(2)	399.6		
Fe1–O1G (Fe4–O1P)	209.8(3)		209.6(3)			
Fe2–O1 (Fe5–O2)	190.4(2)	399.0	189.7(2)	399.6		
Fe2–O1H (Fe5–O1Q)	208.6(3)		209.9(3)			
Fe3–O1 (Fe6–O2)	191.2(2)	398.0	188.4(2)	398.3		
Fe3–O1I (Fe6–O1R)	206.8(3)		209.9(3)			

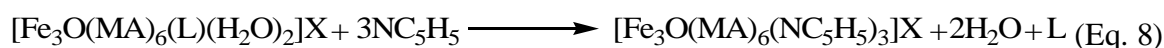
The ethanol-substituted clusters **10–13** did not show the reduced values of the Fe- μ_3 O and Fe-O_{ligand} distance sum. For this reason, methanolysis reactions are more efficient than ethanolysis reactions. The Fe-O_{ligand} distances range from 206.8(3) pm to 209.9(3) pm, while the Fe- μ_3 O distances show values between 188.4(2) pm and 192.1(3) pm. The deviation of the distances is low with 3.1 pm (Fe-O_{ligand}), 3.7 pm (Fe- μ_3 O) and 2.9 pm (sum), compared to the water-substituted compounds. In the mixed-ligand clusters **9**, **12b** and **13**, the coordination of water did not lead to a remarkable change in the Fe-O_{ligand} distance or the distortion of the cluster core.

ATR-IR investigations were performed on the crystalline compounds **7–13**. The methanol compounds **7** and **8** showed many additional bands from co-crystallized by-products, which might originate from methanolysis side reactions during the preparation of the clusters. Such problems were not detected for the ethanol compounds, which showed, with the exception of the chloride compound **13**, the expected bands for the coordinated alcohol.

IR investigations in solution showed the degradation of the clusters in solution, which made alcohol-substituted triiron compounds unsuitable in the nano building block approach and made further efforts to find more stable substituents indispensable.

2.1.7 Clusters of General Formula $[\text{Fe}_3\text{O}(\text{MA})_6(\text{py})_3]\text{X}$

The results of the last chapter suggested that the only possibility to obtain clusters of the general composition $[\text{Fe}_3\text{O}(\text{MA})_6(\text{L})_3]\text{X}$ is a ligand exchange starting from preformed water-substituted cluster. As a matter of fact the control reaction, the reaction of iron(III) chloride with sodium methacrylate in a water/pyridine mixture, yielded undefined precipitates. Therefore, the synthesis of the nitrate **14**, chloride **15** and bromide **16** compounds started from the corresponding water-substituted clusters **1**, **3** and **5** suspended in chloroform, and pyridine was added (equation 8).



	X	L
14	NO ₃	H ₂ O
15	Cl	0.5 HMA / 0.5 H ₂ O
16	Br	0.5 HMA / 0.5 H ₂ O

In all cases, black crystals grew by diffusion of n-pentane into the solutions. It is well known that pyridine-substituted triiron oxo clusters are due to a rearrangement of the pyridine rings at a certain temperature difficult to measure by single crystal XRD. In addition, the obtained crystals contained a lot of solvent molecules in the crystal structure. The amount of solvent was determined gravimetrically for **14**, resulting in about 4 chloroform molecules per cluster. During the measurements the chloroform evaporated and the samples became amorphous. Therefore, although in each case single crystals were obtained and single crystal measurements were performed, no final structure refinement was possible.

The tetrafluoroborate cluster $[\text{Fe}_3\text{O}(\text{MA})_6(\text{py})_3]\text{BF}_4$ **17** was obtained by substitution of the chloride anion in **15** with silver tetrafluoroborate in chloroform. Crystals were again obtained by diffusion of n-pentane, but as in the other cases no structural refinement was accomplished.

The pyridine-substituted clusters will in the following serve as model systems for the synthesis of cluster-reinforced polymers and the interpretation of the physical properties of the final hybrid materials. Therefore, it is necessary to be sure about the constitution of the clusters. As elucidated before, the direct determination of the crystal structure by single crystal X-ray diffraction was not possible, because the crystals decompose during the measurements due to loss of solvent. Therefore, the starting point was the comparison of the IR-data of the different compounds **14–17**. As presented in Figure 2.23, the ATR-IR spectra of the clusters with different anions show exactly the same bands for the coordinated methacrylate ligands with regard to their intensity, position and width. The only difference was found for the nitrate compound **14** that showed, compared to the other compounds **15–17**, two additional bands in the spectrum that originate from the nitrate anion, as discussed in chapter 2.1.2.1.

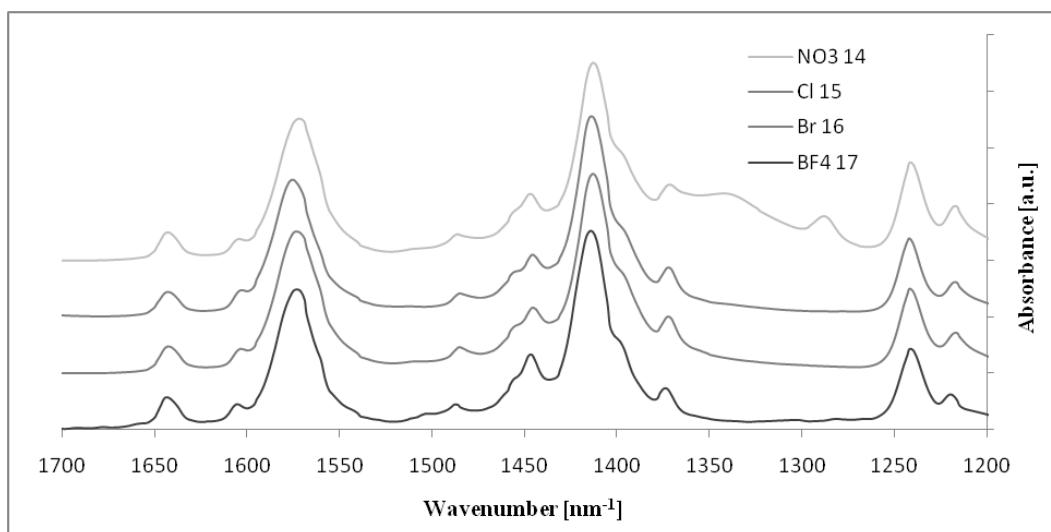


Figure 2.23: Comparison of ATR-IR spectra of compounds **14–17** in the region between 1200 cm^{-1} and 1700 cm^{-1} obtained from crystalline samples.

The coordination of the pyridine was indicated by the band at 1603 cm^{-1} and three bands in the region between 980 cm^{-1} and 1100 cm^{-1} . A comparison of these bands is presented in Figure 2.24. As for the methacrylate bands, the bands for the pyridine are congruent for all compounds **14–17**. The only difference could be obtained for the tetrafluoroborate derivative **17**, because the bands for the B–F stretching vibration are visible in this region.

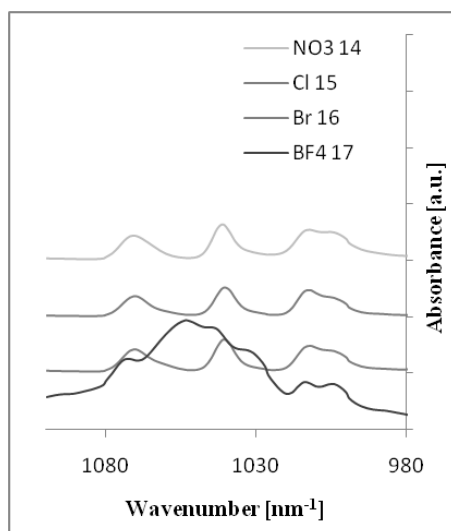


Figure 2.24: Comparison of ATR-IR spectra of compounds **14–17** in the region between 980 cm^{-1} and 1100 cm^{-1} obtained from single crystalline samples.

The last prove of conformity of compounds **14–17** is given by the band for the stretching vibration of the μ_3 -oxygen within the iron(III) ion triangle that was found at 609 cm^{-1} .

It can be concluded that all clusters **14–17** have exactly the same coordination behavior of the methacrylate and pyridine ligands and must therefore have the same symmetry of the cluster core. The only differences are the anions. It will be shown, in chapters 2.1.8 and 2.1.9, that the anions have an effect on the solution stability. The influence of each anion is different in solution. The coordination behavior of the anions affects the cluster and therefore each cluster shows a different behavior in solution. However, this is not the case for the crystalline compounds. Furthermore, it can be concluded that, because all physical properties are determined by the cluster core, every measurement done for one crystalline compound and every result obtained from them can directly be used for all the other clusters.

Two experiments showed the structure of the cluster core. At first, Mössbauer spectra of **15**, discussed in chapter 2.2.1.6, evidenced that only one iron site is present in this compound. Secondly, SQUID measurements, discussed in 2.2.3.7, of **14** showed that the iron(III) ions show spin frustration. This is only possible if the cluster core is highly symmetric. With the information that the cluster bears a Fe_3O unit (see IR) it can be concluded that the iron(III) ions are arranged in an equilateral triangle (this means at least C_3 symmetry) and no further iron(III) ions are present. The structure of the compound is thus $[\text{Fe}_3\text{O}(\text{MA})_6(\text{py})_3]\text{X}$ without coordinated anion.

The methacrylate-substituted cluster $\text{Fe}_3\text{O}(\text{MA})_6(\text{H}_2\text{O})_2(\text{MA})$ **6** behaves differently in a way that the coordinated methacrylato-*O* ligand is stable against substitution with pyridine. The synthesis procedure followed the one mentioned above, including the suspension of $\text{Fe}_3\text{O}(\text{MA})_6(\text{H}_2\text{O})_2(\text{MA})$ **6** in chloroform and the addition of 3 equivalents of pyridine, but in this case $\text{Fe}_3\text{O}(\text{MA})_6(\text{py})_2(\text{MA})$ **18** was obtained. An image of the cluster is presented in Figure 2.25. In contrast to the tris-substituted pyridine clusters it showed a C_{2v} symmetry of the cluster core.

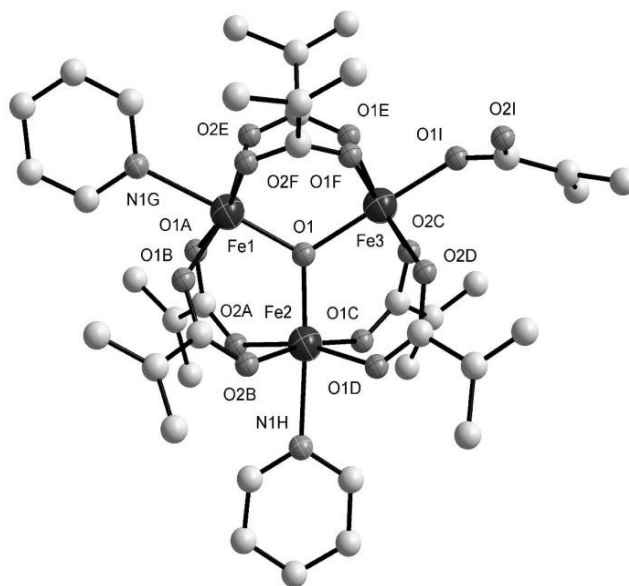


Figure 2.25: Molecular structure of $\text{Fe}_3\text{O}(\text{MA})_6(\text{py})_2(\text{MA})$ **18**.

The most important angles and distances are listed in Table 2.19. The pyridine rings were coplanar the core plane. The iron triangle was distorted showing a $\text{Fe3}-\mu_3\text{O}$ distance of 195.2(5) pm. This value was similar to 194.0(2) pm detected in compound **6**. The other two other iron(III) ions showed distances of 188.0(5) pm and 187.1(5) pm respectively to the central oxygen atom. The $\text{Fe3}-\text{O1I}$ distance was 192.6(7) pm, while the $\text{Fe1}-\text{N1G}$ distance was found to be 218.2(6), and the $\text{Fe2}-\text{N1H}$ 219.6(6) pm.

Table 2.19: Selected bond distances [pm] and angles [$^\circ$] in **18**.

$\text{Fe1}-\text{O1}$	188.0(5)	$\text{Fe3}-\text{O2D}$	199.6(6)
$\text{Fe1}-\text{O2E}$	198.6(6)	$\text{Fe3}-\text{O1E}$	200.4(6)
$\text{Fe1}-\text{O1A}$	100.5(6)	$\text{Fe3}-\text{O1F}$	202.9(6)
$\text{Fe1}-\text{O2F}$	200.7(6)	$\text{Fe3}-\text{O2C}$	205.0(6)
$\text{Fe1}-\text{O1B}$	201.0(6)	$\text{O1I}-\text{C1I}$	1241.(12)
$\text{Fe1}-\text{N1G}$	218.2(6)	$\text{O2I}-\text{C1I}$	130.5(14)
$\text{Fe2}-\text{O1}$	187.1(5)	$\text{O1}-\text{Fe1}-\text{O1A}$	94.4(2)
$\text{Fe2}-\text{O1D}$	198.0(6)	$\text{O1}-\text{Fe1}-\text{O1B}$	96.5(2)
$\text{Fe2}-\text{O1C}$	200.7(7)	$\text{O1}-\text{Fe1}-\text{O2E}$	98.0(3)
$\text{Fe2}-\text{O2A}$	201.6(6)	$\text{O1}-\text{Fe1}-\text{O2F}$	95.5(2)
$\text{Fe2}-\text{O2B}$	202.2(6)	$\text{Fe2}-\text{O1}-\text{Fe1}$	119.3(3)
$\text{Fe2}-\text{N1H}$	219.6(6)	$\text{Fe2}-\text{O1}-\text{Fe3}$	120.2(2)
$\text{Fe3}-\text{O1I}$	192.6(7)	$\text{Fe1}-\text{O1}-\text{Fe3}$	120.4(2)
$\text{Fe3}-\text{O1}$	195.2(5)		

2.1.8 IR Investigations

The substitution of water against pyridine could easily be followed by ATR-IR. The spectrum of $[\text{Fe}_3\text{O}(\text{MA})_6(\text{py})_3]\text{Cl}$ **15** is representatively presented in Figure 2.26. The most important bands are listed in Table 2.20.

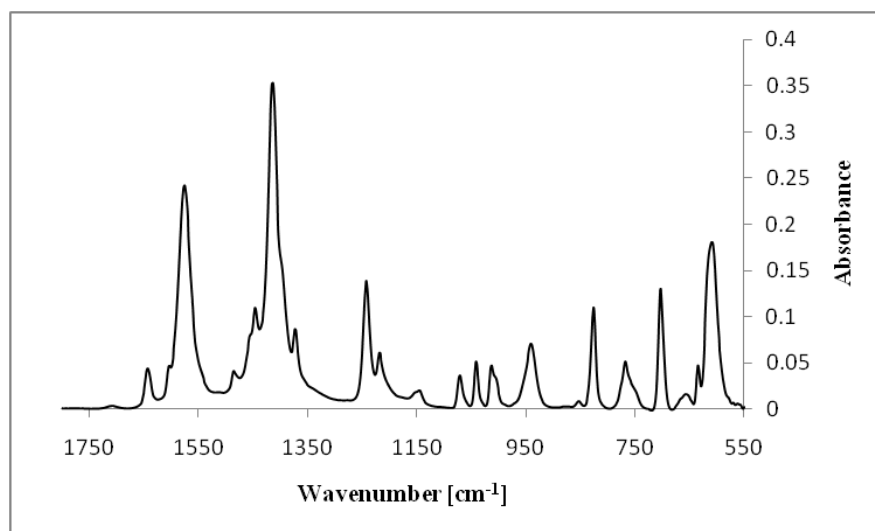


Figure 2.26: ATR-IR spectrum of crystalline $[\text{Fe}_3\text{O}(\text{MA})_6(\text{py})_3]\text{Cl}$ **17** in the region between 1800 cm^{-1} and 550 cm^{-1} .

Table 2.20: Comparison of the most important bands of crystalline compounds **14–18** [cm^{-1}].

Compound	$\nu(\text{C}=\text{C})$	$\nu_{\text{asym}}(\text{CO}_2)$	$\nu_{\text{sym}}(\text{CO}_2)$	$\nu_{\text{sym}}(\text{Fe}_3\text{O})$
14	1643	1572	1413	609
15	1643	1576	1415	609
16	1642	1574	1413	609
17	1644	1574	1415	609
18	1644	1575	1414	609

The spectra were dominated by the asymmetric and symmetric stretching vibration of the coordinated carboxylates at around 1575 cm^{-1} and 1415 cm^{-1} respectively. The double bond of the methacrylate was found at around 1642 cm^{-1} and the stretching vibration of the μ_3 -oxygen was located at around 609 cm^{-1} . The coordination of the pyridine could be followed by several characteristic bands recorded in literature.^{59,80,88,89} The fundamental ring vibration of pyridine shifted after the coordination to higher wavenumbers and was found at 1602 cm^{-1} . Another ring vibration at 1454 cm^{-1} was visible as a shoulder of the larger methacrylate band at 1446 cm^{-1} .⁵⁹ At 1071 cm^{-1} , 1041 cm^{-1} and 1013 cm^{-1} , characteristic bands for the C–H vibrations were observed.

For the nitrate compound **14**, the anion was indicated by a broad band at 1342 cm^{-1} , while the tetrafluoroborate of compound **17** was detectable by a broad band with a maximum at 1052 cm^{-1} .

For the bis-pyridine-substituted compound **18**, a similar spectrum, with regards to the intensities and position of the signals compared to the tris-substituted clusters was detected. The coordinated methacrylate anion was indicated by a small band at 1712 cm^{-1} and a shoulder at 1546 cm^{-1} .

Solution FT-IR measurements were performed in CHCl_3 , to investigate the solution stability of the pyridine-substituted triiron clusters. The results for $[\text{Fe}_3\text{O}(\text{MA})_6(\text{py})_3]\text{BF}_4$ **17** are presented in Figure 2.27. The main bands of the crystalline compound were found as well in the spectra of the chloroform solution. At 1645 cm^{-1} , the band for the C=C double bond was visible. The bands at 1607 cm^{-1} and the shoulder at 1456 cm^{-1} indicated the presence of coordinated pyridine. No evidence for free pyridine was found in the spectrum. In contrast to the water- and alcohol-substituted clusters, the spectrum did not show any bands in the region above 1650 cm^{-1} , which indicate different or non-coordinated methacrylate species or methacrylic acid. Together with the fact that all important bands were retained, it can be concluded that the cluster was stable in solution. The only characteristic difference comparing the spectrum in solution with the crystalline compound was the shift of the two carboxylate bands. The asymmetric signal shifted from 1574 cm^{-1} to 1579 cm^{-1} , while the symmetric was found at 1422 cm^{-1} compared to 1415 cm^{-1} for the crystals. This effect was caused by the higher degree of freedom of the methacrylate groups in solution, due to the lack of packing effects and hydrogen bonds. Ligands could rotate freely, which led to the higher symmetry D_{3h} accompanied by sharper bands compared to the ones of the crystals. The results are verified by the NMR results discussed below.

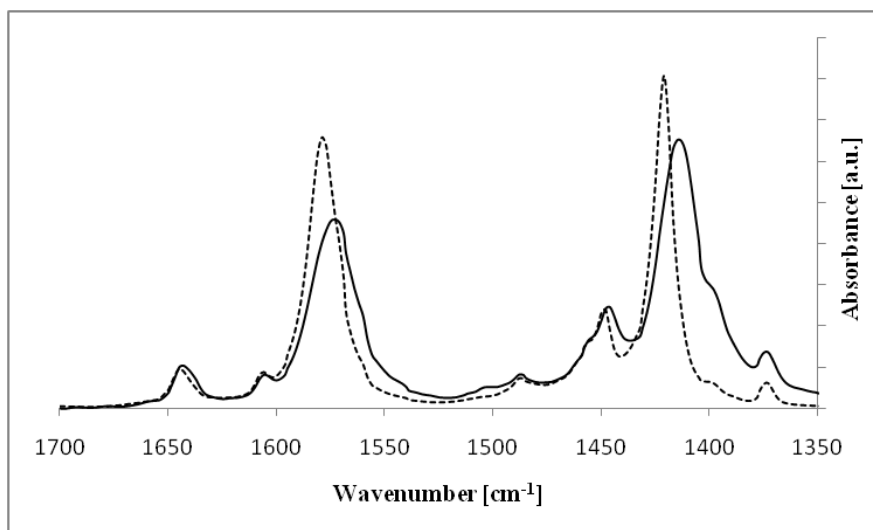


Figure 2.27: Comparison of the IR spectra of $[\text{Fe}_3\text{O}(\text{MA})_6(\text{py})_3]\text{BF}_4$ **17** as crystals (solid line) and in CHCl_3 solution (dashed line).

The chloroform solution spectrum of $[\text{Fe}_3\text{O}(\text{MA})_6(\text{py})_3]\text{BF}_4$ **17** was compared to the solution spectra of the nitrate **14** and chloride **15** compounds. The result for $[\text{Fe}_3\text{O}(\text{MA})_6(\text{py})_3]\text{Cl}$ **15** is exemplarily presented in Figure 2.28. Neither the nitrate nor the

chloride compound showed additional methacrylate bands and were consequently stable in solution. Although, as discussed above, the ATR-IR spectra of the crystalline samples were equal, the two spectra showed little, but characteristic differences compared to **17**, which were mainly manifested in the asymmetric vibration of the carboxylate. The band was shifted two wavenumbers to 1581 cm^{-1} , but even more convincing the band was broader and showed tailing to higher wavenumbers. Therefore, the band for the coordinated pyridine at 1607 cm^{-1} was present only as a shoulder of the asymmetric carboxylate band. The symmetric vibration broadening of the band at lower wavenumbers, but less pronounced compared to the symmetric vibration.

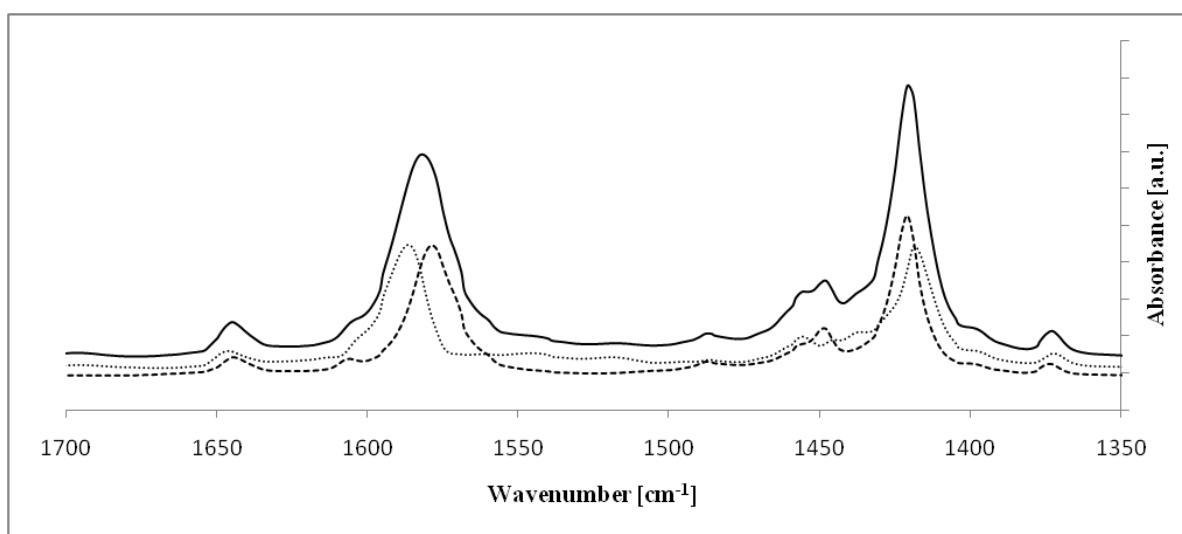


Figure 2.28: Comparison of the IR spectrum of a 3.125 mg/ml $[\text{Fe}_3\text{O}(\text{MA})_6(\text{py})_3]\text{Cl}$ **15** chloroform solution (solid line) with the chloroform solution of $[\text{Fe}_3\text{O}(\text{MA})_6(\text{py})_3]\text{BF}_4$ **17** (dashed line) in the region between 1350 cm^{-1} and 1700 cm^{-1} ; the dashed line is the difference between the two spectra.

To further investigate this phenomenon, the spectrum of **17** was subtracted from **15**. The results are presented in Figure 2.28. The resulting spectra indicated that in solutions of **15** one or even more different coordinated methacrylate species additional to that of the triiron compound are present. The position of the bands indicated, like in the case of the triiron compound, a μ_2 -coordinated carboxylate.

IR investigations of **15** in chloroform with different cluster concentrations were performed. The obtained spectra are reported in Figure 2.29. By increasing the concentration of the cluster from 3.125 mg/ml to 25 mg/ml, a slight shift from 1582 cm^{-1} to 1581 cm^{-1} of the position of the asymmetric band occurred, accompanied by the decrease of the band in the region above 1585 cm^{-1} . This means that with higher cluster concentration the band became more and more like the band of **17**. It should be pointed out that for the tetrafluoroborate compound **17** no concentration dependent changes in the IR spectrum were observed. This evidences the stability of cluster **17** in solution.

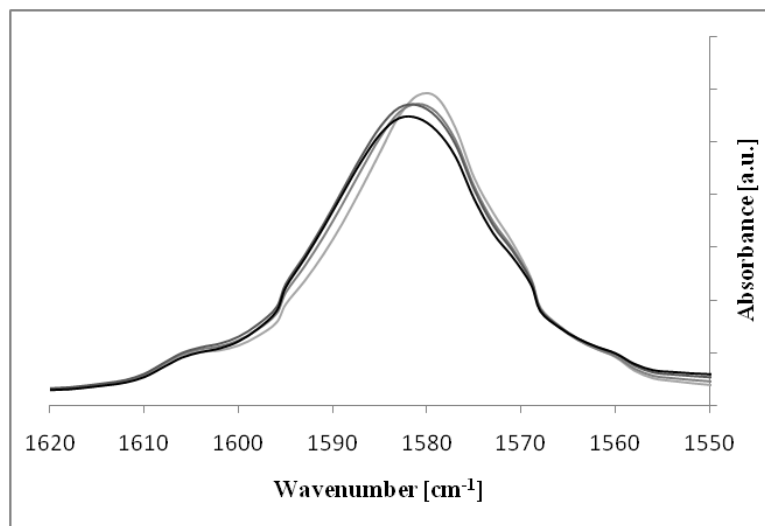


Figure 2.29: Comparison of the IR spectra of $[\text{Fe}_3\text{O}(\text{MA})_6(\text{py})_3]\text{Cl}$ **15** with a cluster concentration of 3.125 mg/ml (black), 6.25 mg/ml (dark gray), 12.5 mg/ml (middle gray) and 25 mg/ml (light gray) in the region between 1550 cm^{-1} and 1620 cm^{-1} .

2.1.9 NMR Investigations

To further investigate the observed differences in the IR spectra of the compounds **14–18**, NMR investigations were additionally performed. Earlier investigations on water- and alcohol-substituted clusters **1–13** did not yield any reasonable results, because the clusters were not stable in solution and showed many different decomposition products that cannot be assigned to the different signals. Since the stability of pyridine-substituted compounds was proven by liquid FT-IR, the compounds were characterized by NMR techniques as well. A comparison of ^1H NMR measurements in d_6 -acetone solutions with a concentration of 20 mg/ml is illustrated in Figure 2.30.

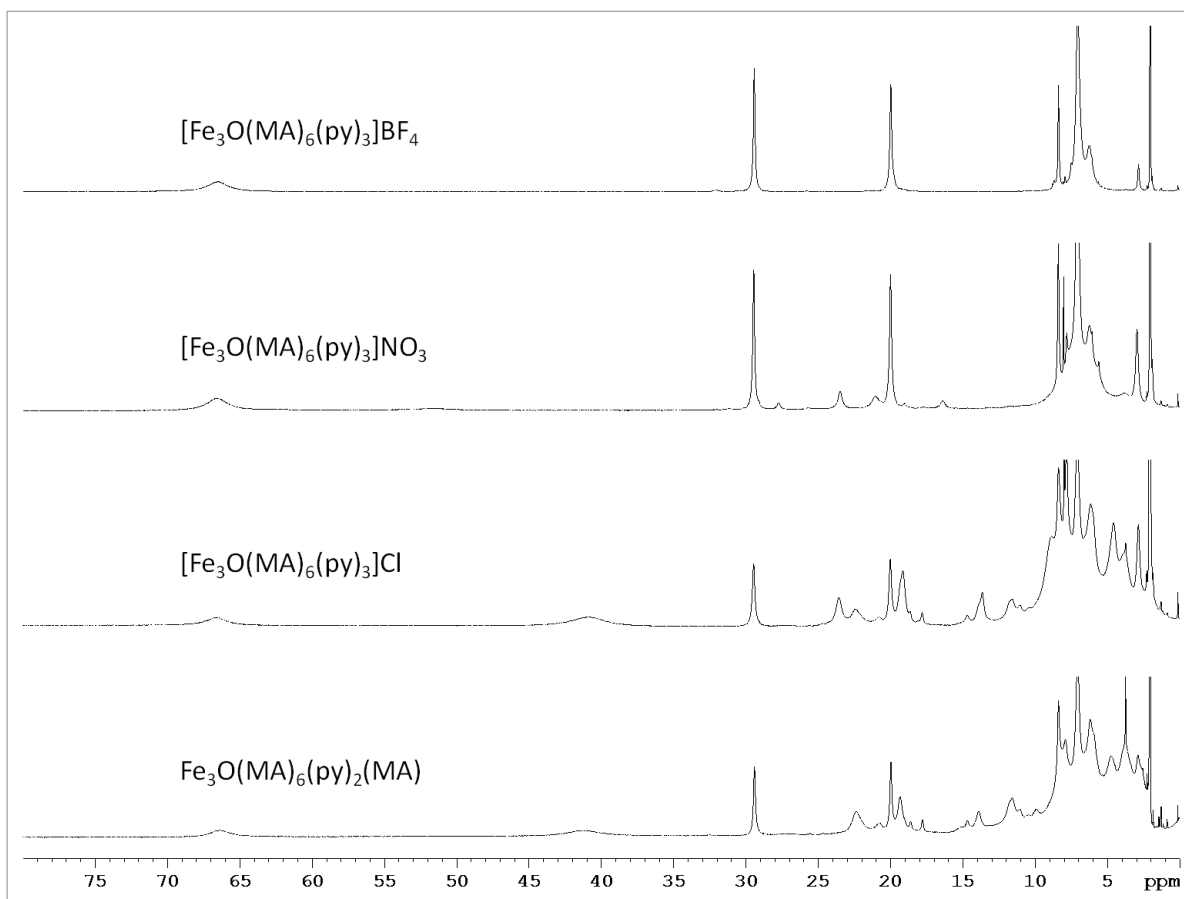


Figure 2.30: Comparison of ^1H liquid NMR measurements of the pyridine-substituted iron(III) oxo clusters **17** (t), **14** (ct), **15** (cb) and **18** (b) in d_6 -acetone solution with a cluster concentration of 20 mg/ml in the region from 0 ppm to 80 ppm.

The ^1H NMR spectrum of $[\text{Fe}_3\text{O}(\text{MA})_6(\text{py})_3]\text{BF}_4$ **17** showed sharp signals in the region from 0 to 80 ppm. The most intense peak is the solvent signal of d_6 -acetone at 2.05 ppm. Only very weak signals assigned to free pyridine, methacrylate or methacrylic acid could be detected. It can therefore be concluded that this compound was completely stable in solution and could serve as model system for the other bis- and tris-pyridine-substituted compounds.

Five signals, as expected for a D_{3h} symmetric cluster, indicated the coordinated methacrylate and pyridine ligands. No correlation between the integrals of the signals and the amount of protons or carbon atoms in the system were observed, due to the faster relaxation of the nuclear spins closer to the paramagnetic centers. The fast relaxation led to broad signals as well. Therefore, coupling of the protons was not detectable and only singlets were obtained. Hence, the signals could not be assigned to the related protons by standard methods. The biggest paramagnetic shift accompanied by the most pronounced broadening of the signals, caused by the Coulomb field of the paramagnetic centers, the fast relaxation and the dilation of the d-orbital SOMOs, should be assigned to stereoscopic proximity of the protons and the carbon atoms. This however did not help to distinguish between protons originating from the pyridine or from the methacrylate ligands.

To further investigate the solution stable compound $[\text{Fe}_3\text{O}(\text{MA})_6(\text{py})_3]\text{BF}_4$ **17**, ^{13}C , COSY and HMBC liquid NMR measurements were performed. The results for the ^{13}C and for the HMQC measurements are presented in Figure 2.31 and Figure 2.32.

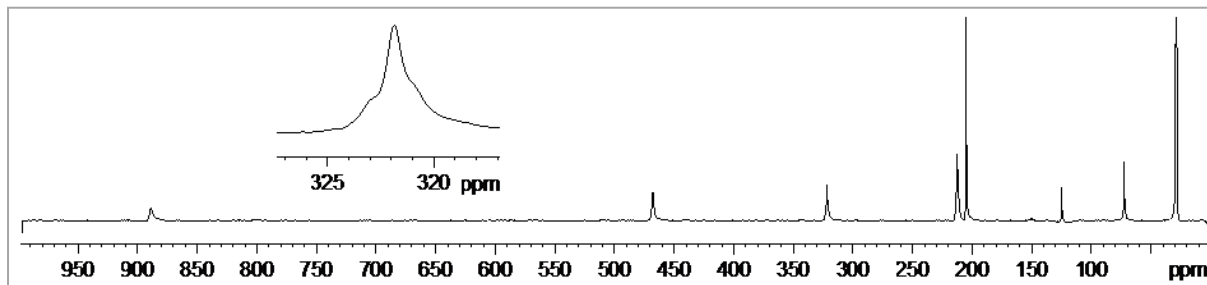


Figure 2.31: ^{13}C NMR spectrum of $[\text{Fe}_3\text{O}(\text{MA})_6(\text{py})_3]\text{BF}_4$ **17** in d_6 -acetone in the region between 0 ppm and 1000 ppm.

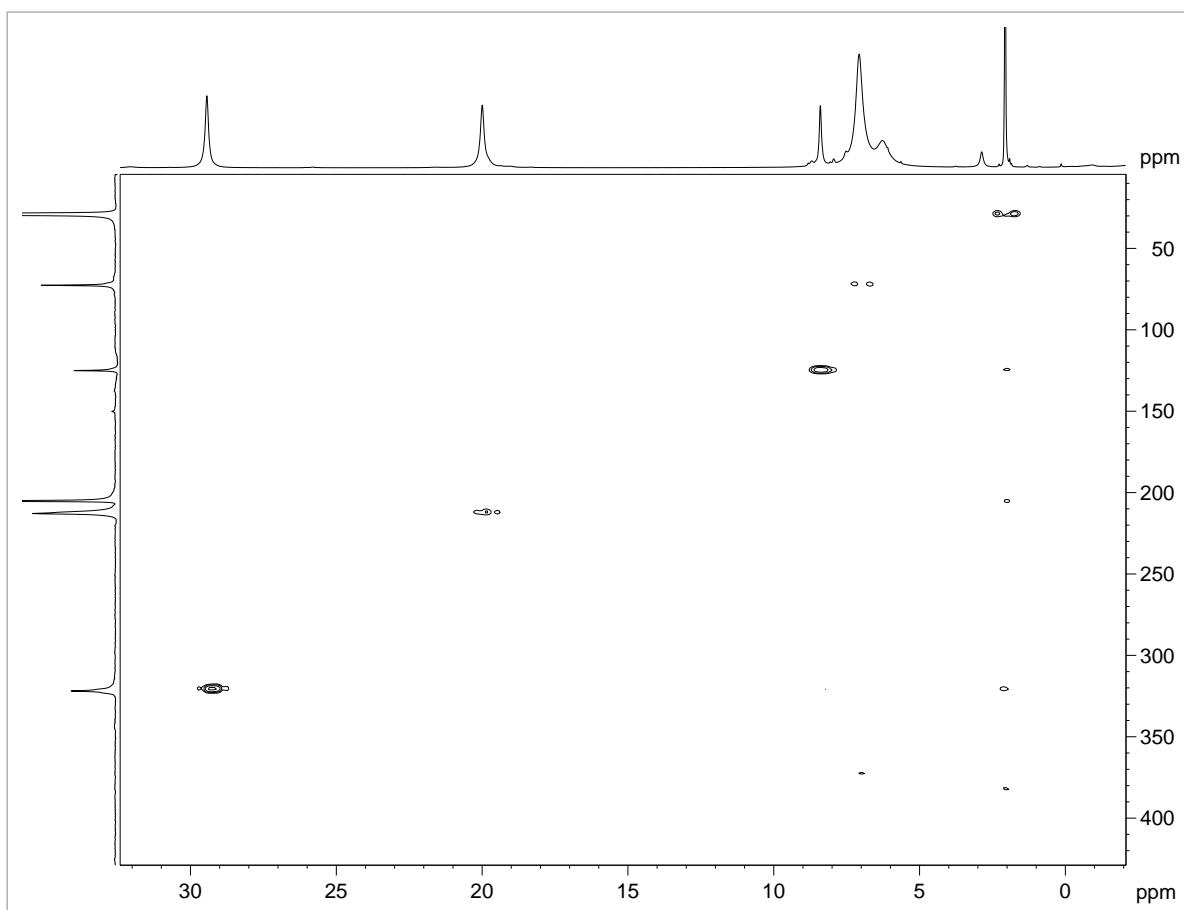


Figure 2.32: HMQC spectrum of a 20 mg/ml solution of $[\text{Fe}_3\text{O}(\text{MA})_6(\text{py})_3]\text{BF}_4$ **17** in d_6 -acetone.

The COSY hydrogen-hydrogen correlation spectrum only showed signals, between the β -H of the coordinated pyridine ring at 29.4 ppm and the γ -H at 8.4 ppm. The two protons are located next to each other and had enough distance to the paramagnetic centers. No correlation was found for the α -H of the pyridine or the CH_2 or CH_3 of the methacrylate

ligands. The HMQC spectrum assigned the carbon signals at 321.9 ppm to the β -C and the one at 125.1 ppm to the γ -C of the pyridine. Two more signals were visible, which were assigned to the CH₂ group of the methacrylato ligand at 212.8/19.9 ppm and the CH₃ group at 72.6/7.1 ppm. As in the COSY spectrum, no correlation could be found for the α -C/H of the pyridine, but after the assignment of the other peaks the signals at 467.9/66.6 ppm were related. The missing two carbon signals of the methacrylato ligand were found as a shoulder at 212.3 for the β -C and a very small peak at 888.8 ppm for the carbon atom nearest to the paramagnetic centers.

An additional overlapping signal was, as presented in Figure 2.31, detected for the peak of the pyridine β -C at 321.9 ppm. Furthermore, small signals assigned to free pyridine could be found at 150.0 ppm, 137.2 ppm and 124.0 ppm in the ¹³C NMR spectrum. Both indicated exchange or substitution reactions on the cluster that take place to minor extent.

In the ¹H NMR spectrum of the nitrate compound **14** presented in Figure 2.30, small peaks in the region of the double bond of the methacrylato ligands and the β -H of the pyridine arose, additional to the signals of **17**. Additional free methacrylic acid and free pyridine were visible in the spectrum.

The same results were obtained for the spectrum of [Fe₃O(MA)₆(py)₃]Cl **15**, but even more pronounced. Numerous additional signals were visible, which were nearly as high as the ones for the triiron cluster. A second broad signal obtained at 41.9 ppm indicates a differently coordinated pyridine. A high proportion of non-coordinated methacrylic acid and pyridine were visible in the spectrum. Interestingly, the spectrum of the di-substituted compound **18** showed great similarities to the spectrum of **15**. The cluster has an C_{2v} approximate symmetry and should therefore show two signals for the bridging coordinated methacrylato ligands, one for the coordinated pyridines and one for the methacrylate-*O* ligands. The most prominent peaks in the ¹H NMR spectrum of **18** were found to be the signals for the tri-substituted compound. In addition, four intense signals were present that indicate the expected structure of the compound.

Measurements with different cluster concentrations were performed in analogy to the solution FT-IR measurements for cluster **15**. The results are presented in Figure 2.33.

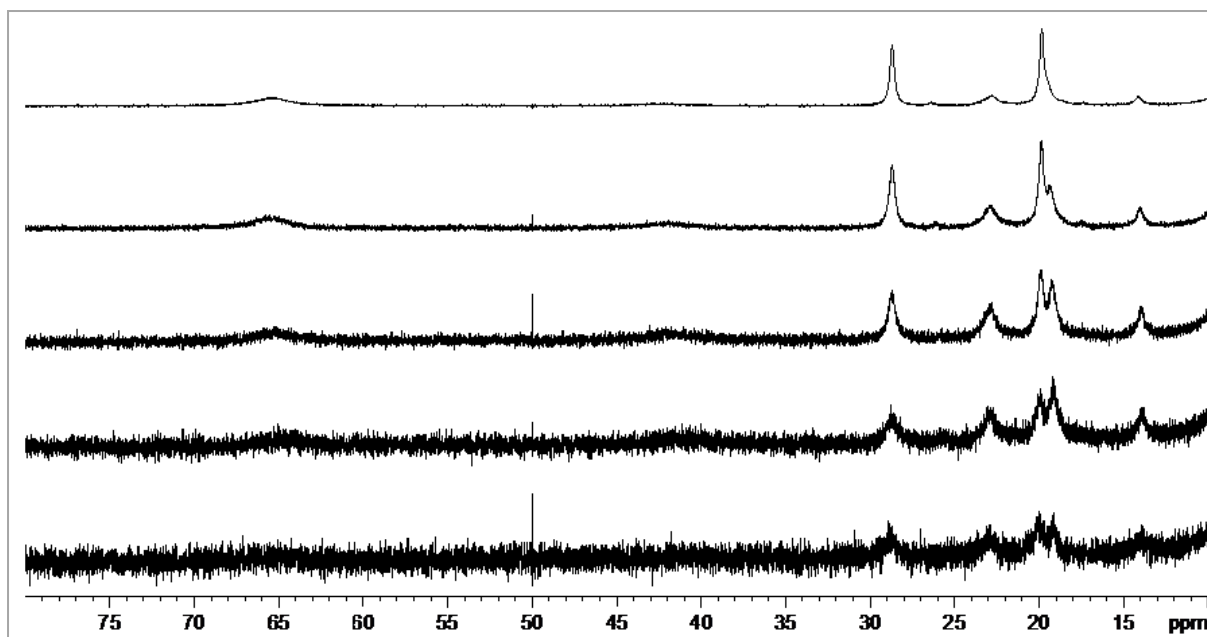


Figure 2.33: ^1H liquid NMR measurements of **15** in CDCl_3 with cluster concentrations from bottom to top of 3.125 mg/ml, 6.25 mg/ml, 12.5 mg/ml, 25 mg/ml and 50 mg/ml in the region between 10 ppm and 80 ppm.

The ^1H NMR spectrum of the CDCl_3 solution with 50 mg/ml cluster **15** showed great similarities to the proton spectrum of the stable compound **17**. Only little additional signals were observed and, as well, only marginal amounts of free methacrylates and pyridine. By decreasing the concentration of cluster in the solution, the additional signals became more intense. For the smallest cluster concentration, they were even higher than the peaks of the triiron compound. The change in the peak pattern had also an influence on the performable measurement techniques. Only for the sample with a higher cluster concentration HMQC and COSY spectra could be obtained.

As the concentration of the cluster, the solvent had an influence on the obtained spectra as well. The results of a comparison of spectra in varying solvents with 25 mg/ml cluster concentration are presented in Figure 2.34. For simplicity reasons, only the region between 10 ppm and 80 ppm is taken into consideration.

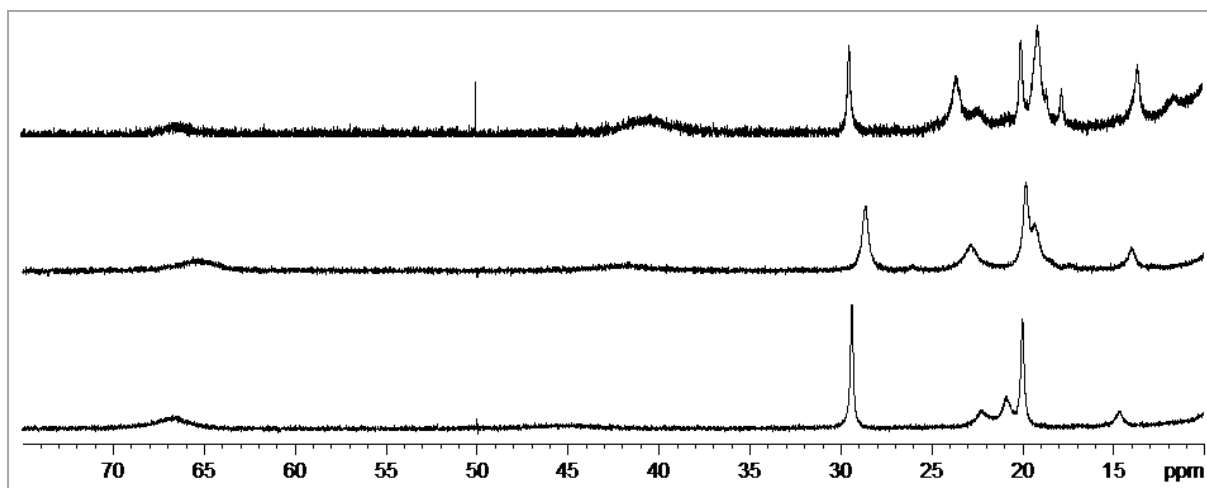


Figure 2.34: Comparison of the ^1H NMR spectra of a 25 mg/ml solution of **15** in CD_3NO_2 (b), CDCl_3 (m) and $(\text{CD}_3)\text{CO}$ (t).

The three spectra show major differences in the intensity and number of additional signals. In each case, the appearance of new signals went along with the detection of free methacrylates, methacrylic acid and pyridine. The cluster appeared to be most stable in nitromethane showing four new signals. Three signals and a broad one at around 43 ppm were obtained in d-chloroform, in addition to the signals of the triiron cluster. For the d_6 -acetone solution, the signals of the differently-substituted compound were more intense than the ones of the triiron cluster. There were six new signals present in the spectrum and the broad signal at 41.9 ppm was found to be larger than the one at 66.6 ppm. As elucidated before, the integrals did not reflect the proportion of compounds and therefore no quantitative conclusions could be drawn.

2.1.10 Discussion and Conclusion

A series of pyridine-substituted oxo centered triiron clusters **14–18** with varying anions was presented in this chapter. The synthesis started from the water-substituted clusters **1**, **3** and **5** presented in 2.1.1. According to the results of 2.1.4, the compounds were suspended in chloroform and the coordinated water molecules were substituted by addition of pyridine. This procedure resulted in $[\text{Fe}_3\text{O}(\text{MA})_6(\text{py})_3]^+$ clusters with nitrate **14**, chloride **15** and bromide **16** anions.

To further investigate the role of the anion for the stability of the clusters in solution, a compound with non-coordinating tetrafluoroborate $[\text{Fe}_3\text{O}(\text{MA})_6(\text{py})_3]\text{BF}_4$ **17** was synthesized by substitution of the chloride in **15** with silver tetrafluoroborate. Solution FT-IR investigations revealed the stability in chloroform solution. 1D ^1H and ^{13}C NMR were measured and the obtained signals could be assigned to the corresponding proton and carbon atoms by 2D COSY and HMQC measurements. The tetrafluoroborate cluster **17** was used as model system for solution FT-IR and NMR investigations of the other clusters.

Liquid FT-IR measurements evidenced the solution stability of compounds **14** and **15**, but the signals were broader compared to the one of **17**. The comparison of the ^1H NMR spectrum of the tetrafluoroborate with that of the nitrate and the chloride compounds in d_6 -acetone resulted in additional signals for the latter two, more intense for the chloride cluster. To understand these additional signals and identify the corresponding compounds, the behavior of the clusters in varying solvents turned out to be of major interest. d_6 -Acetone was used in the beginning, because all the compounds, especially **17**, which was not soluble in CDCl_3 or CD_3NO_2 , were well soluble in this solvent. **15** was measured in CDCl_3 and the number of additional signals decreased to four. With the knowledge that the signals for **18** are similar to **15**, the conclusion that these signals originate from $\text{Fe}_3\text{O}(\text{MA})_6(\text{py})_2\text{Cl}$, a bis-pyridine-substituted cluster with an attached chloride, was drawn. Compared to **15**, which has a D_{3h} symmetry in solution, the new compound is C_{2v} symmetric and therefore shows four signals for the protons in the region above 10 ppm, one signal for the α - and β -pyridine protons respectively and two peaks for the methacrylate CH_2 . The tris-pyridine and bis-pyridine compounds show an equilibrium in solution that is dependent on the solvent. NMR measurements of **15** in CD_3NO_2 again led to four additional, but remarkably smaller peaks compared to the chloroform spectrum. This was related to the better solvation of the chloride anion in the more polar solvent and the according shift of the equilibrium to the tris-pyridine compound. As the polarity of the solvent, the affinity of the anion to iron(III) ions influenced the proportion of bis-substituted cluster in the solution. Smaller signals for the bis-substituted compound were detected accordingly for the nitrate compound **14**.

The situation gets even more complicated when a coordinating solvent, like d_6 -acetone, is involved. In this case, the coordinated pyridine cannot only be displaced by an anion, but as well by a solvent molecule. In the ^1H NMR spectrum of the nitrate compound **14** in d_6 -acetone, for instance, 5 additional signals were present, while in the case of **15** and **18** 11 new signals were visible. The new signals were accompanied by the detection of free pyridine that originated from substitution reactions on the cluster. A list of the possible compounds in solution, their symmetry and the number of expected signals between 10 ppm and 35 ppm is presented in Table 2.21. The CD_3 groups of the d_6 -acetone will get invisible by coordination to the paramagnetic center and were therefore not taken into consideration.

Table 2.21: List of possible coordination compounds in d_6 -acetone solution, their symmetry and number of expected NMR signals in the region between 10 ppm and 35 ppm for the β -pyridine and the methacrylate CH_2 ; py = pyridine, ac = d_6 -acetone and X = NO_3^- or Cl^- .

Coordinated Molecules	Symmetry	Number of Signals	β -pyridine	CH_2
py py py	D_{3h}	2	1	1
py py ac	C_{2v}	3	1	2
py ac ac	C_{2v}	3	1	2
ac ac ac	D_{3h}	1	0	1
X py py	C_{2v}	3	1	2
X py ac	C_s	4	1	3
X ac ac	C_{2v}	2	0	2

The number of signals in the 1H NMR spectrum of **15** indicated that for the chloride compound nearly all differently coordinated species were present in solution. It is noteworthy that it was possible to recrystallize **15** from the acetone solution in good yield, which indicates that all substitution reactions are reversible. Nevertheless, DLS measurements showed the absence of any agglomerates in solution. Interestingly, as in the case of $CDCl_3$, smaller and fewer new signals were observed for the nitrate compound in d_6 -acetone solutions and no anion-substituted compounds were detected for tetrafluoroborate.

To conclude, in this chapter a stable compound $[Fe_3O(MA)_6(py)_3]BF_4$ **17** was established and the spectroscopic properties were investigated. It was shown that the compound does show only minor decomposition or ligand substitution reactions even in coordinating solvents. Therefore, this cluster is a good candidate for the use in the nano building block approach and was applied in the synthesis of cluster-reinforced polymers.

2.2 Cluster-Reinforced Polymers

2.2.1 Solution Co-Polymerization of $[Fe_3O(MA)_6(py)_3]BF_4$

Investigations on the influence of the different ligands and counter anions on the stability and behavior of triiron oxo clusters in chapter 2.1 resulted in the synthesis of the solution-stable compound $[Fe_3O(MA)_6(py)_3]BF_4$ **17**. Solution FT-IR and NMR experiments evidenced the stability of **17** in solution with only little tendency for ligand substitution reactions. On the other hand, compound **17** was badly soluble in any non-coordinating organic monomer and solvent. Previous investigations showed that in a coordinating solvent the coordinated ligands at the cluster are successively substituted, but the cluster core with the coordinated bridging carboxylates stayed unchanged.⁹⁰ Therefore, solution polymerization in pyridine was performed, because substitution reactions of the solvent would be degenerate.

2.2.1.1 Preliminary Investigations on Neat Polystyrene and PMMA

Little is known about solution polymerization in pyridine and about polymerization of late transition metal oxo clusters. Therefore, the first goal was to investigate the dependency of the initiator proportion, the reaction temperature and the influence of the cluster proportion on the polymerization reaction. The first two parameters were optimized by experiments with neat styrene and methylmethacrylate. The optimization parameter for all three tasks were the yield of the polymerization reactions after purification of the products by reprecipitation.

The starting point for all further experiments were the reaction conditions used by Ghosh et al. in their investigations on the influence of pyridine on the polymerization kinetics and the chain transfer rate in the synthesis of polystyrene and polymethylmethacrylate.^{91,92} On the basis of these results, a volume ratio of 1:1 between the pyridine solvent and organic monomer, 0.005 g/ml (0.35 mol%) initiator proportion, and a reaction temperature of 60 °C were chosen. Because of the results of Hamza, who proved that by using dibenzoyl peroxid as initiator, the oxygen located radicals are quenched by transition metals, in his case copper, AIBN was used instead of dibenzoyl peroxide.⁹³ After the polymerization reaction, the polymers were dissolved in toluene and precipitated in n-pentane to remove residual monomers.

The first reactions with styrene resulted in low yields of about 20 % after 17 hours reaction time. To improve the reaction rate, the initiator proportion was increased from 0.015 g/ml (1.03 mol%) to 0.030 g/ml (2.05 mol%) and 0.045 g/ml (3.04 mol%), which resulted in significantly higher yields. The results are presented in Table 2.22 and Figure 2.35. The reaction temperature was increased to 80 °C in a second attempt, which improved the yield to 40 %. 97 % yield were obtained for the reaction with 0.045 g/ml (3.04 mol%) initiator.

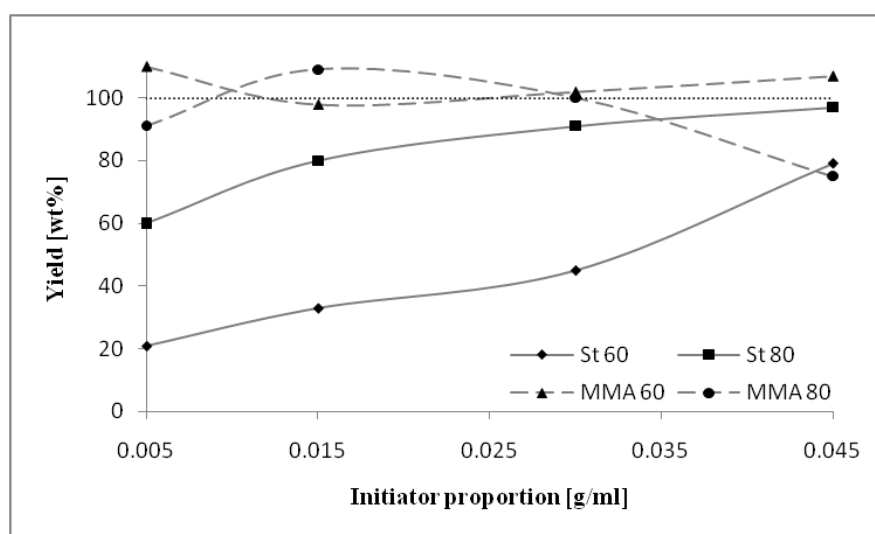


Figure 2.35: Comparison of the polymerization yields of polystyrene (St) and PMMA (MMA) polymerized at 60 °C and 80 °C respectively.

Table 2.22: Comparison of the yields of the polymerization reaction in pyridine.

Initiator Prop.	Initiator Prop. St	Yield St 60	Yield St 80	Initiator Prop. MMA	Yield MA 60	Yield MA 80
[g/ml]	[mol%]	[wt%]	[wt%]	[mol%]	[wt%]	[wt%]
0.005	0.35	21	60	0.32	110	91
0.015	1.03	33	80	0.96	98	109
0.03	2.05	45	91	1.91	102	100
0.045	3.04	79	97	2.84	107	75

Methylmethacrylate is known to be more reactive than styrene and therefore the yields were quantitative, even for low initiator proportions. The reaction at 60 °C with 0.005 g/ml (0.32 mol%) initiator proportion resulted in 110 % yield. It can be concluded that all monomers were already polymerized under this conditions. The yield above 100 % might be caused by residual solvent or by the insertion of pyridine into the polymer chain. The yield of the samples polymerized at 60 °C was constant by varying the initiator proportion, while the polymerizations at 80 °C showed a yield maximum at 0.015 g/ml (0.96 mol%). This is caused by the larger number of the more reactive radicals that lead to quenching of the polymerization and results in short polymer chains. Such short oligomers get lost during the purification process and reduce the overall yield.

2.2.1.2 GPC Investigations on the Neat Polymers

GPC analyses were performed on the polystyrene samples. To avoid exchange reactions at the cluster, toluene was used instead of common THF. The results are presented in Figure 2.36. For small AIBN proportions, the molar mass decreased by increasing the initiator proportion, and was nearly constant for higher initiator proportions. This effect can be explained by the availability of monomer in the solution. While for small initiator proportions enough monomer is present in the solution for every radical to start a polymerization reaction, for larger initiator proportion the first radicals consume all monomers and the remaining radicals are quenched without a polymerization reaction. The molar mass of the samples, polymerized at 60 °C, is generally higher than that of the 80 °C samples. This is caused by the enhanced chain initiation, which results in larger numbers of radicals present at higher temperature. As a result, the chain termination processes are increased and shorter chains were obtained. The polydispersity M_w/M_n of the samples was in the range of 1.59–1.73, typical for solution polymerization.

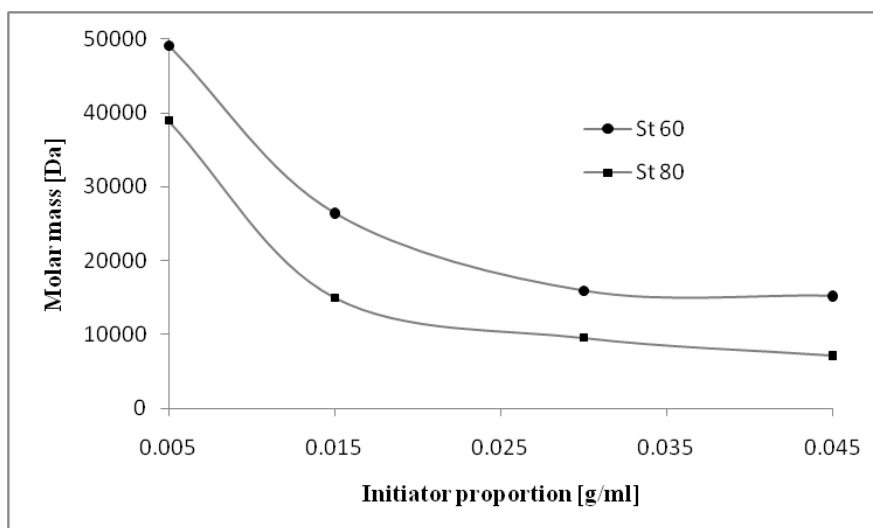


Figure 2.36: Comparison of the GPC determined molar masses of polystyrene samples polymerized at 60 °C and 80 °C, respectively.

Table 2.23: Comparison of the molar masses and polydispersity indices determined by GPC for the neat polymers with 0.005, 0.015, 0.03 and 0.045 g/ml initiator polymerized at 60 °C or 80 °C.

Initiator Proportion [g/ml]	Initiator Proportion [mol%]	St 60 [Da]	Polydispersity	St 80 [Da]	Polydispersity	Calc. Chain Length [Da]
0.005	0.35	49141	1.65	38934	1.67	29757
0.015	1.03	26419	1.70	15000	1.68	10112
0.030	2.05	15912	1.71	9555	1.64	5080
0.045	3.04	15222	1.73	7167	1.59	3426

2.2.1.3 Preparation of the Cluster-Co-Polymers

The use of clusters as building blocks in the nano building block approach is determined by i) the stability in solution, ii) the solubility in organic monomers and iii) the stability during the polymerization reaction.

NMR-experiments of $[\text{Fe}_3\text{O}(\text{MA})_6(\text{py})_3]\text{BF}_4$ **17** in d_5 -pyridine solution verified, on the one hand, the fast degenerate substitution of the coordinated pyridine, indicated by disappearance of the signals of the coordinated pyridine, and on the other hand showed the stability of the cluster in this medium by unchanged methacrylato- O, O' ligand signals.

Compound **17** was reacted with AIBN in toluene solution to investigate the stability of the cluster towards radical reactions. The cluster was dissolved in toluene followed by the addition of one equivalent of AIBN. The solution was heated to 60 °C over night. ATR-IR as well as liquid NMR investigations proved the stability of the cluster, but as well showed that no homo-polymerization of the cluster did occur.

After investigating the basic requirements, compound **17** was used as co-monomer in the synthesis of inorganic-organic hybrid materials. The use of polyfunctional clusters usually

leads to highly crosslinked insoluble resins.³² Therefore according to the results with the neat polymers, the first experiments were done with 0.03 g/ml (2.05 mol%) initiator at 60 °C. Comparison of the yields for these reactions is presented Figure 2.37. In contrast to the expected behavior, the yield of the reaction decreased with increasing cluster loading. The cluster apparently inhibited the polymerization. Therefore, first the initiator proportion was increased to 0.045 g/ml (3.04 mol%), resulting in higher yields. In a second step, the reaction temperature was increased to 80 °C. In contrast to the samples polymerized at 60 °C, the yields were generally high between 90 % and 100 %. The yield did not decrease by increasing the cluster proportion, but improved slightly for the highest cluster loadings. This indicated that under this conditions the clusters crosslink the polymer chains.

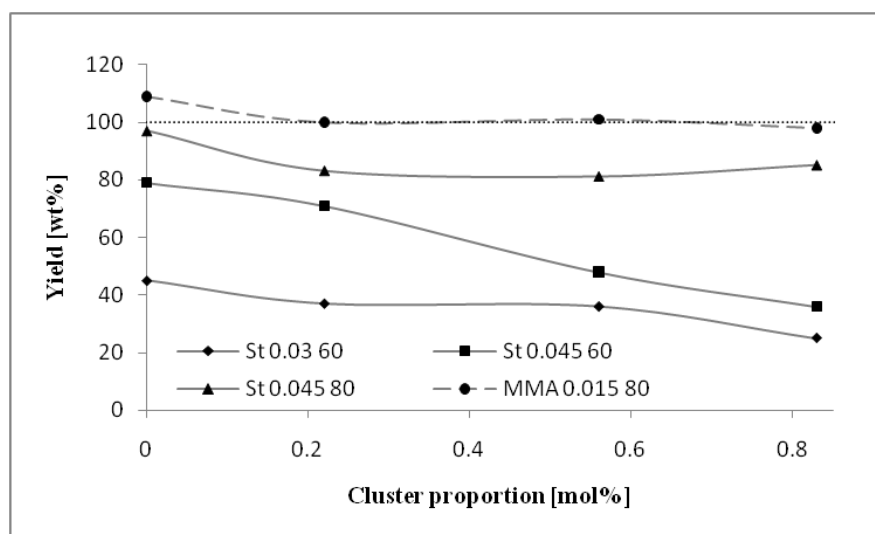


Figure 2.37: Comparison of the polymerization yields of cluster-co-styrene (St) polymers polymerized with 0.03 g/ml (2.05 mol%) and 0.045 g/ml (3.04 mol%) initiator at 60 °C and 80 °C and a cluster-co-methylmethacrylate (MMA) polymerized with 0.015 g/ml (0.96 mol%) at 80 °C.

As for the neat polymers, the reaction works out better for the methylmethacrylate-co-polymers due to the higher reactivity of the monomer. According to the results of styrene, higher initiator proportions (0.015 g/ml; 0.96 mol%) and temperature (80 °C) were used for MMA from the beginning. The reactions resulted in yields of about 100 % after the purification step.

Table 2.24: Comparison of the polymerization yields of cluster-co-styrene (St) polymers polymerized with 0.03 g/ml (2.05 mol%) and 0.045 g/ml (3.04 mol%) initiator at 60 °C and 80 °C and a cluster-co-methylmethacrylate (MMA) polymerized with 0.015 g/ml (0.96 mol%) at 80 °C.

Cluster Proportion St [mol%]	St 0.03 60 [wt%]	St 0.045 60 [wt%]	St 0.045 80 [wt%]	Cluster Proportion MMA [mol%]	MMA 0.015 80 [wt%]
0	45	79	97	0	109
0.22	37	71	83	0.22	100
0.56	36	48	81	0.55	101
0.83	25	36	85	0.82	98

2.2.1.4 GPC Investigations on the Cluster-Co-Polymers

As mentioned above in earlier works, the cluster-co-polymers were insoluble after the polymerization.³² In contrast, the materials obtained by solution polymerization in pyridine were well soluble in toluene and chloroform, respectively. This opens the possibility to purify the polymers and remove the residual monomer and also allows the use of standard polymer analysis techniques like GPC. The results for the molar mass determination are presented in

Figure 2.38.

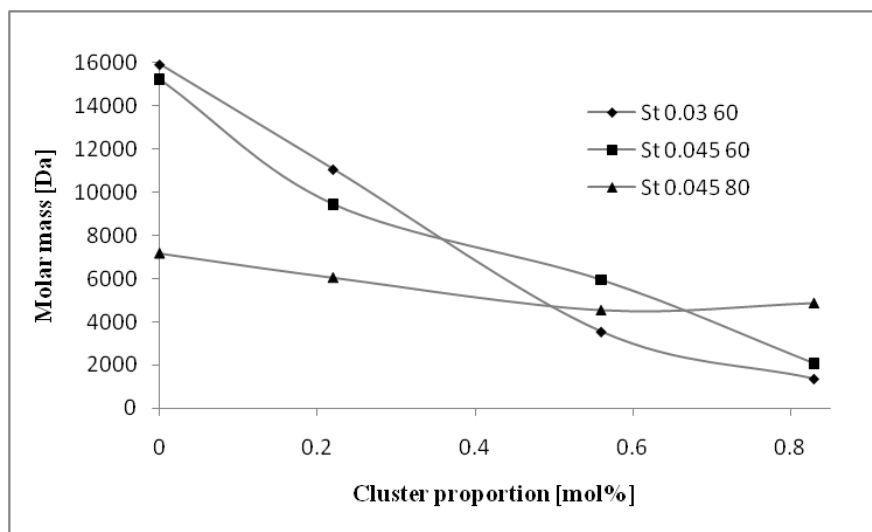


Figure 2.38: Comparison of the GPC determined molar mass of the cluster-co-polystyrene (St) with 0.03 g/ml and 0.045 g/ml initiator proportion polymerized at 60 °C and 80 °C.

For the experiments at 60 °C with different initiator proportions (0.03 g/ml and 0.045 g/ml), a similar behavior could be detected. The molar mass decreases constantly with increasing cluster proportion, indicating the suppression of the polymerization reaction by the cluster as well as the lack of crosslinking in the system.

The reduced molar mass upon addition of the cluster can be explained by the electron transfer properties, described in one particular case for the transfer between the Fe(II,III,III) and the Fe(III,III,III) cluster in solution.⁵⁷ The cluster is able to influence the total molar mass

in two ways: i) it acts as an electron (radical) transfer agent and therefore shortens the chain length of the obtained polymers and ii) it crosslinks the shorter polymer chains to obtain larger fragments.

Comparing the samples polymerized at 60 °C, for undoped samples and for 0.22 mol% cluster loading the molar mass of the 0.03 g/ml initiator proportion samples is, as expected, larger than of the samples with 0.045 g/ml initiator. This behavior changes by further increase of the cluster loading. Due to the higher degree of crosslinking, the samples with 0.045 g/ml initiator showed larger molar mass.

The situation is different for the samples polymerized at 80 °C. As shown before, the neat polymers showed low molar mass due to the high initiator proportion and the increased temperatures. In contrast to the other experiments, the addition of cluster did not lead to a drastic decrease in the molar mass and even to slightly higher mass for high cluster proportion. This behavior can be traced back to an (over)compensation of the molar mass reduction by the crosslinking of these shorter units.

To prove this theory, the molar mass of the polymer chains in the cluster-co-polymer were determined. To this end the cluster had to be destroyed and separated from the polymer. The first attempts to decompose the cluster with concentrated aqueous HCl directly added on the hybrid polymer did not result in the destruction of the cluster even after two days. This indicated the successful introduction of the cluster into the polymer. Therefore, the cluster-co-polymers were dissolved in toluene and extracted with concentrated aqueous HCl. GPC measurements of the resulting white powders led to chain lengths of 4501 Da (1.90 polydispersity index) for the samples with 0.56 mol% and 3268 Da (2.65 polydispersity index) for the sample with 0.83 mol% cluster proportion. This analysis demonstrated that the chain length of the individual polymer chains is indeed reduced, but this is compensated by the crosslinking of the clusters. The values are in the range of the theoretical chain length in the case that every radical initiate a polymerization reaction, which is a typical behavior for the cluster acting as a transfer agent for the polymerization.

Table 2.25: Comparison of the molar mass and polydispersity determined by GPC for the $[\text{Fe}_3\text{O}(\text{MA})_6(\text{py})_3]\text{BF}_4$ -co-styrene hybrid materials with 0.03 g/ml and 0.045 g/ml initiator proportion polymerized at 60 °C and with 0.045 g/ml initiator proportion polymerized at 80 °C with 0, 0.22, 0.56 and 0.83 mol% cluster.

Cluster Proportion [g/ml]	Cluster Proportion [mol%]	St 0.03 60 [Da]	Poly-dispersity	St 0.045 60 [Da]	Poly-dispersity	St 0.045 80 [Da]	Poly-dispersity
0	0	15912	1.71	15222	1.73	7167	1.59
0.020	0.22	11061	1.88	9441	2.05	6034	1.62
0.050	0.56	3543	2.23	5934	4.06	4521	1.88
0.075	0.83	1364	3.65	2063	4.91	4850	1.71

2.2.1.5 IR Investigation of the Cluster-Co-Polymers

Instead of comparing the spectra of the cluster-co-polymers with one another, much more information can be obtained by subtracting the spectra of the neat polymers from the hybrid materials. The processed spectrum shows only the bands of the polymerized cluster. This opens the possibility to easily investigate the stability of the cluster during the polymerization.

By subtraction of two spectra, the Lambert-Beer law has to be taken into consideration. Only spectra of compounds with the same composition are, due to changes in the absorption coefficient, allowed to be subtracted from one another. This is not the case for cluster-reinforced polymers, because, as shown above, the molecular structure of the polymers changes due to the addition of the cluster. The situation gets even more complicated by measuring ATR-IR spectra, because the intensity of the bands is dependent on the grain size, the contact pressure and so on. However, the position of the bands does not change and the intensity should only shift to some extent. Therefore, only qualitative investigations are possible.

Due to the high sensitivity of IR spectroscopy, even small cluster proportions can be investigated. It is possible to follow shifts of bands which give insights in the coordination behavior of the ligands in the final material. As in the previous chapters, the symmetric and asymmetric CO₂ vibration of the coordinated bridging methacrylate ligands indicated the stability of the cluster. The band of the double bond gives additional information about the crosslinking density of the clusters. It is known that due to the low intensity of the double bond signal residual double bond proportions can be detected to a maximum amount of 5 mol%, therefore, in principle, the analysis of the double bonds is only characteristic for the samples with 0.83 mol% (4.9 % double bond). In contrast to previous studies, on cluster-co-polymers prepared in pyridine by solution polymerization a purification step could be applied to get rid of the residual monomer. Therefore, any band of a double bond must originate from the bridging methacrylate ligands, coordinated to the cluster.

The cluster-co-styrene samples, polymerized at 60 °C first, were investigated. The results are presented in Figure 2.39. The evaluation of the data showed the limits of this method. For the samples with 0.11 mol% and 0.22 mol% cluster, the spectra were noisy and no clear bands could be observed. The processed spectra of the other two samples with 0.56 mol% and 0.83 mol% cluster proportions showed great similarities to the vibrations of the pure cluster. The bands were generally broader than for the cluster in solution and showed similarities to the bands obtained for crystalline [Fe₃O(MA)₆(py)₃]BF₄ **17**. This indicated that by incorporation of the cluster in the polymer matrix the symmetry of the cluster decreases.

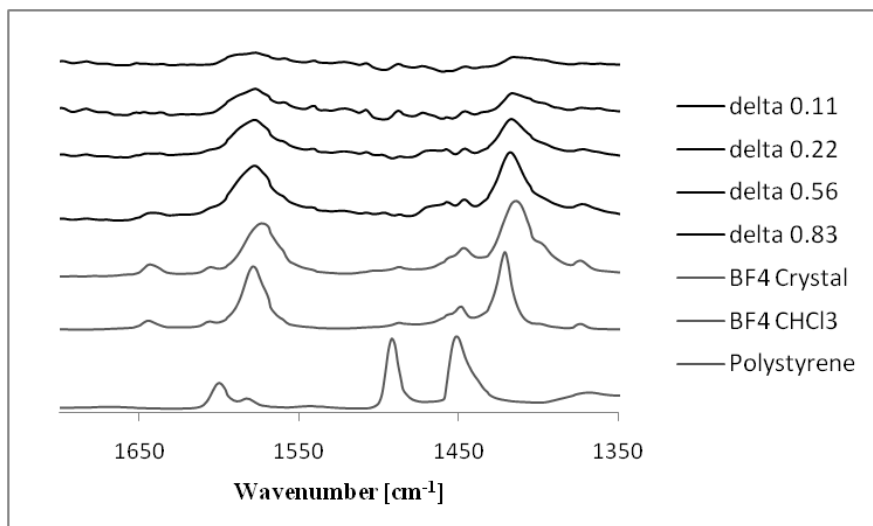


Figure 2.39: Comparison of the cluster-co-styrene ATR-IR spectra after the subtraction of polystyrene (δ) with 0.11 mol%, 0.22 mol%, 0.56 mol% and 0.83 mol% cluster proportion, polymerized with 0.045 g/ml (3.04 mol%) AIBN at 60 °C, with the neat cluster as crystals and in CHCl₃ solution and the neat polystyrene.

The double bonds, indicated by a band at around 1645 cm⁻¹, were still visible for all 60 °C co-polymerized samples. The unreacted double bonds of the methacrylate ligands indicated the crosslinking density, which is the reason for the low yields in the synthesis of the cluster-co-polymers.

A different behavior was detected for the samples polymerized at 80 °C. The results are presented in Figure 2.40. The band indicating the double bonds was not visible, accompanied by higher yields and crosslinking density. As for the 60 °C polymerized samples, the bands for the symmetric and asymmetric stretching vibration of the CO₂ groups were found at similar positions as for the crystalline compound **17**, which indicated the stability of the cluster during the polymerization reaction. However, a remarkable broadening of the bands was detected, which was assigned to the presence of polymerized and non-polymerized methacrylate ligands randomly attached on the cluster. This results in different symmetries for the individual cluster and a broadening of the signal.

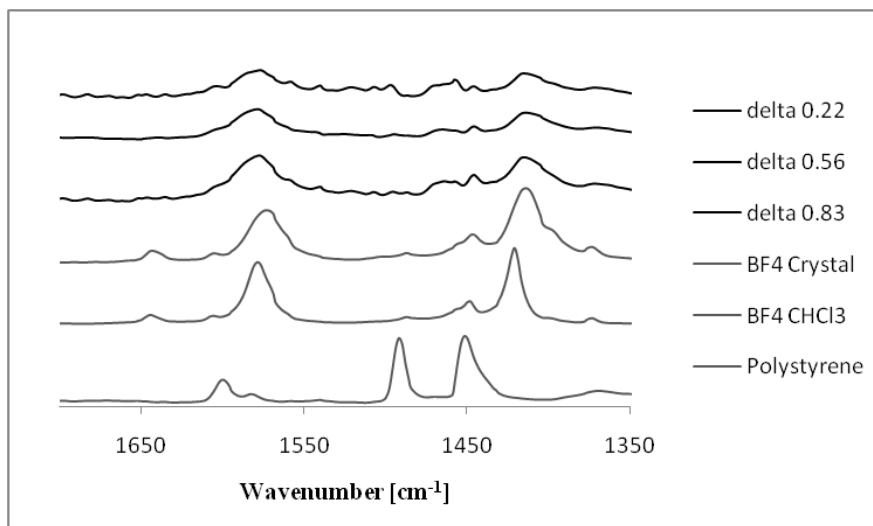


Figure 2.40: Comparison of the cluster-co-styrene ATR-IR spectra after the subtraction of undoped polystyrene (delta) with 0.22 mol%, 0.56 mol% and 0.83 mol% cluster proportion, polymerized with 0.045 g/ml (3.04 mol%) AIBN at 80 °C, with the neat cluster as crystals and in CHCl₃ solution and the neat polystyrene.

ATR-IR investigations were carried out on the cluster-co-MMA hybrid materials. The maximum of the asymmetric CO₂ vibration was shifted to 1604 cm⁻¹, while the symmetric vibration shifted to lower wavenumbers. These shifts indicated a change in the coordination of the carboxylato ligands, which is assigned to the decomposition of the cluster during the polymerization reaction.

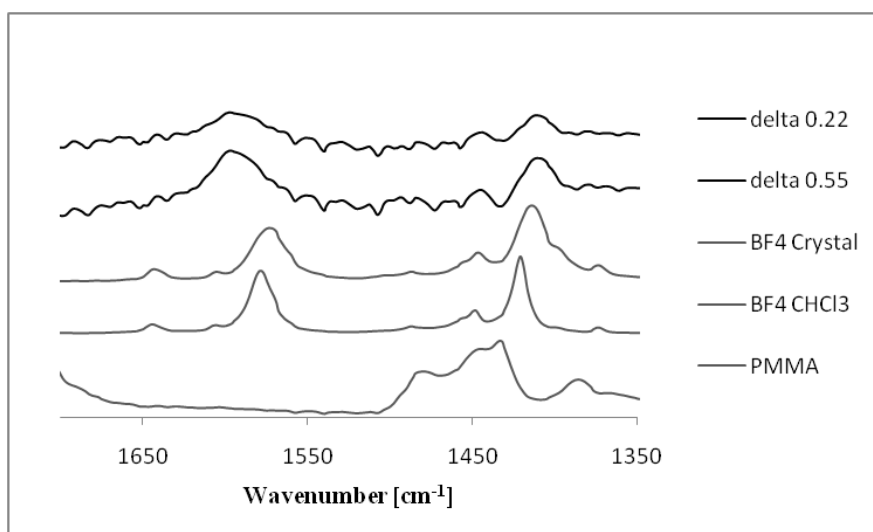


Figure 2.41: Comparison of the cluster-co-PMMA ATR-IR spectra after the subtraction of undoped polystyrene (delta) with 0.22 mol% and 0.55 mol% cluster proportion, polymerized with 0.015 g/ml (0.96 mol%) AIBN at 80 °C, with the neat cluster as crystals and in CHCl₃ solution and the neat PMMA.

2.2.1.6 Mössbauer Investigations

To further investigate the stability of the clusters during the polymerization reaction Mössbauer spectroscopy was performed. Two model clusters were chosen to investigate the properties of the triiron oxo clusters before the incorporation in the polymers and compare the results to the cluster-reinforced hybrid materials. Therefore, measurements on a batch of single crystals of the symmetric compound $[\text{Fe}_3\text{O}(\text{MA})_6(\text{py})_3]\text{Cl}$ **15** and the distorted compound $\text{Fe}_3\text{O}(\text{MA})_6(\text{py})_2(\text{MA})$ **18** were done. The results are presented in Figure 2.42.

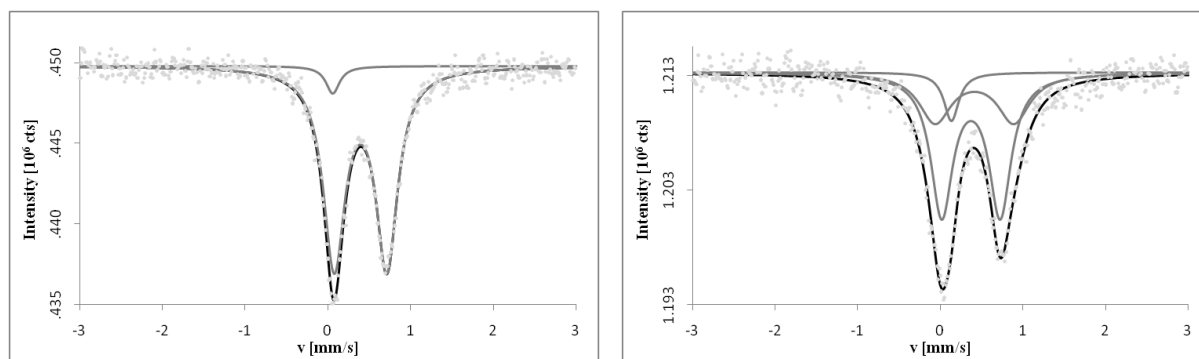


Figure 2.42: Mössbauer spectra of crystal batches of $[\text{Fe}_3\text{O}(\text{MA})_6(\text{py})_3]\text{Cl}$ **15** (l) and $\text{Fe}_3\text{O}(\text{MA})_6(\text{py})_2(\text{MA})$ **18** (r); the measurement points are indicated by light gray dots, the fitting curves by gray lines and their sum by the black line.

The spectrum of compound **15** showed the typical doublet for a high spin iron(III) ion. The most important fit parameters are listed in Table 2.26. As expected for the highly symmetric compound, the obtained curve could be fitted with one doublet, which indicated the presence of only one iron site. The signal showed a low line width and therefore only one sort of iron(III) ion is present in the sample. The asymmetry in the intensity of the doublet resulted in an additional singlet fit curve. Previous investigations showed that this is due to an artifact of the measurement that disappears at lower temperatures.⁴⁸

Table 2.26: Fit parameters for the Mössbauer spectra of $[\text{Fe}_3\text{O}(\text{MA})_6(\text{py})_3]\text{Cl}$ **15**, $\text{Fe}_3\text{O}(\text{MA})_6(\text{py})_2(\text{MA})$ **18** and for the hybrid material with 0.075 g/ml cluster and 0.045 initiator proportion polymerized at 80 °C; the values marked with an asterisk were fixed during the fitting.

	CS	D	A	w	Population
	[mm/s]	[mm/s]	[counts mm/s]	[mm/s]	[atom %]
$[\text{Fe}_3\text{O}(\text{MA})_6(\text{py})_3]\text{Cl}$					
Singlet 1	0.056(67)		570(260)	0.097(55)	4.5(20)
Doublet 1	0.3940(75)	0.636(14)	12140(430)	0.1586(72)	95.5(34)
$\text{Fe}_3\text{O}(\text{MA})_6(\text{py})_2(\text{MA})$					
Singlet 1	0.134(30)		1430(420)	0.109(42)	7.1(21)
Doublet 1	0.412(32)	0.953(96)	6241.19*	0.234(47)	31.1008
Doublet 2	0.370(11)	0.707(33)	12393.3*	0.162(13)	61.7576
cluster-co-polymer					
Singlet 1	-0.028(43)		4200(1400)	0.175(64)	9.5(31)
Doublet 1	0.500(13)	0.705(21)	40200(2000)	0.236(14)	90.5(44)

A different result was obtained for compound **18**. In contrast to **15**, this cluster is C_{2v} symmetric and therefore showed two doublets for two different iron sites, one for the iron(III) ion with the coordinated methacrylato-*O* anion and one for the two pyridine coordinated iron(III) ions. To obtain better fitting results, the ratio between the two signals was kept constant at 1:2 with the possibility to refine this ratio to improve the goodness of fit. The proportion of iron(III) ions after the fitting (see Table 2.26) matched quite well with the expected ratios. The parameters for the pyridine-substituted iron(III) sites, indicated by doublet 2, showed great similarities to the results for cluster **15** with a comparable isomer shift and quadrupole splitting. The small differences can be explained by the changes of the Fe- $\mu_3\text{O}$ distances caused by the coordination of the methacrylate anion. For doublet 1, representing the methacrylato-*O* coordinated iron(III) site, bigger isomer shifts, quadrupole splittings and line widths were detected. As in the case of **15**, an additional singlet was necessary to obtain good fit parameters.

The cluster-reinforced polystyrene with the largest cluster proportion (0.83 mol%) and 0.045 g/ml (3.05 mol%) initiator polymerized at 80 °C was measured. The results of the measurement are presented in Figure 2.43, the fit parameters are listed in Table 2.26. The anions do not influence the iron(III) sites within the clusters and therefore the results for the polymerized compound **17** are directly comparable to the results of **15**.

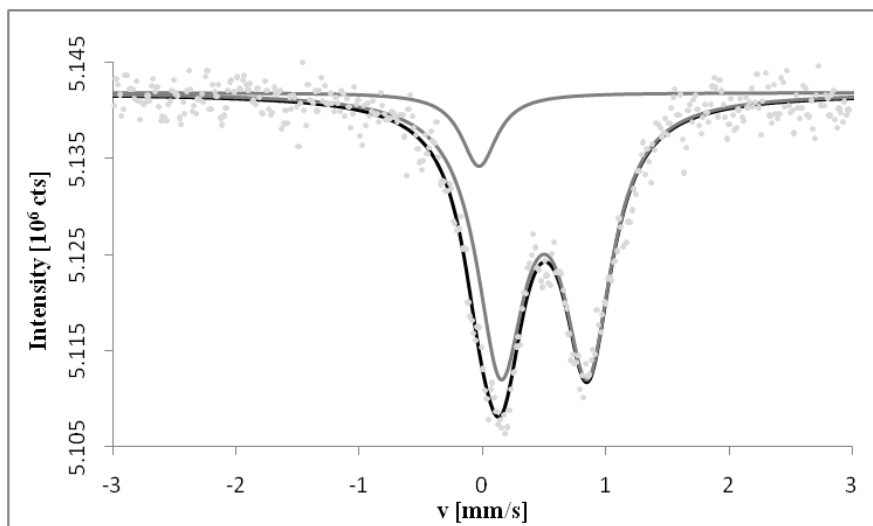


Figure 2.43: Mössbauer spectrum of the cluster-co-polystyrene with 0.83 mol% cluster **17** and 0.045 g/ml (3.05 mol%) AIBN polymerized at 80 °C; the measurement points are indicated by light gray dots, the fitting curves by gray lines and their sum by the black line.

The spectrum of the cluster-co-polymer showed the expected doublet in the region for high spin iron(III) ions. As for the crystalline compounds, the signal of the doublet at lower isomer shift has a larger intensity than the other. One singlet and one doublet were chosen for the fitting. The doublet showed a larger isomer shift than found for the model compounds. The quadrupole splitting as well as the line width was in the expected range. Therefore, it was concluded that the clusters were stable during the polymerization. The larger quadrupole shift of the signal was assigned to the polymerization of the bridging methacrylate ligand double bonds and was due to the lower symmetry of the clusters. This fact was as well reflected in the enhanced line width that can be explained by the presence of many nearly, but not exactly similar iron(III) ion sites in the polymerized clusters. Keeping in mind that even small changes of the distances within the cluster core led to annihilation of the spin frustration such a behavior must not be present for magnetic cluster-reinforced polymers.

2.2.1.7 SAXS Investigations

To investigate the distribution of the cluster in the polymer, small angle X-ray scattering was performed on the cluster-co-styrene materials polymerized with 0.045 g/ml (3.05 mol%) initiator proportion at 80 °C. After background correction from air and parasitic scattering, the data were normalized at $q = 7 \text{ nm}^{-1}$. The resulting scattering curves are presented in Figure 2.44.

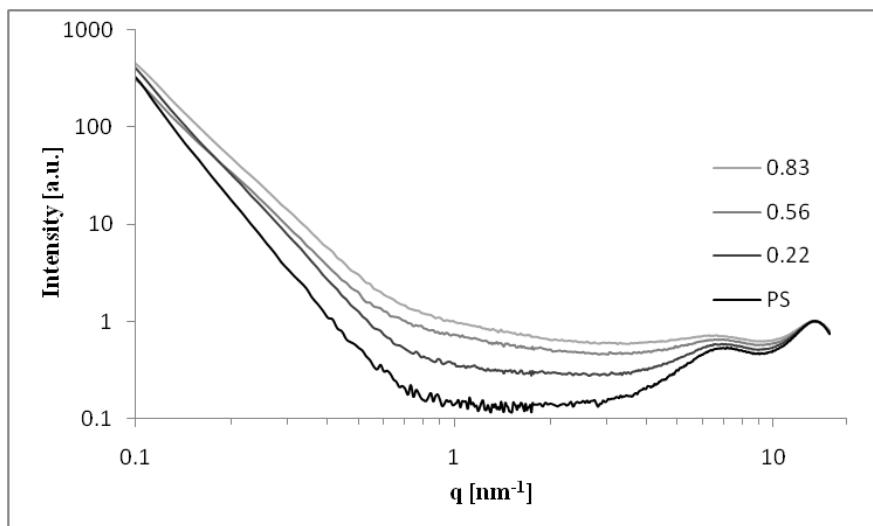


Figure 2.44: SAXS curves of undoped polystyrene and the $[\text{Fe}_3\text{O}(\text{MA})_6(\text{py})_3]\text{BF}_4$ **17**-co-styrene materials after background correction and normalization.

The scattering curve of the neat polystyrene showed the typical signals at $q = 6.92 \text{ nm}^{-1}$ for the ordering in the polystyrene chain and $q = 13.55 \text{ nm}^{-1}$ for the distance between the polystyrene rings that are arranged by π - π stacking. With increasing cluster proportion the scattering intensity clearly increased. This is due to the good scattering properties of the iron atoms in the clusters that lead to an increased base line. Therefore, signal to noise for the doped samples was generally bad. The signal at $q = 13.55 \text{ nm}^{-1}$ did not change significantly, indicating that polymer chains are still present in the material. However, the signal at $q = 6.92 \text{ nm}^{-1}$ changes in two ways. First, it gets less intense with increasing cluster proportion. This indicates that the long range order of the polymer is changing due to the crosslinking of the polymer chains. Secondly, the maximum of the signal shifts to lower q values. The curve of neat polystyrene was subtracted from the curves of the cluster-reinforced polymers. The results are presented in Figure 2.45.

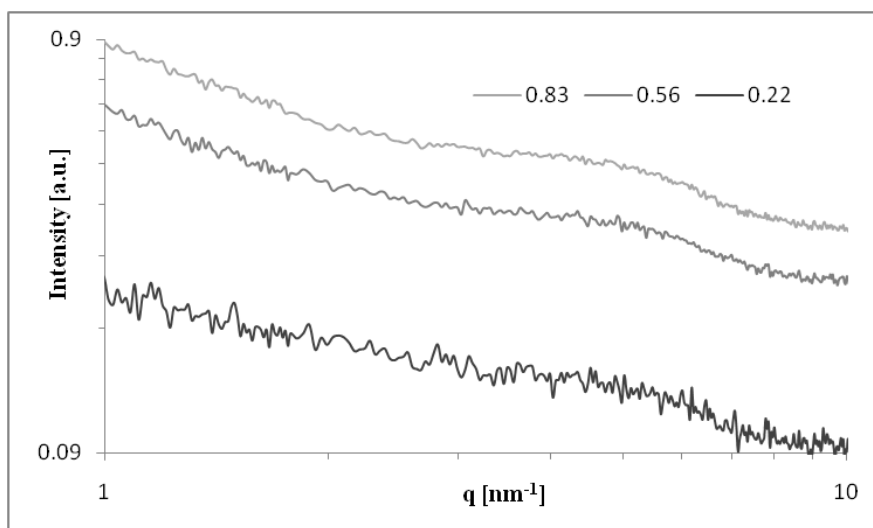


Figure 2.45: SAXS curves the $[\text{Fe}_3\text{O}(\text{MA})_6(\text{py})_3]\text{BF}_4$ 17-co-styrene materials after background correction and normalization and the subtraction of the neat polystyrene curve from the samples with 0.22 mol%, 0.56 mol and 0.83 mol% cluster proportion.

As elucidated before the signal to noise ratio was high for all samples. The new maximum was assigned to assemblies of clusters. The signal shifted to lower q values with increasing cluster proportion, which according to $d = (2\pi/q)$ means that the assemblies get bigger. In other words, the clusters form inorganic islands during the polymerization. With increasing cluster proportion these islands grow.

Information on the macroscopic size regime can be obtained from the curve progression in the $q = 0.1\text{--}0.5 \text{ nm}^{-1}$ region. Compared to the undoped polystyrene, the cluster-co-polymers show a broad shoulder, which becomes more pronounced with higher cluster proportions. The evaluation for the polymers with 0.22 and 0.56 mol% cluster proportion results in inhomogeneities of 30 nm to 50 nm. A bimodal result was obtained with sizes around 40 nm and sizes around 80 nm for the sample with 0.83 mol% cluster proportion. This means that structures with approximately equal sizes were formed during the polymerization or during the re-precipitation.

2.2.1.8 Thermal Properties of the Cluster-Co-Styrene Materials

The introduction of clusters into a polymer matrix is known to increase the decomposition temperature of the hybrid material due to the crosslinking. To investigate this effect, the cluster-co-styrene polymers were analyzed by TGA. The results are presented in Figure 2.46.

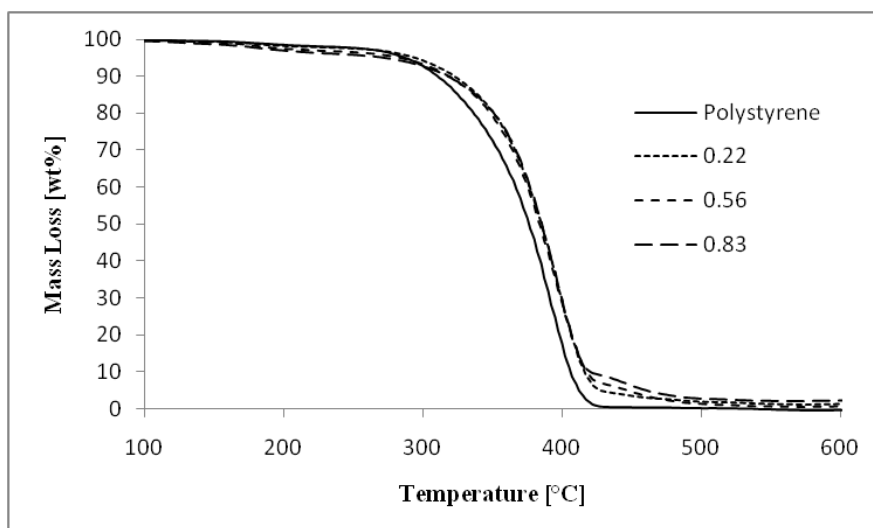


Figure 2.46: Comparison of the TGA results for the cluster-co-styrene materials with 0, 0.22, 0.56 and 0.83 mol% cluster, polymerized with 0.045 g/ml initiator at 80 °C.

The results for the thermogravimetric analysis of neat polystyrene showed the thermal stability of the polymer with neglectable mass loss up to 344 °C, followed by the rapid, complete decomposition of the sample.

The cluster-reinforced polymers showed a first mass loss in the temperature range between 150 °C and 250 °C assigned to the decoordination and loss of the coordinated pyridine. The most characteristic temperatures are listed in Table 2.27. The quantity of the first decomposition step increased accordingly with increasing cluster proportion. The second onset temperature associated with the decomposition of the hybrid polymer itself was detected at 353 °C to 355 °C, 9 °C to 11 °C higher compared to the neat clusters. Char formation was detected for the cluster-co-polymer, more pronounced for increased cluster proportions. Increased char formation is assigned to higher crosslinking density. This observation fits well to the results of the GPC and ATR-IR analysis.

Table 2.27: Thermal data for undoped and $[\text{Fe}_3\text{O}(\text{MA})_6(\text{py})_3]\text{BF}_4$ 17 doped polystyrene

Cluster Proportion [mol%]	Mass Loss 1 [wt%]	Onset 2 [°C]	Mass Loss 2 [wt%]	Onset 3 [°C]	Mass Loss3 [wt%]	Residual Mass [wt%]	Residual Mass calc. [wt%]
0	2.30	344	97.98	-	0	-0.28	0
0.22	2.45	353	91.95	440	4.77	0.83	0.48
0.56	3.47	352	87.47	440	7.49	1.57	1.17
0.83	4.18	355	85.61	437	8.23	1.98	1.71

2.2.2 Discussion and Conclusion

In this chapter, the preparation of $[\text{Fe}_3\text{O}(\text{MA})_6(\text{py})_3]\text{BF}_4$ -co-styrene and MMA cluster-reinforced polymers was described. The cluster was badly soluble in all organic monomers and therefore solution polymerization in pyridine was performed.

The solvent had an influence on the polymerization, indicated by yield reduction and increased reaction times. Therefore, the temperature was increased and the initiator proportion was optimized. Compared to styrene, lower temperatures and initiator proportions had to be applied for the more reactive MMA to obtain full conversion of the monomer.

The addition of the cluster did not result in the expected insoluble resins, but instead soluble polymers were obtained. GPC investigations showed that with increasing cluster proportion the molar mass was reduced. This behavior was traced back to the radical (electron) transfer properties of the cluster during the polymerization reaction. The molar mass for the materials synthesized at 60 °C decreased constantly due to the lack of crosslinking of the clusters, while this effect was compensated by crosslinking in the case of the 80 °C samples.

ATR-IR investigations were performed on the different hybrid materials. It was shown that the bands for the methacrylate ligands did not change during the radical polymerization in the case of the styrene samples, which was assigned to the stability of the clusters during the reaction. The results from the GPC measurements for the crosslinking of the chains could be verified. The samples polymerized at 60 °C showed residual cluster double bonds, while no band was detected for the 80 °C samples. In contrast, a remarkable shift in the methacrylate signals was detected for the MMA samples and traced back to the instability of the clusters during the polymerization.

Although the clusters appeared to be stable during the synthesis, a large line width of signals in the Mössbauer spectrum was detected, which is only possible if all clusters have lower symmetry due to the polymerization.

The thermal stability was determined by TGA measurements. Due to the crosslinking of the polymer chains the onset temperature was increased 3.2 %, but stayed nearly constant for all cluster proportions.

2.2.3 Bulk Co-Polymerization of $[\text{Fe}_3\text{O}(\text{MA})_6(4\text{-vpy})_3]\text{NO}_3$

2.2.3.1 Synthesis of $[\text{Fe}_3\text{O}(\text{MA})_6(4\text{-vpy})_3]\text{NO}_3$ (19)

Even though good results were obtained with solution polymerization in pyridine, the method of choice for the preparation of cluster-reinforced polymers is bulk polymerization. This could be realized by the use of 4-vinylpyridine as the organic co-monomer, which combines the properties of the pyridine solvent with that of the styrene monomer. To avoid the delivery of pyridine by substitution reactions of the ligand against the monomer on the one

hand and the presence of fluorine in the hybrid material on the other the 4-vinylpyridine-substituted cluster $[\text{Fe}_3\text{O}(\text{MA})_6(4\text{-vpy})_3]\text{NO}_3$ **19** was synthesized, analogous to the pyridine compounds, by a reaction starting from $[\text{Fe}_3\text{O}(\text{MA})_6(\text{H}_2\text{O})_3]\text{NO}_3$ **1**.

2.2.3.2 IR Investigations of $[\text{Fe}_3\text{O}(\text{MA})_6(4\text{-vpy})_3]\text{NO}_3$ **19**

The spectra of $[\text{Fe}_3\text{O}(\text{MA})_6(4\text{-vpy})_3]\text{NO}_3$ **19** showed the typical bands for bridging methacrylate ligands by two intense bands at 1573 cm^{-1} and 1415 cm^{-1} indicating the asymmetric and symmetric stretching vibration of the carboxyl group, while the double bond was represented by two bands, one at 1642 cm^{-1} for the C=C bond and another at 1008 cm^{-1} for the CH_2 bending. The nitrate anion was indicated by a broad band at 1347 cm^{-1} . Additional bands were obtained from the coordinated 4-vinylpyridine. The band at 1595 cm^{-1} , indicating the ring vibration, was shifted to 1614 cm^{-1} indicating the coordination of the nitrogen to the iron(III) ion of the cluster in agreement with the literature.

2.2.3.3 Preparation of Cluster-Co-Polymers

The cluster **19** was dissolved in 4-vinylpyridine and the polymerization was started by the addition of 0.5 g/ml AIBN. The reaction was performed as a stepwise free radical bulk polymerization. Starting from $50\text{ }^\circ\text{C}$ the temperature was increased to 80, 120 and $150\text{ }^\circ\text{C}$ for seven and seventeen hours, respectively. This procedure was necessary, because the polymerization was inhibited by the clusters (see chapter 2.2.1.4) and different cluster proportions need different reaction temperatures to obtain full conversion of the monomer. IR studies confirmed the absence of residual monomer in the materials after this procedure. It should again be mentioned that IR is only able to detect residual double bonds of about 5 %, but is an easy and quick method to get a first impression of the conversion. The proportion of the cluster was varied from 0 over 0.05, 0.1, 0.25, 0.49, 0.98, 1.47, 2.35 up to 3.43 mol% resulting in insoluble black resins after the reaction.

In contrast to previous results on Zr- and Ti-oxo clusters, the gelation time did not linearly increase with increasing cluster proportion for the iron(III) oxo cluster, but showed, due to the radical transfer properties of the clusters, a strong dependency on the cluster proportion. At low cluster proportions, the gelation time increased with increasing cluster proportions until a maximum at 0.49 mol%. Neat poly-(4-vinylpyridine) was converted to a solid after one night at $50\text{ }^\circ\text{C}$, while the sample with 0.49 mol% cluster needed two days with temperatures up to $120\text{ }^\circ\text{C}$ to get solid. This trend inverted and the gelation time was decreased again for samples with cluster proportions higher than 0.49 mol%. The samples with 2.45 mol% and 3.43 mol% cluster gelled overnight at $50\text{ }^\circ\text{C}$.

This effect was traced back to the radical transfer properties of the iron clusters. At first the polymerization is only inhibited by the clusters. Above 0.49 mol% cluster proportion, the crosslinking properties get relevant. At these cluster concentrations, a large proportion of

double bonds originate from the clusters. Hence, only short polymer chains have to be formed, that are then crosslinked by the clusters, resulting in a crosslinked network.

The first reactions were performed without stirring. Interestingly phase separation occurred for all cluster proportions. The cluster-co-polymers precipitated as a black solid at the bottom of the reaction vessel. The rest of the material consists of colorless poly-(4-vinylpyridine). This experiment gave insight in the hybrid network formation. At the beginning of the polymerization the clusters react preferentially, and inorganic-rich phases were formed that precipitate due to a high degree of crosslinking. In the following, the bulk material polymerizes around these phases. These results indicated that the stirring rate has a direct influence on the size of the inorganic phases, and therefore on the properties of the cluster-reinforced polymers. Therefore, it was kept at 750 rpm for all experiments.

The materials properties change with increasing cluster proportion. The resins were obtained by smashing the surrounding flask and therefore first impressions of the mechanical properties were obtained. While the neat polymer was obtained as a whole block, all the other cluster-co-polymers broke during the glass smashing procedure. For materials with low cluster proportion, few big pieces were obtained, while the highly loaded samples break into many small pieces.

2.2.3.4 IR Investigations on the Hybrid Materials

The cluster-co-polymers had to be milled to obtain a powder suitable for ATR-IR spectroscopy. The milling of the samples was performed with a ball mill and appeared to be difficult for samples with lower cluster proportion, while quite simple for the highly loaded samples. This indicates, as the splattering during the synthesis, the increasing brittleness of the hybrid polymers.

The investigation of the co-polymers confirmed the absence of residual double bonds in the final materials. The polymerizable double bonds of 4-vinylpyridine were indicated by two bands, one at 924 cm^{-1} for the bending of the CH_2 group and another at 1633 cm^{-1} for the stretching of the double bond. Both bands disappeared during the polymerization reaction except for the samples with the highest cluster proportions (2.45 mol% and 3.43 mol%), where small bands at 1643 cm^{-1} were detected. This means that all monomer units have reacted and also all groups on the cluster are crosslinking the polymers. As mentioned before, IR spectroscopy is only able to detect residual double bonds in the range of 5 %, while the highest cluster proportion was 3.43 mol% and the double bond proportion 17.7 %.

The subtraction procedure established for $[\text{Fe}_3\text{O}(\text{MA})_6(\text{py})_3]\text{BF}_4$ **17**-co-polystyrene materials could not be applied for the poly-(4-vinylpyridine) materials, because the most intense bands of the polymer were located exactly at the same positions as the carboxyl stretching vibrations. Therefore, only the spectra of the polymers were compared. With increasing cluster proportion the bands get broader. This could be interpreted in means that

the structure of the polymer becomes less uniform. This result fits quite well to the results of the SAXS investigations.

2.2.3.5 SAXS Investigations

SAXS investigations were performed to investigate the distribution of the cluster in the hybrid material. After background correction from air and parasitic scattering, the data were normalized at $q = 7 \text{ nm}^{-1}$. The resulting scattering curves are presented in Figure 2.47.

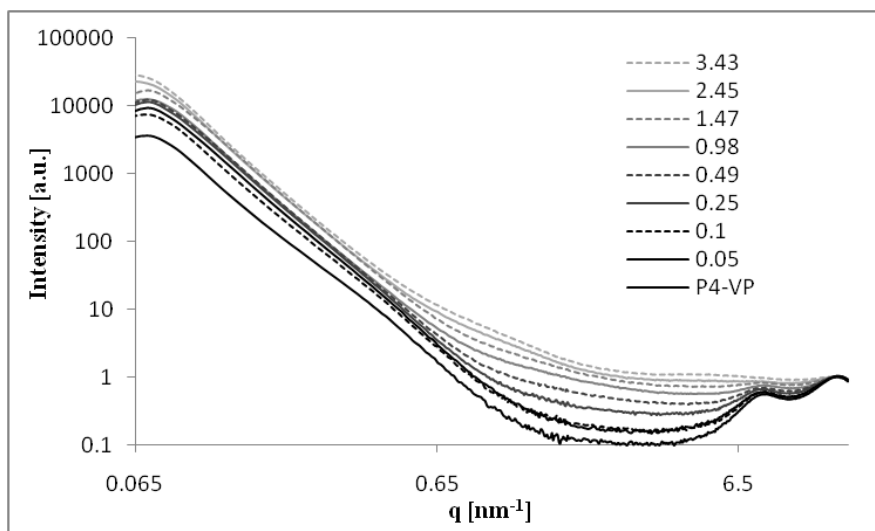


Figure 2.47: SAXS curves of undoped poly-(4-vinylpyridine) and the $[\text{Fe}_3\text{O}(\text{MA})_6(4\text{-vpy})_3]\text{NO}_3$ **19**-co-poly-(4-vinylpyridine) materials with 0.05, 0.1, 0.25, 0.49, 0.98, 1.47, 2.45 and 3.43 mol% cluster proportion after background correction and normalization.

As in the case of the neat polystyrene, neat poly-(4-vinylpyridine) showed two maxima, one at $q = 7.9 \text{ nm}^{-1}$ for the ordering of the polymer chains and one at $q = 13.9 \text{ nm}^{-1}$ for the arrangement of the aromatic rings. With increasing cluster proportion the background scattering increased, which is due to the good scattering properties of the iron atoms. This was accompanied by the decrease of the signal to noise ratio. The maximum at $q = 13.9 \text{ nm}^{-1}$ is constant, while the maximum at $q = 7.9 \text{ nm}^{-1}$ shifted to lower q values with increasing cluster proportion. To further investigate this effect, the scattering curve of the undoped poly-(4-vinylpyridine) was subtracted from that of the cluster-reinforced polymers. The results are presented in Figure 2.48.

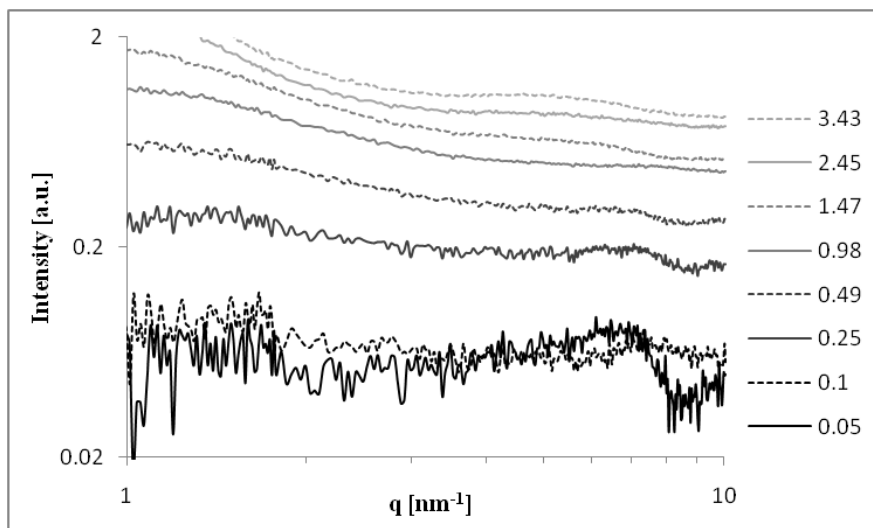


Figure 2.48: SAXS curves of $[\text{Fe}_3\text{O}(\text{MA})_6(4\text{-vpy})_3]\text{NO}_3$ **19**-co-poly-(4-vinylpyridine) materials with 0.05, 0.1, 0.25, 0.49, 0.98, 1.47, 2.45 and 3.43 mol% cluster proportion after background correction, normalization and the subtraction of the neat poly-(4-vinylpyridine) curve in the region between $q = 1$ to 10 nm^{-1} .

All subtracted curves exhibit a maximum that gets broader and shifts to lower q values with increasing cluster proportion. This feature could not be fitted with any model. Instead, they seemed to indicate the size of aggregates in the materials that increase with increasing cluster proportion. In Table 2.28, the dependency of the diameter of the cluster aggregates from the cluster proportion is presented. Due to the bad signal to noise ratio, the maximum for the hybrid material with 0.05 mol% cluster proportion could not be fitted. Due to the lack of sharp signals in the scattering curves it was concluded that the aggregates were amorphous and therefore were interpreted as a random assemblies of iron ions. This result fit quite well to the magnetic measurements discussed in chapter 2.2.3.7.

Table 2.28: Calculated diameters of the cluster aggregates in the $[\text{Fe}_3\text{O}(\text{MA})_6(4\text{-vpy})_3]\text{NO}_3$ **19**-co-poly-(4-vinylpyridine) materials with different cluster proportions.

Cluster Proportion [mol%]	d [nm]
0.05	-
0.1	0.93
0.25	1.04
0.49	1.06
0.98	1.09
1.47	1.31
2.35	1.86
3.43	2.09

More information about the macroscopic assembly of the material were obtained by evaluation of the $q = 0.1$ to 0.5 nm^{-1} region. All curves follow a q^{-4} dependency, which is assigned to the presence of inhomogeneities above 100 nm. The results fit to the observations of the polymerization without stirring that resulted in a complete phase separation. Both

results suggested that the material consists of macroscopic (>100 nm) cluster-reinforced units that are surrounded by a continuous nearly undoped polymer phase.

2.2.3.6 Mössbauer Investigations

A Mössbauer measurement was performed on the hybrid material with 2.45 mol% cluster proportion. The result is presented in Figure 2.49.

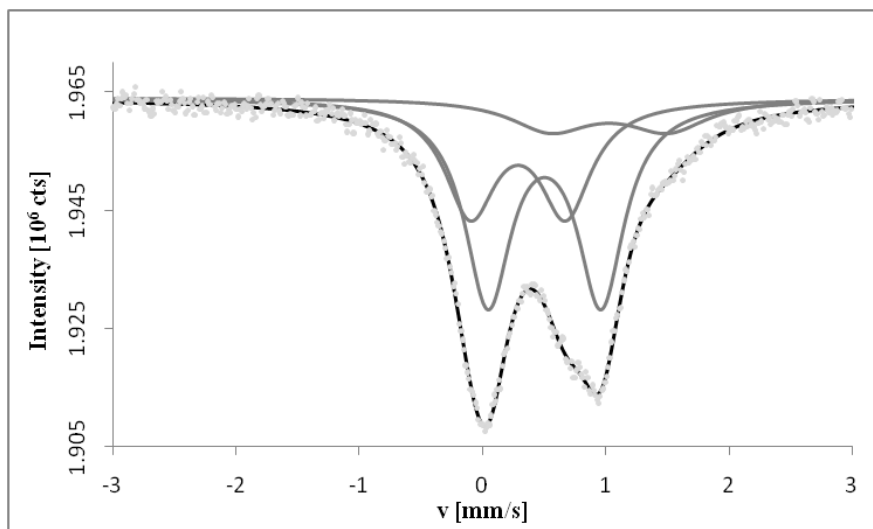


Figure 2.49: Mössbauer spectrum of the cluster-co-poly-(4-vinylpyridine) with 2.45 mol% cluster; the measurement points are indicated by light gray dots, the fitting curves by gray lines and their sum by the black line.

The obtained spectrum showed an asymmetric doublet with noticeable broadening of the higher maximum and a shoulder at higher isomer shift around 1.7 mm/s. The spectrum had to be fitted with at least three doublets, but none of the fitting results were satisfying. The dominant doublet 3 with an isomer shift of 0.503 showed with 0.917 mm/s a large quadrupole splitting, commonly known from iron(II) ions. Doublet 1 can be assigned to a typical iron(III) signal. The shoulder at around 1.7 mm/s is part of doublet 2 with an isomer shift of 1.03(11) mm/s and a quadrupole splitting of 0.95(10) mm/s, typical for iron(II) ions. All obtained fit curves showed a high line width, which was, as in the case of the $[\text{Fe}_3\text{O}(\text{MA})_6(\text{py})_3]\text{BF}_4$ -co-styrene hybrid material, assigned to different iron species in the sample. It can therefore be assumed that the cluster was degraded and no defined species was any longer present in the material. The iron(III) ions were partially reduced to iron(II) during the polymerization reaction.

Table 2.29: Fit parameters for the Mössbauer spectra of cluster-co-polyvinylpyridine with 0.25 g/ml cluster.

	CS	D	A	w	Population
	[mm/s]	[mm/s]	[counts mm/s]	[mm/s]	[atom%]
Doublet 1	0.288(23)	0.772(41)	30000(7900)	0.253(27)	32.8(86)
Doublet 2	1.03(11)	0.95(10)	12700(5200)	0.39(11)	13.9(57)
Doublet 3	0.503(12)	0.917(13)	49000(11000)	0.228(26)	53(12)

2.2.3.7 SQUID Investigations

To investigate the magnetic properties of the cluster-co-polymers, SQUID measurements were performed. As in the case of the Mössbauer measurements, a symmetric cluster $[\text{Fe}_3\text{O}(\text{MA})_6(\text{py})_3]\text{NO}_3$ **14** and a distorted cluster $\text{Fe}_3\text{O}(\text{MA})_6(\text{py})_2(\text{MA})$ **18** were investigated first as model systems. The results are presented in Figure 2.50.

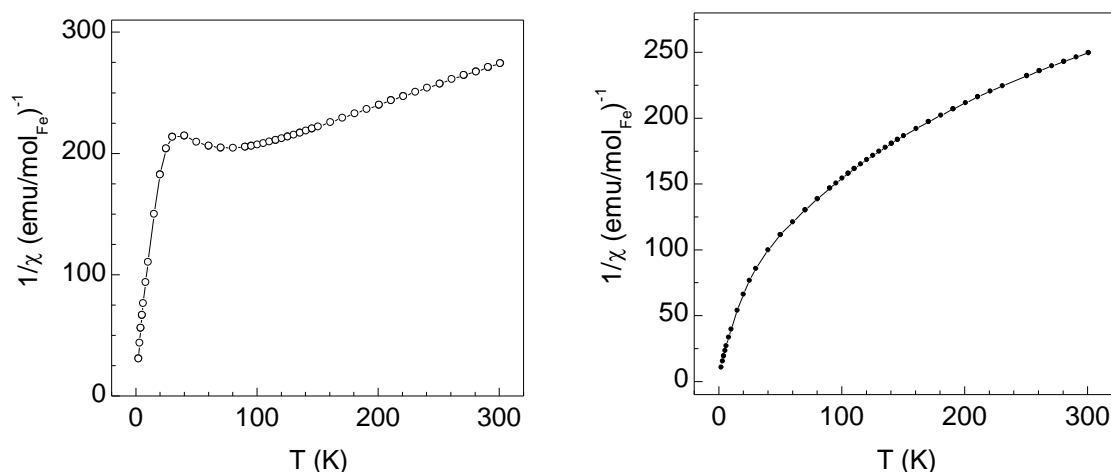


Figure 2.50: The reciprocal susceptibility plot versus temperature of $[\text{Fe}_3\text{O}(\text{MA})_6(\text{py})_3]\text{NO}_3$ **14** (l) and $\text{Fe}_3\text{O}(\text{MA})_6(\text{py})_2(\text{MA})$ **18** (r).

Three regions can clearly be distinguished in the reciprocal susceptibility versus temperature plot of $[\text{Fe}_3\text{O}(\text{MA})_6(\text{py})_3]\text{NO}_3$ **14**. In the first temperature range from 1.8 K to about 20 K, the energy of the system is far below the population of the first high spin level of the cluster. Therefore, a linear dependence on the temperature can be found, the slope of which is assigned to a spin of $S = 1/2$. In the temperature range above 150 K, the high spin levels of the cluster are populated and the slope of the curve indicates a spin of $S = 5/2$. In the intermediate range, an intermediate domain is present that shows a spin frustration of the system. The $S = 1/2$ spin ground state was nearly constant until the transition temperature was reached. A spontaneous transition into the $S = 5/2$ spin state takes place at this point.

For compound **18**, no such regions were present in the reciprocal susceptibility versus temperature plot. As for **14**, the linear approximation of the measurement points at the lowest temperatures showed a $S = 1/2$ ground state and a $S = 5/2$ spin state for high temperatures. No

spin frustration was detected in the system. The transition between the two spin states happened continuously over a wide temperature range.

To determine the spin at 1.8 K, magnetization versus magnetic field measurements were done for compound **14** and **18**. The curves were fitted with Brillouin functions to determine the spin of one magnetic center (J). The results of the fitting are presented in Table 2.30. The Landé g-factor was kept at 2 without any anisotropy for all the fittings. The number of magnetic centers per magnetic center (N) was set constant to 1 for the first fitting and a free optimizeable parameter in the second.

Table 2.30: Fitting parameter for the Brillouin function to model the results of the magnetization versus applied field plot; for the fitting of the cluster-reinforced polymer with 2.45 mol% cluster a linear term was additionally used; the values marked with an asterisk were fixed during the fitting.

	N	Standard Error	g	J	Standard Error	T	Goodness of Fit	d	Standard Error
	[mol ⁻¹]		[]	[]		[K]		[Am ⁻¹ mol ⁻¹]	[Am ⁻¹ mol ⁻¹]
14_1	1*		2*	0.386	7.91·10 ⁻⁴	1.8*	0.99954		
14_2	1.323	0.022	2*	0.300	4.69·10 ⁻³	1.8*	0.99994		
19_1	1*		2*	0.666	1.61·10 ⁻³	1.8*	0.99928		
19_2	0.885	0.021	2*	0.742	1.58·10 ⁻²	1.8*	0.99951		
2.45_1	1*		2*	0.921	7.19·10 ⁻³	1.8*	0.99162		
2.45_2	0.641	0.028	2*	1.358	5.12·10 ⁻²	1.8*	0.99681		
2.45_3	0.290	0.007	2*	2.200	3.61·10 ⁻²	1.8*	0.99985	8.538·10 ⁻⁶	3.135·10 ⁻⁷

The differences in the magnetic properties of the compounds **14** and **18** are caused by the different molecular structure. Spin frustrated systems are characterized by equal spin exchange between the participating ions. This exchange is determined by the overlap of the orbitals and, accordingly, by the distance of the ions from one another. Only symmetric arrangements of atoms can fulfill these requirements. Therefore, the symmetric core of [Fe₃O(MA)₆(py)₃]NO₃ **14** shows spin frustration, while the distorted core of Fe₃O(MA)₆(py)₂(MA) **18** does not show spin frustration.

SQUID measurements were performed on [Fe₃O(MA)₆(4-vpy)₃]NO₃-co-polyvinylpyridine with a cluster proportion of 2.45 mol%. The results are presented in Figure 2.51.

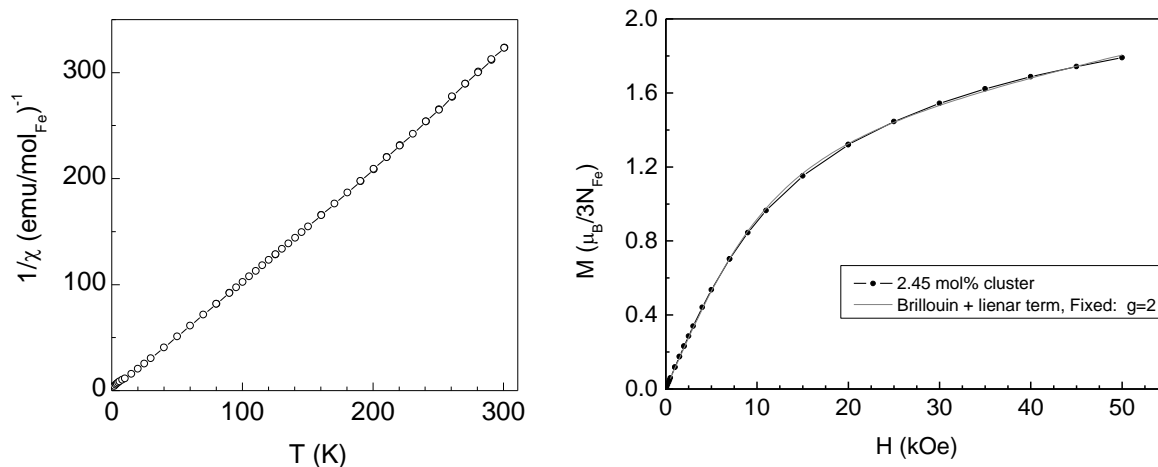


Figure 2.51: The reciprocal susceptibility plot versus temperature of $[\text{Fe}_3\text{O}(\text{MA})_6(4\text{-vpy})_3]\text{NO}_3$ -co-polyvinylpyridine with a cluster proportion of 2.45 mol% (l); The magnetization versus applied field plot with the fitting for the Brillouin functions with additional linear term (r).

In contrast to the two model compounds, the reciprocal susceptibility versus temperature plot was a nearly linear but slightly concave, following the Curie law without any transition in the total spin. The slight concaveness of the curve led to a decrease in the χT value, which must not exist in a pure paramagnetic systems. The magnetization versus magnetic field plot at 1.8 K was, as for the model systems, used to determine the spin state of the molecules at this temperature. The results for the fitting are listed in Table 2.30. In contrast to the model compounds, the fitting led only to good results when a linear parameter was added to the Brillouin function. This is indicating a ferromagnetic coupling between the iron ions. SAXS investigations had shown that no crystalline domains were present in the cluster-reinforced polymers. Therefore, these ferromagnetic interactions must originate from individual iron assemblies within the inorganic islands. On the other hand the value for the amount of iron(III) ions in the hybrid material of $N = 0.290$ was found. This means that a big proportion of the iron ions are antiferromagnetically coupled and are not detectable in the SQUID measurement.

In conclusion, the SQUID measurements confirmed the SAXS and Mössbauer results that the clusters are decomposed during the polymerization. The majority of the iron ions is paramagnetic, but interactions between the individual ions ranging from antiferromagnetic to ferromagnetic could be detected as well.

2.2.3.8 Nano-Indentation Investigations

The cluster-co-polymers were obtained with many bubbles for low cluster proportion or as fractions for the ones with high cluster proportion respectively, which render them insufficient for impact resistance, bending strength and tensile strength experiments. Compacting with and without preliminary milling did not lead to any satisfying result. The only sufficient analysis technique to determine the mechanical properties of such samples are

nano-indentation experiments that were performed to determine the hardness and the brittleness. In previous papers, it was shown that this technique is a powerful tool to investigate the behavior of cluster-reinforced hybrid materials.²⁷

As mentioned above and verified below, the brittleness of the samples increases remarkably with increasing cluster proportion. Therefore, the samples with low cluster proportion could be cut and polished before performing the indentation experiment, while the one with high cluster proportions (1.47, 2.45 and 3.43 mol%) only were cleaned with a soft towel before analysis.

The results for the indentation hardness are presented in Table 2.31 and plotted in Figure 2.52 against the cluster proportion of the co-polymers. Only small changes were observed for small cluster proportions with a small decrease in hardness compared to the neat polymer. This effect was traced back to the reduction of the polymer chain length due to the presence of a transfer agent. The value increased slowly for the samples with 0.1 and 0.25 mol% cluster and increased remarkably the slope for the samples with 0.49 and 0.98 mol%, which was assigned to the increased crosslinking and the nano filler effect. The slope decreased again for the hybrid materials with 1.47, 2.45 and 3.43 wt% cluster. The standard deviation was quite small for small cluster proportion (~2–4 %), but increased drastically for samples with higher proportions (9–17 %) due to the rougher surface. Therefore over 30 indentations were necessary to obtain good distribution.

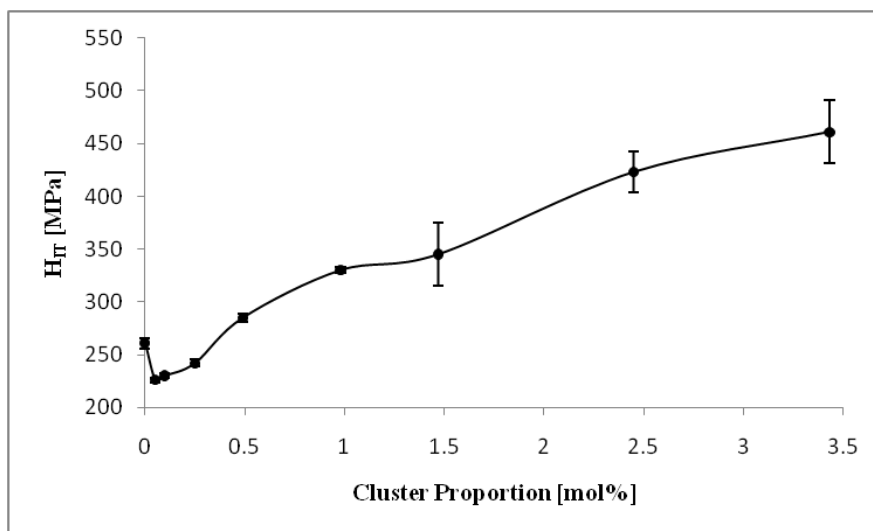


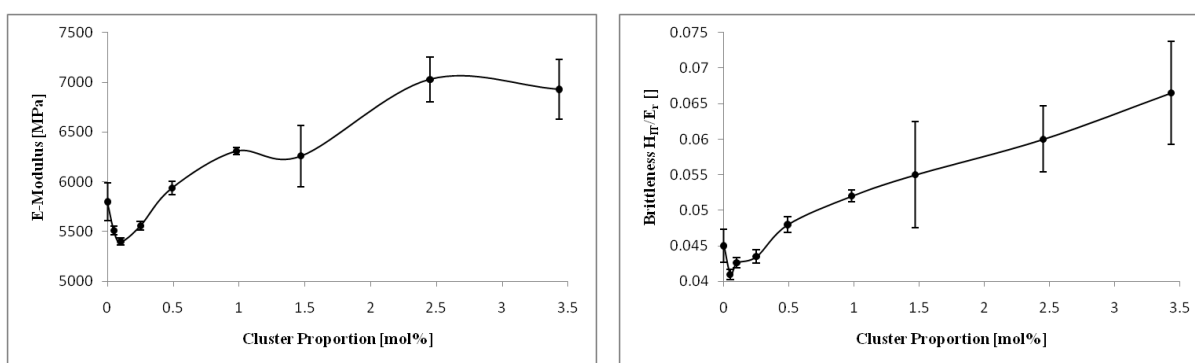
Figure 2.52: Indentation hardness of the $[\text{Fe}_3\text{O}(\text{MA})_6(4\text{-vpy})_3]\text{NO}_3$ -co-poly-(4-vinylpyridine) materials as a function of the cluster proportion.

Table 2.31: Comparison of the micro hardness, the Young's modulus and the brittleness of the $[\text{Fe}_3\text{O}(\text{MA})_6(4\text{-vpy})_3]\text{NO}_3$ -co-poly-4-vinylpyridine materials determined by nano-indentation measurements

Cluster Proportion [mol%]	H_{IT} [MPa]	\pm	E_r [MPa]	\pm	H_{IT} / E_r	
					[]	\pm
0	261	9.9	5800	377	0.045	0.0046
0.05	226	4.5	5510	82	0.041	0.0014
0.1	230	4.6	5400	74	0.0426	0.0014
0.25	242	6.4	5560	83	0.0435	0.0018
0.49	285	7.1	5940	133	0.048	0.0023
0.98	330	6.1	6310	77	0.052	0.0016
1.47	345	60	6260	616	0.055	0.015
2.45	423	38	7030	453	0.06	0.0093
3.43	461	60	6930	601	0.0665	0.0144

The addition of cluster obviously led to reinforcement of the polymers. When comparing the neat polymer with the hybrid material with 3.43 mol% cluster proportion, the hardness increased to an extent of 76.2 %.

The indentation Young's modulus, as the hardness, decreased for low cluster proportions compared to the neat cluster, showing a minimum for the sample with 0.1 mol% cluster. The results are presented in Table 2.31 and plotted in Figure 2.53. After reaching the minimum, the Young's modulus increased again and showed in the end a flattening of the curve. The uneven curve as well as the broad standard deviation for large cluster proportions was explained by the different procedure of the sample preparation for the analysis (polished or just cleaned). The increase in the Young's modulus was not that large as detected for the hardness and equals 19.5 % comparing the neat polymer with the 3.43 mol% cluster proportion sample.

**Figure 2.53:** Indentation Young's modulus (ℓ) and brittleness (r) of the $[\text{Fe}_3\text{O}(\text{MA})_6(4\text{-vpy})_3]\text{NO}_3$ -co-poly-(4-vinylpyridine) materials as a function of the cluster proportion.

The plasticity of the system was calculated by dividing the hardness through the Young's modulus. The value follows more or less the behavior of the hardness with a strong

fluctuation at the beginning followed by a strong increase. The results are presented in Table 2.31 and plotted in Figure 2.53.

2.2.3.9 TGA Investigations

Thermogravimetric analyses (TGA) were performed between 25 and 700 °C in synthetic air with a heating rate of 10 °C/min. The evaluation of the TGA curves of the individual samples is presented in Figure 2.54. The neat polymer showed a first decomposition step at 344 °C and a small second step at 497 °C indicating the formation of organic char. As it was shown in previous work, this formation of char is increased with increasing cluster proportion. No big differences were detected comparing neat polymer and cluster-co-polymers with cluster proportion from 0.05 to 0.98 mol%, except the continuous increase of the char amount, which reached 25 wt% for samples with 0.98 and 1.43 mol% cluster. The samples with 1.43 and 2.45 mol% cluster showed an additional new decomposition step at 249 °C, more pronounced for the higher cluster proportion. The sample with 3.43 mol% cluster showed a completely different decomposition behavior. In contrast to the other samples, the decomposition temperature was decreased and also no char formation was detected. The decomposition started at 243°C, in the range of the temperatures for the co-polymers with 1.43 and 2.45 mol% cluster, and a second step was visible with an onset at 312 °C. Although the decomposition temperature was strongly decreased, the hybrid material did also show enhanced thermal stability compared to the unreacted cluster (see Figure 2.54).

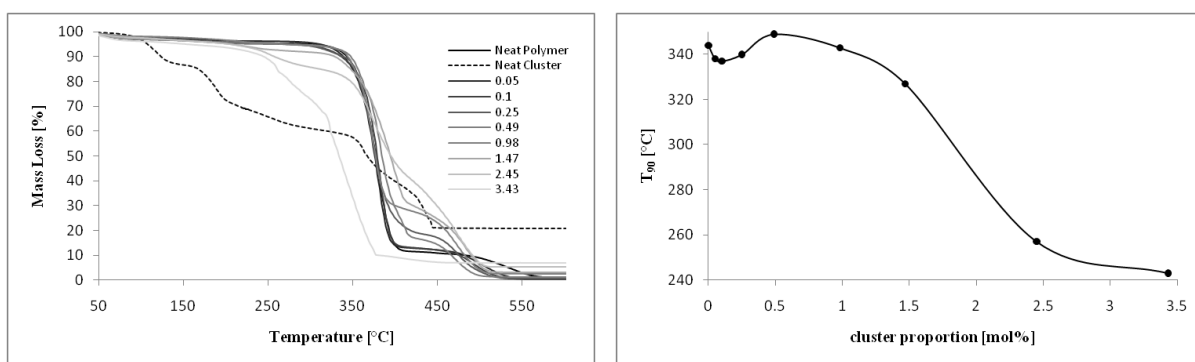


Figure 2.54: Comparison of the TGA results of the $[\text{Fe}_3\text{O}(\text{MA})_6(4\text{-vpy})_3]\text{NO}_3$ -co-poly-(4-vinylpyridine) materials with 0.05, 0.1, 0.25, 0.49, 0.98, 1.47, 2.45 and 3.43 mol% cluster proportion with the neat polymer and the unreacted cluster (l); comparison of the onset temperatures of the second decomposition step (r).

The evaluation of the decomposition temperatures is presented in Figure 2.54. The temperature where 90 wt% was decomposed (T_{90}) was taken into account, because the usually used T_{95} temperature does not reproduce the behavior of the material. The neat polymer showed a T_{90} of 344 °C, which decreases 6 °C for the sample with 0.05 mol% cluster. By increasing the cluster proportion, the thermal stability of the co-polymers again increased slightly until its maximum at 0.49 mol% and 349 °C was reached. Then it decreased again strongly for samples with higher cluster proportions, mainly due to a second decomposition

step at 249 °C, resulting in a 100 °C lower T_{90} temperature for the sample with 3.43 mol% cluster in the co-polymer.

Table 2.32: Thermal data for undoped and $[\text{Fe}_3\text{O}(\text{MA})_6(4\text{-vpy})_3]\text{NO}_3$ **22** doped polyvinylpyridine

Cluster Proportion [mol%]	Mass Loss 1 [wt%]	Onset 2 [°C]	Mass Loss 2 [wt%]	Onset 3 [°C]	Mass Loss3 [wt%]	Residual Mass [wt%]	Residual Mass calc. [wt%]
0	4.5	344	83.7	497	10.7	0.9	0.00
0.05	3.9	338	83.2	473	12.2	0.3	0.12
0.1	5.1	337	81.8	471	12.8	0.2	0.24
0.25	4.8	340	75.7	458	18.7	0.5	0.60
0.49	4.9	349	78.7	454	15.0	1.1	1.17
0.98	4.8	343	66.4	450	26.3	2.3	2.35
1.47	7.3	327	62.4	461	23.0	3.2	3.52
2.45	9.1	257	51.2	422	34.4	5.4	5.87
3.43	11.5	243	19.8	312	61.9	6.8	8.22

2.2.3.10 DSC investigations

The glass transition temperature (T_g) was determined by differential scanning calorimetry (DSC). To remove absorbed water, originating from the milling process, the samples were heated with 10 °C/min heating rate from -50 °C to 250 °C. No exothermic signals assigned to further polymerization processes were obtained. Measurements were performed in a range from 100 °C to 250 °C for all samples with a heating rate of 10 °C/min. The results are presented in Figure 2.55 and Table 2.33. The sample with 3.43 mol% cluster had to be measured in a range from 100 °C to 300 °C for exact determination of T_g . The signal for the glass transition temperature decreased with increasing cluster proportion due to the crosslinking of short polymer chains.

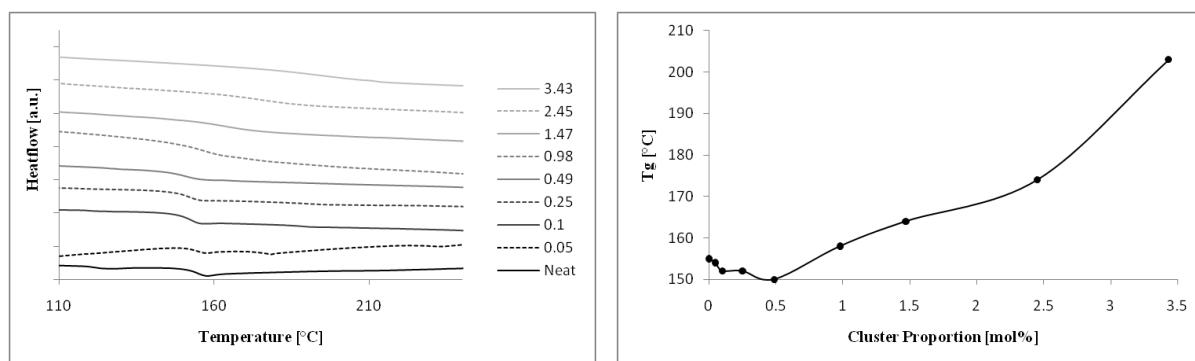


Figure 2.55: Comparison of the DSC curves of the $[\text{Fe}_3\text{O}(\text{MA})_6(4\text{-vpy})_3]\text{NO}_3$ -co-poly-4-vinylpyridine materials (l) and the comparison of the glass transition temperature versus the cluster proportion (r).

Table 2.33: Values of the glass transition temperature of the $[\text{Fe}_3\text{O}(\text{MA})_6(4\text{-vpy})_3]\text{NO}_3$ -co-poly-4-vinylpyridine materials with different cluster proportions.

Cluster Proportion [mol%]	T_g [°C]
0	155
0.05	154
0.1	152
0.25	152
0.49	150
0.98	158
1.47	164
2.45	174
3.43	203

The evaluation of the glass transition temperatures versus cluster proportion results in the inverse behavior of the material compared to the decomposition temperature. The neat polymer showed a glass transition temperature of 155 °C. Until the minimum for 0.49 wt% at 150 °C (−3.2 %) was reached, T_g was slowly decreasing 5 °C from 155 °C for the neat sample. Afterwards, an increase was detected resulting in a T_g of 203 °C for the cluster-co-polymer with 3.43 mol%, which is 48 °C (31.0 %) higher than that for the neat sample.

2.2.4 Conclusion

The synthesis as well as the thermal, magnetic and mechanical characterization of $[\text{Fe}_3\text{O}(\text{MA})_6(4\text{-vpy})_3]\text{NO}_3$ **19**-co-poly-(4-vinylpyridine) materials were reported in this chapter.

The first issue, the modification of the cluster and the organic co-monomer, to perform bulk polymerization, was achieved by using the coordinating monomer 4-vinylpyridine and the 4-vinylpyridine-substituted nitrate cluster $[\text{Fe}_3\text{O}(\text{MA})_6(4\text{-vpy})_3]\text{NO}_3$ **19**.

The great advantage of this system was the good solubility of the cluster in the monomer. Therefore, hybrid materials with up to 3.43 mol% cluster were synthesized by radical bulk polymerization. Due to the radical transfer properties of the clusters a stepwise polymerization was performed to be ensure that all monomers were reacted.

First analyses of the materials by ATR-IR did not show any signals for residual double bonds within the detection limits. In the Mössbauer spectrum of the hybrid materials, a shift of the iron signal occurred compared to the clusters before the polymerization, due to the decomposition of the clusters and the formation of undefined species. Signals clearly assigned to iron(II) were as well visible in the Mössbauer spectrum and a clear sign for redox reactions and radical transfer of the iron ions during the polymerization reaction. The SQUID results indicated the decomposition of the clusters as well by showing different magnetic properties of the hybrid materials compared to the unreacted cluster compounds. The results showed that various different magnetic interactions, from antiferromagnetic to ferromagnetic, were present

in the material, which proved the random distribution of the iron ions in the material and of the position of the iron ions relative to each other.

SAXS investigations evidenced that during the polymerization the clusters decompose and undefined aggregates were formed in the material that grew with increasing cluster proportion. These nanometer-sized aggregates did not show any sharp maxima in the SAXS curve and therefore crystalline domains were excluded. The evaluation showed that in the material domains with high cluster proportion are present that are surrounded by nearly undoped polymer.

Even though the clusters decompose during the synthesis, the iron ions in the material have an influence on the hardness and the Young's modulus. Nano-indentation investigations evidenced that the hardness was decreased by addition of small cluster proportions due to the presence of a transfer agent and the resulting shorter chain lengths of the polymers in the material. Above 0.49 mol% cluster, this effect was overcompensated by the crosslinking properties of the iron ions that therefore reinforce the material. For the material with 3.43 mol% cluster, the hardness increased by 76.2 %. The Young's modulus showed similar, but less pronounced behavior compared to the hardness. The maximum improvement was found for the sample with 3.43 mol% cluster with 19.5 % change. The brittleness was low for hybrid materials with low cluster proportion and increased up to 47.8 % for the material with 3.43 mol% cluster.

In contrast to the mechanical properties, the thermal stability was not much influenced over a wide cluster proportion range with little decrease in the decomposition temperature up to 0.49 mol% cluster proportion due to the shorter chain length. The onset temperature started to decrease rapidly above 1.47 mol% cluster proportion.

The glass transition temperature showed similar behavior as the mechanical properties. At first the value decreased, and increased above 0.98 mol% cluster proportion. The hybrid material with 3.43 mol% cluster showed a 31.0 % higher glass transition temperature than the neat polymer.

The reason for this behavior was the presence of the iron oxo clusters with radical transfer properties. The properties of the material were influenced in two ways. By addition of small cluster proportions, the polymer chain length is reduced, which leads to a softer material (reduction of the hardness, Young' modulus, brittleness and glass transition temperature) with reduced thermal stability. The increase of the cluster proportion leads to the crosslinking of the shorter polymer chains and therefore to improved mechanical and thermal stability.

A remarkable observation is obtained by a closer look at the general property changes. Each individual property showed the minimum (or maximum) at a different cluster proportion. This means that the properties are differently dependent on the nanofiller effect, the polymer chain length and the crosslinking density in the system.

3 Summary

The combination of organic materials with inorganic moieties is the characteristics of hybrid materials. This idea gained much attention during the last decades, resulting in several types of different synthetic approaches and material classes. In general, the materials can be classified in two main groups: In class I hybrid material systems the inorganic and organic component only show weak interactions, while in class II hybrid materials the two components are linked through strong chemical bonds, such as covalent or coordinative interactions.

Cluster-reinforced polymers are one recent approach to improve the properties of polymeric compounds. Compared to other inorganic moieties, clusters are well defined in their size and shape, can be purified by crystallization and do not show any distribution in their physical properties. Class I hybrid materials can be obtained by the use of non-functional ligands, while polymerizable ligands lead to class II hybrid materials. The crosslinking density is determined by the number of functional groups per cluster unit.

In this work, the so called nano building block approach was used to prepare cluster-reinforced hybrid polymers based on iron(III) oxo clusters. Little is known about the behavior of iron(III) oxo clusters in solution on the one hand and about late transition metal clusters in polymerization reactions on the other. Therefore, the focus of this work was to investigate these two issues.

The well known oxo cluster $[\text{Fe}_3\text{O}(\text{OOCR})_6(\text{L})_3]\text{X}$ was used as model compound. The cluster core consists of a triangle of iron(III) ions regularly arranged around a central μ_3 -oxygen, resulting in a D_{3h} symmetry of the cluster core. Two carboxylato-*O,O'* ligands bridge every edge of the Fe_3 triangle and a coordinated solvent ligand completes the octahedral coordination sphere of the iron(III) ions.

$[\text{Fe}_3\text{O}(\text{OOCR})_6(\text{L})_3]\text{X}$ has the advantage that i) the carboxylates (OOCR), ii) the ligands (L) and iii) the anion (X) can be easily varied. By controlling the composition, the desired properties and sufficient stability of the clusters were obtained. Therefore, a large variety of differently-substituted trinuclear, oxo-centered iron(III) clusters were prepared and their stability in solution was investigated. In the following, only methacrylate-modified iron(III) clusters will be discussed.

The reaction of iron(III) salts with sodium methacrylate in water resulted in the formation of differently-substituted iron(III) oxo clusters depending on the anion of the precursor salt. Therefore, the results will be discussed separately for each anion.

Two different clusters were obtained starting from iron(III) nitrate. Direct reaction of iron(III) nitrate with sodium methacrylate in water led to the expected formation of $[\text{Fe}_3\text{O}(\text{MA})_6(\text{H}_2\text{O})_3]\text{NO}_3$ (MA = methacrylate), but in the crystal structure $\text{Fe}_3\text{O}(\text{MA})_6(\text{H}_2\text{O})_2\text{NO}_3$ was present as well. In this compound, one coordinated water

molecule was substituted by the nitrate anion, resulting in an uncharged cluster. It was possible to separate the compound by crystallization in chloroform. The coordination of the anion had no influence on the distances within the cluster core and therefore, the D_{3h} symmetry was retained.

$[\text{Fe}_3\text{O}(\text{MA})_6(\text{H}_2\text{O})_{2.5}(\text{MAH})_{0.5}]\text{Cl}$ (MAH = methacrylic acid), a compound with two different clusters in the crystal structure was obtained by reaction of iron(III) chloride with sodium methacrylate in water. One, $[\text{Fe}_3\text{O}(\text{MA})_6(\text{H}_2\text{O})_3]\text{Cl}$, was isostructural to the expected tris-water-substituted cluster, while at the other, $[\text{Fe}_3\text{O}(\text{MA})_6(\text{H}_2\text{O})_2(\text{MAH})]\text{Cl}$, one coordinated water molecule was replaced by a methacrylic acid. As in the case of nitrate, it was possible to crystallize the derivative $[\text{Fe}_3\text{O}(\text{MA})_6(\text{H}_2\text{O})_3]\text{Cl}$ separately from organic solvents. Investigations starting from iron(III) bromide led to the same structural motives as mentioned above.

A totally different behavior was found starting from iron(III) sulfate. The reaction with sodium methacrylate in water yielded in $\text{Fe}_3\text{O}(\text{MA})_6(\text{H}_2\text{O})_2(\text{MA})$ without any sulfate present in the crystal structure. Instead, methacrylate was coordinated directly to the cluster core. The structure showed remarkable differences to $\text{Fe}_3\text{O}(\text{MA})_6(\text{H}_2\text{O})_2\text{NO}_3$. The distance between the central oxygen and the methacrylate-*O* substituted iron(III) ion was elongated resulting in a C_{2v} symmetry of the cluster core.

To apply the nano building block approach, all components must be stable in solution. Therefore, solution FT-IR investigations were performed. All tris-water-substituted compounds were either not soluble in common organic solvents or showed degradation in solution.

The results for the synthesis and the behavior of water-substituted iron(III) oxo clusters led to the following conclusions:

- The reaction of different iron salts leads to differently coordinated clusters, according to the different coordination behavior of the anions.
- Chloride and bromide lead to the same clusters.
- The anion is able to substitute one water molecule and coordinate directly to one iron(III) ion of the cluster core.
- The anion coordination leads to two types of clusters with either an unchanged cluster core (C_{3v} symmetric) or the distortion of angles and distances resulting in a C_{2v} symmetric core.
- To obtain a triiron oxo cluster, the anion has to be coordinating, but must not have too much affinity to iron(III) ions.
- Water-substituted clusters are badly soluble in organic solvents.
- Water-substituted clusters are not stable in solution and therefore not suitable for the nano building block approach.

The bad solubility prevented a detailed investigation of the cluster behavior in solution and rendered it impossible to use such compounds in the nano building block approach. Therefore, in a first attempt, the water ligands were substituted against methanol and ethanol. As in the case of the water-substituted clusters, different products were obtained according to the used anion.

Three different synthetic routes were applied:

- Substitution of the water ligands against methanol or ethanol starting from preformed water clusters.
- Direct synthesis of the clusters in methanol or ethanol.
- Dissolving the preformed water clusters in methanol or ethanol.

Each of these synthesis methods yielded different products. This effect was especially evident for the chloride compounds. Substitution of the ligands starting from the water- and methacrylic acid-substituted compound $[\text{Fe}_3\text{O}(\text{MA})_6(\text{H}_2\text{O})_{2.5}(\text{MAH})_{0.5}]\text{Cl}$ led to the formation of the expected tris-alcohol-substituted derivatives $[\text{Fe}_3\text{O}(\text{MA})_6(\text{HOR})_3]\text{Cl}$, with $\text{R} = \text{Me}, \text{Et}$, while the direct synthesis in the corresponding alcohol yielded $[\text{Fe}_3\text{O}(\text{MA})_6(\text{H}_2\text{O})(\text{HOR})_2]\text{FeCl}_4$. Due to the different solvent a cluster with tetrachloroferrate was formed. By direct synthesis in alcohol, using different solvents for the crystallization, it was even possible to crystallize $[\text{Fe}_3\text{O}(\text{MA})_6(\text{H}_2\text{O})_{0.5}(\text{HOR})_{2.5}]\text{Cl}$, a product where both clusters $[\text{Fe}_3\text{O}(\text{MA})_6(\text{HOR})_3]^+$ and $[\text{Fe}_3\text{O}(\text{MA})_6(\text{H}_2\text{O})(\text{HOR})_2]^+$ with exclusively chloride anions were present in the crystal structure.

For the nitrate compounds, the first two synthetic methods led to the formation of the tris-alcohol-substituted compounds $[\text{Fe}_3\text{O}(\text{MA})_6(\text{HOR})_3]\text{NO}_3$ with $\text{R} = \text{Me}, \text{Et}$.

The third synthetic route led to the precipitation of a yellow solid independent of the used cluster or anion. ATR-IR investigations evidenced the presence of bridging methoxy and methacrylate groups, which were assigned to ferric wheel compounds. The precipitate was insoluble in all common organic solvents and therefore a detailed characterization could not be performed.

Solution FT-IR investigations were performed on all alcohol-substituted compounds. Although the clusters were well soluble in chloroform, the spectra evidenced the presence of differently coordinated methacrylate ligands and free methacrylic acid in solution that could only originate from the decomposition of the clusters.

The results for the synthesis and the behavior of alcohol-substituted iron(III) oxo clusters led to following conclusions:

- Tris-alcohol-substituted clusters with chloride anions are exclusively obtained by substitution of the water molecules from a preformed water cluster.
- The synthesis starting from iron(III) chloride in the coordinating solvent leads to tetrachloroferrate clusters.

- For nitrate, both synthetic routes lead to tris-alcohol-substituted compounds.
- Dissolving triiron clusters in methanol or ethanol leads to the presumable formation of ferric wheel compounds independent on the anion.
- The alcohol-substituted clusters are all soluble in chloroform, but decompose in solution. Therefore, these compounds are not suitable for the nano building block approach.

Based on these results, pyridine-modified iron(III) oxo clusters were synthesized. The coordinated water molecules from the preformed water-substituted clusters were substituted by pyridine. Nitrate, chloride, bromide and tetrafluoroborate clusters with the general formula $[\text{Fe}_3\text{O}(\text{MA})_6(\text{py})_3]\text{X}$ were obtained this way. In contrast to all other reported clusters, no single crystal X-ray analysis of a tris-pyridine-substituted cluster was obtained. Therefore, the structure was verified by ATR-IR, Mössbauer and SQUID measurements.

The substitution of the water molecules from $\text{Fe}_3\text{O}(\text{MA})_6(\text{H}_2\text{O})_2(\text{MA})$ resulted in $\text{Fe}_3\text{O}(\text{MA})_6(\text{py})_2(\text{MA})$. After the reaction the methacrylate anion was still coordinated to the cluster core.

The solution stability of the clusters was determined by solution FT-IR and NMR investigations. $[\text{Fe}_3\text{O}(\text{MA})_6(\text{py})_3]\text{BF}_4$ with the non-coordinating tetrafluoroborate anion was found to be stable in solution and therefore dealt as model compound for further investigations.

Solution FT-IR and NMR experiments on $[\text{Fe}_3\text{O}(\text{MA})_6(\text{py})_3]\text{NO}_3$ and $[\text{Fe}_3\text{O}(\text{MA})_6(\text{py})_3]\text{Cl}$ resulted in the conclusion that both clusters showed dynamic substitution reactions in solution. In non-coordinating solvents, this was attributed to the substitution of one coordinated pyridine against an anion, which was reflected in the appearance of four new signals for $\text{Fe}_3\text{O}(\text{MA})_6(\text{py})_2\text{X}$ ($\text{X} = \text{NO}_3^-, \text{Cl}^-$) in the NMR spectra. Chloride has a larger affinity to iron(III) ions and therefore coordinated better than nitrate. This fact was reflected in the detection of a larger amount of anion coordinated clusters for $[\text{Fe}_3\text{O}(\text{MA})_6(\text{py})_3]\text{Cl}$ in solution. However, in coordinating solvents the situation got even more complicated, because, additional to the anions, the solvent was as well coordinating to the cluster core resulting in numerous different cluster species. Interestingly, even these substitution reactions were mediated by the affinity of the anions to the iron(III) ions.

The results for the synthesis and the behavior of pyridine-substituted iron(III) oxo clusters led to following conclusions:

- Tris-pyridine-substituted clusters are obtained by substitution of the water molecules from preformed water-substituted clusters.
- The coordinated methacrylate anion of the distorted cluster $\text{Fe}_3\text{O}(\text{MA})_6(\text{H}_2\text{O})_2(\text{MA})$ is stable against substitution with pyridine.
- $[\text{Fe}_3\text{O}(\text{MA})_6(\text{py})_3]\text{BF}_4$ is stable in solution and is therefore suitable for the nano building block approach.

- Coordinating anions lead to the appearance of undefined species in solution. The affinity of the anions to the iron(III) ions determine the proportion of differently coordinated species
- Coordinating solvents enhance this effect and lead to a large number of differently coordinated species, while non-coordinating polar solvents better solvate the anions and stabilize the clusters.

As mentioned above, $[\text{Fe}_3\text{O}(\text{MA})_6(\text{py})_3]\text{BF}_4$ was found to be stable in solution and therefore the first polymerization reactions were based on this cluster. The compound was not soluble in any common organic monomer or non-coordinating solvent. To overcome this problem, solution polymerization in pyridine was performed using the organic monomers styrene and methylmethacrylate (MMA).

In contrast to the expected polymerization behavior of styrene, pyridine as the solvent had an influence on the polymerization reaction by reducing the reaction rate. Hence, the initiator concentration and the polymerization temperature had to be optimized. Compared to styrene, MMA showed full conversion even at low temperatures and initiator proportion due to the higher reactivity of the monomer.

The addition of cluster led to a further decrease of the reaction rate and accordingly to lower molar mass of the polymer. This effect was traced back to radical transfer properties of the clusters. Additional GPC investigations indicated that the clusters did not crosslink the polymer chains when reacted at low temperatures.

ATR-IR investigations were performed on the different hybrid materials. By subtraction of the spectra of the neat polymers from that of the hybrid materials the bands of the clusters after the polymerization were enhanced. The clusters embedded in the polystyrene hybrid materials showed similar bands to the unreacted cluster, while in the MMA samples a significant shift was obtained that was attributed to the decomposition of the clusters during the synthesis. For polystyrene samples that were reacted at low temperatures, bands for residual double bonds at the clusters were observed, which verified the GPC results. These bands were not observed for the hybrid materials reacted at elevated temperatures.

Mössbauer measurements supported the results of the ATR-IR investigations. The spectrum for the hybrid material showed an increase of the line width and the isomer shift, that indicated that the clusters were retained during the reaction but changed their symmetry.

TGA analyses of the undoped polymer and the hybrid materials showed an increase of the decomposition temperature due to the introduction of the clusters. The onset temperature for the decomposition showed a strong increase, comparing the neat polymer with the material with the lowest cluster proportion. Further increase of the cluster proportion only led to little changes in the decomposition temperature.

The results for the synthesis and the characterization of $[\text{Fe}_3\text{O}(\text{MA})_6(\text{py})_3]\text{BF}_4$ reinforced hybrid materials led to following conclusions:

- Pyridine reduces the reaction rate and more initiator has to be used.
- Only short polymer chains can be obtained by a solution polymerization in pyridine.
- MMA polymerizes better than styrene.
- The clusters act as transfer agent and inhibit the polymerization. Therefore, the polymer chain length decreases with increasing cluster proportion.
- The crosslinking density is dependent on the reaction temperature.
- The clusters are stable during the polymerization reaction with styrene, but change their symmetry.
- The clusters decompose during the polymerization reaction with MMA.
- Although compared with the undoped polymers the polymer molar mass is reduced by the addition of clusters, the decomposition temperature is enhanced.

Although good results were obtained by solution polymerization in pyridine, the method of choice for the preparation of cluster-reinforced polymers is bulk polymerization. Therefore 4-vinylpyridine, a coordinating solvent, was used instead of styrene and $[\text{Fe}_3\text{O}(\text{MA})_6(4\text{-vpy})_3]\text{NO}_3$ instead of the tetrafluoroborate derivative to avoid fluorine moieties in the material.

The advantage of the system was the good solubility of the cluster in the monomer. Hybrid materials with up to 3.43 mol% cluster were synthesized by free radical bulk polymerization. The cluster inhibits the polymerization, which rendered a stepwise polymerization at different temperatures necessary. For the highest cluster proportions (2.45 and 3.43 mol%), the reaction time was decreased due to the crosslinking of the system. Insoluble black resins were obtained after polymerization.

The Mössbauer spectrum showed significant differences to the unreacted clusters. The doublet was remarkably shifted to higher isomeric shifts and showed a shoulder in the region of iron(II) ions. This behavior was assigned to the decomposition of the individual clusters during the polymerization reaction. The presence of iron(II) evidences redox reactions of the iron ions during the radical reaction.

SQUID measurements indicated as well the decomposition of the clusters by showing different magnetic properties of the hybrid materials compared to the unreacted cluster compounds. The results illustrate that in the material various different magnetic interactions, from antiferromagnetic to ferromagnetic, were present.

The decomposition of the clusters was as well indicated by the results of SAXS investigations. The scattering curves appeared to indicate two sizes of aggregates in the materials. In the nanometer regime, aggregates are formed that increase with increasing cluster proportion. Within these aggregates an irregular arrangement of the iron ions is expected due to the lack of sharp maxima in the SAXS curves. On the other hand, the curves indicate a macroscopic phase separation of the hybrid material from the undoped polymer.

Although the clusters decompose during the synthesis, the clusters or iron ions have an influence on the mechanical properties of the hybrid materials. Nano-indentation investigations were used to determine the hardness and the Young's modulus. For small cluster proportions, the material gets softer due to the reduction of the chain length caused by the presence of a radical transfer agent. Above 0.49 mol% cluster, this effect was overcompensated by the crosslinking properties of the iron ions that therefore reinforce the material. The hardness, Young's modulus and brittleness increase monotonously with increasing cluster proportion. The hybrid material with the highest cluster proportion (3.43 mol%) showed 76 % increased hardness, 20 % increased Young's modulus and 48 % increased brittleness.

The decomposition temperature decreased, related to the undoped polymer, for small cluster proportions due to the shorter chain length followed by an increase and a maximum at 0.49 mol% cluster. For cluster proportions higher than 1.47 mol%, the onset temperature started to decrease rapidly and was found 100 °C lower for the hybrid material with 3.43 mol% cluster. Although the decomposition temperature was that much decreased, the hybrid material still showed higher thermal stability compared to the unreacted clusters.

The glass transition temperature showed similar behavior to the mechanical properties. At first, the value decreased followed by an increase above 0.98 mol% cluster proportion. The hybrid material with 3.43 mol% cluster showed a 31 % higher glass transition temperature than the neat polymer.

The results for the synthesis and the characterization of hybrid materials prepared from $[\text{Fe}_3\text{O}(\text{MA})_6(4\text{-py})_3]\text{NO}_3$ led to following conclusions:

- The clusters inhibit the polymerization at small cluster proportions due to the radical transfer properties, and decrease the gelation time for high cluster proportions due to the crosslinking of the network.
- The hybrid materials show phase separation during the polymerization.
- The clusters decompose during the polymerization reaction.
- Inorganic islands are formed during the polymerization that grow with increasing cluster proportion. Random magnetic interactions are present within these assemblies due to the irregular arrangement of the iron ions.
- The hardness, Young's modulus, brittleness, decomposition temperature and glass transition temperature decreased for small cluster proportions and increased again by further increase.
- The minimum of each individual property was found at different cluster proportions.

4 Experimental Section

4.1 General Methods and Materials

All manipulations for the cluster synthesis were carried out in air. Chloroform was filtered through basic alumina before use. 4-Vinylpyridine was purified and degassed before use. All other chemicals and solvents were used as received.

For the polymer preparation, all manipulations were carried out in moisture- and oxygen-free atmosphere of dry argon. All monomers were purified and degassed before use. All solids were excessively dried. For the reactions standard Schlenk techniques were used.

The solvents for the NMR experiments were as well used as received. A list of all used chemicals is presented in Table 4.1.

Table 4.1: Chemicals used

Name	Supplier	Purity
iron(III) nitrate nonahydrate	Aldrich	98+ %
iron(III) chloride hexahydrate	Aldrich	97 %
iron(III) bromide	Aldrich	98 %
iron(III) sulfate hydrate	Aldrich	97 %
sodium methacrylate	Aldrich	99 %
4-vinylpyridine	Aldrich	95 %
styrene	Aldrich	99 %
azo-bis-(isobutyronitril)	Acros	98 %
silver tetrafluoroborate	Aldrich	98 %
pyridine	Aldrich	99.5+ %
methanol	Aldrich	puriss.
ethanol	Merck	z.A.
d-chloroform	euriso-top	99.8 % D
d ₆ -acetone	euriso-top	99.9 % D
d ₅ -pyridine	euriso-top	99.5 % D

4.2 Analytical Techniques

4.2.1 IR Spectroscopy

ATR-IR spectra were recorded on a Bruker Tensor 27 equipped with an ATR MicroFocusing MVP-QL with a ZnSe crystal or a PIKE MIRacle with diamante window and

ZnSe optics. Solution FT-IR was done with a CaF₂ cell in chloroform solution. The software used for analysis was OPUS version 4.0.

4.2.2 Single Crystal X-Ray Diffraction

Selected crystals were mounted on a Siemens SMART diffractometer with a CCD area detector or a Bruker AXS KAPPA diffractometer with an APEX II CCD area detector. Graphite-monochromated Mo-K_α radiation ($\lambda = 71.073$ pm) was used for all measurements. The data were collected at 100 K in a nitrogen stream or at room temperature. Three sets of exposures were recorded with different Φ angle to cover a hemisphere of the reciprocal space. Each exposure covered 0.3° in ω . The data were corrected for polarization and Lorentz effects and an empirical absorption correction (SADABS) was applied. The cell dimensions were refined with all unique reflections. The structures were solved by direct methods (SHELXS97). Refinement was carried out with the full-matrix least-squares method based on F^2 (SHELXL93) with anisotropic thermal parameters for all non-hydrogen atoms. The positions of the hydrogen atoms were calculated and their position was refined riding on their corresponding atoms.

4.2.3 NMR Spectroscopy

¹H (d1 = 0.1 s) and ¹³C (d1 = 0.05 s) 1D NMR experiments were performed on a Bruker AVANCE 250 (250.13 MHz {¹H}, 62.86 MHz {¹³C}) and a Bruker AVANCE 300 (300.13 MHz {¹H}, 75.47 MHz {¹³C}) spectrometer, both equipped with a 5 mm broadband probe head and a z-gradient unit. The 2D spectra were exclusively recorded on the Bruker AVANCE 300 spectrometer. COSY (Correlated Spectroscopy) and HMQC (Heteronuclear Multiple Quantum Correlation) were measured with Bruker standard pulse sequences.

4.2.4 Elemental Analysis

Elemental analysis was carried out on a 2400 CHN Analyzer by Perkin Elmer operated by the Microanalytical Laboratory at the Institute of Physical Chemistry, University of Vienna.

4.2.5 Gel Permeation Chromatography

Gel permeation chromatography (GPC) was performed in toluene using a Waters system with a 515 HPLC pump, a 717 autosampler, a 2410 differential refractive index detector and Styragel columns (HR 0.5, 3 and 4, linear and GPC phase SDV 50/100/10E5A) at 40 °C at a rate of 1 ml/min applying linear polystyrene standards.

4.2.6 Small Angle X-Ray Scattering

The data were recorded using a pinhole camera with a rotating anode generator (Ni-monochromated Cu-K α radiation) and a Bruker AXS area detector. All SAXS patterns were first corrected for background scattering from the experimental setup. The pattern was radially averaged to obtain the scattering intensity $I(q)$, where $q = (4\pi/\lambda) \sin \theta$ is the scattering vector, 2θ being the angle between the incident and the diffracted beam, and $\lambda = 0.154$ nm the X-ray wavelength. Scattering curves in the q range between 0.1 nm^{-1} and 14 nm^{-1} were obtained by combining data measured at two different sample-detector distances.

4.2.7 Thermogravimetric Analysis

Mass changes as a function of temperature were recorded on a Netzsch TG 209C Iris thermal analyzer in synthetic air flow. The temperature was increased from $25 \text{ }^\circ\text{C}$ to $700 \text{ }^\circ\text{C}$ with a heating rate of $10 \text{ }^\circ\text{C}/\text{min}$.

4.2.8 Magnetic Measurements

Magnetic experiments were performed while warming the samples from 1.8 K to room temperature on an MPMS-5 SQUID Quantum Design magnetometer. Dc susceptibility measurements were performed on the samples with an applied field of $H = 100 \text{ Oe}$. Magnetization experiments were recorded at 1.8 K with an applied field from 0 kOe to 50 kOe .

4.2.9 Nano-Indentation

Hardness and indentation elastic moduli were measured at $23 \text{ }^\circ\text{C}$ on a Nanoindenter XP (MTS Systems) equipped with a Berkovich indenter. The penetration was performed with a maximum depth of $2 \text{ }\mu\text{m}$ and a penetration velocity of $100 \text{ nm}/\text{s}$. Coplanar sample surfaces were obtained for samples below $1 \text{ mol}\%$ cluster by pressing the samples with at increased temperatures and for samples above by applying an abrasive paper. The analysis followed the method of Oliver and Pharr and ISO 14577, respectively.⁹⁴

4.2.10 Differential Scanning Calorimetry

Enthalpy as a function of temperature measurements were recorded on a Mettler Toledo DSC 823 $^\circ$ in a nitrogen flow of $200 \text{ ml}/\text{min}$. The temperature was increased with $10 \text{ }^\circ\text{C}/\text{min}$ and decreased with $20 \text{ }^\circ\text{C}/\text{min}$ in a temperature range between $-50 \text{ }^\circ\text{C}$ and $200 \text{ }^\circ\text{C}$. STARE Software was used to analyze the results.

4.3 Methacrylate-Modified Iron(III) Oxo Clusters

4.3.1 Water-Substituted Clusters

4.3.1.1 Synthesis of $[\text{Fe}_3\text{O}(\text{MA})_6(\text{H}_2\text{O})_3]\text{NO}_3 \cdot 10\text{H}_2\text{O}$ (1)

An amount of 10 g of $\text{Fe}(\text{NO}_3)_3 \cdot 9\text{H}_2\text{O}$ (24.8 mmol) was dissolved in 60 ml of deionized water and two equivalents of sodium methacrylate (49.5 mmol, 5.35 g) were added. The color turned from orange to red, and after 15 min an orange-red precipitate was formed. After stirring overnight, the reaction mixture was filtered and the solid redissolved in 60 ml of an acetone/water mixture (1:1). Red crystals (3.28 g, 49 % yield) were obtained after evaporation of acetone over a period of three days.

IR (ATR) ν/cm^{-1} : 1642 m, 1573 s, 1454 m, 1415 vs, 1374 m, 1336 m, 1242 s, 1042 w, 1008 w, 946 m, 826 m, 662 w, 612 s

Anal. Calcd. (wt %): C 32.40 H 4.08 N 1.57

Found (wt %): C 35.09 H 4.42 N 1.59

4.3.1.2 Synthesis of $\text{Fe}_3\text{O}(\text{MA})_6(\text{H}_2\text{O})_2\text{NO}_3 \cdot \text{CH}_2\text{Cl}_2$ (2)

An amount of 10 g of $\text{Fe}(\text{NO}_3)_3 \cdot 9\text{H}_2\text{O}$ (24.8 mmol) was dissolved in 60 ml of deionized water and two equivalents of sodium methacrylate (49.5 mmol, 5.35 g) were added. The color turned from orange to red, and after 15 min an orange-red precipitate was formed. After stirring overnight, the reaction mixture was filtered.

An amount of 0.2 g (2.2 mmol) of the precipitated powder was dried over P_4O_{10} and then dissolved in 10 ml of dry CH_2Cl_2 . The solution was filtered after one hour. After the addition of n-hexane, CH_2Cl_2 was allowed to evaporate during one week, and 72.5 mg (37 % yield) crystals suitable for single crystal XRD were obtained.

IR (ATR) ν/cm^{-1} : 1641 m, 1570 s, 1452 m, 1413 vs, 1301 m, 1241 s, 1008 w, 944 m, 825 m, 654 w, 611 s

4.3.1.3 Synthesis of $[\text{Fe}_3\text{O}(\text{MA})_6(\text{H}_2\text{O})_{2.5}(\text{HMA})_{0.5}]\text{Cl} \cdot 4.5\text{H}_2\text{O}$ (3)

An amount of 10 g of $\text{FeCl}_3 \cdot 6\text{H}_2\text{O}$ (37 mmol) was dissolved in 60 ml of deionized water, and 2 equivalents of sodium methacrylate (74 mmol, 8 g) were added. The solution turned from orange to dark red, and after 15 min a red precipitate was obtained. The suspension was stirred overnight. After filtration, the solid was washed with 10 ml of water and redissolved in 60 ml of an acetone/water mixture (1:1). Slow evaporation of the acetone during three days resulting in 2.55 g (26 % yield) of large dark red crystals.

IR (ATR) ν/cm^{-1} : 1678 w, 1642 m, 1569 s, 1518 m, 1454 m, 1414 vs, 1374 m, 1242 s, 1210 w, 1007 w, 943 m, 826 m, 659 w, 612 s

Anal. Calcd. (wt %): C 35.76 H 4.40 Cl 3.77 Re 25.47

Found (wt %): C 37.1 H 4.57 Cl 4.60 Re 26.10

4.3.1.4 Synthesis of $[\text{Fe}_3\text{O}(\text{MA})_6(\text{H}_2\text{O})_3]\text{Cl} \cdot 1.5\text{H}_2\text{O} \cdot \text{CH}_2\text{Cl}_2$ (4)

An amount of 10 g of $\text{FeCl}_3 \cdot 6\text{H}_2\text{O}$ (37 mmol) was dissolved in 60 ml of deionized water, and 2 equivalents of sodium methacrylate (74 mmol, 8 g) were added. The solution turned from orange to dark red, and after 15 min a red precipitate was obtained. The suspension was stirred overnight.

An amount of 0.5 g (0.66 mmol) of the orange solid was dried over P_4O_{10} and dissolved in dry dichloromethane. Diethyl ether was then allowed to diffuse into the solution, resulting in crystals of **4** suitable for single crystal X-ray diffraction in low yields.

IR (ATR) ν/cm^{-1} : 1642 m, 1573 s, 1454 m, 1415 vs, 1374 m, 1242 s, 1008 w, 946 m, 826 m, 659 w, 612 s

4.3.1.5 Synthesis of $[\text{Fe}_3\text{O}(\text{MA})_6(\text{H}_2\text{O})_{2.5}(\text{HMA})_{0.5}]\text{Br} \cdot 2.75 \text{H}_2\text{O}$ (5)

Anhydrous FeBr_3 (16.9 mmol, 5 g) was dissolved in 50 ml of water and 2 equivalents (33.8 mmol, 3.66 g) of sodium methacrylate were added, accompanied by a color change to dark red. An orange precipitate was formed after 15 min, which was filtered off. The precipitate was dissolved in 60 ml of an acetone/water (1:1) mixture, and acetone was allowed to evaporate within one week. Crystals (1.53 g, 32 % yield) suitable for single crystal X-ray diffraction were obtained.

IR (ATR) ν/cm^{-1} : 1678 w, 1641 m, 1570 s, 1517 w, 1488 w, 1454 m, 1414 vs, 1374 m, 1242 s, 1007 w, 946 m, 825 m, 659 w, 613 s

4.3.1.6 Synthesis of $\text{Fe}_3\text{O}(\text{MA})_6(\text{H}_2\text{O})_2(\text{MA}) \cdot 1.5\text{H}_2\text{O} \cdot \text{HMA}$ (6)

$\text{Fe}_2(\text{SO}_4)_3 \cdot 5\text{H}_2\text{O}$ (10 g, 20.41 mmol) was dissolved in 60 ml of water, and sodium methacrylate (8.83 g, 81.64 mmol) was added to the solution. The color turned from orange-red to dark red, and after 30 min an orange precipitate was obtained, which was filtered off, washed with 10 ml of water and dried *in vacuo*. Yield 3.22 g (29 %). Crystals could be obtained by dissolving the cluster in an acetone/water mixture and slow evaporation of the acetone.

IR (ATR) ν/cm^{-1} : 1690 w, 1644 m, 1629 w, 1579 s, 1542 s, 1515 w, 1454 m, 1414 vs, 1372 m, 1243 s, 1212 w, 1006 w, 939 m, 827 m, 660 w, 613 s

Anal. Calcd. (wt %): C 39.18 H 4.62

Found (wt %): C 40.41 H 4.66

4.3.2 Alcohol-Modified Clusters

4.3.2.1 Synthesis of $[\text{Fe}_3\text{O}(\text{MA})_6(\text{MeOH})_3]\text{NO}_3 \cdot 1.5\text{CH}_2\text{Cl}_2$ (7)

Method I: Dried crystals of **1** (0.5 g, 0.6 mmol) were suspended in 10 ml of dichloromethane and 3 equivalents of methanol (75 μl , 1.8 mmol) were added. The solid dissolved accompanied by a color change to dark red. The solution was stirred for one hour, filtered through a syringe filter and n-pentane was allowed to diffuse into the solution. After one day 0.27 g (53 % yield) big red crystals were obtained suitable for single crystal X-ray diffraction.

Method 2: Iron(III)nitrate nonahydrate (5 g, 12.4 mmol) was dissolved in 60 ml of methanol and sodium methacrylate was added to the solution. The liquid turned dark red and after few minutes a white precipitate was formed which was removed by filtration. The solvent was removed *in vacuo*, 50 ml of CH_2Cl_2 were added to the residue and removed to remove last traces of methanol. Then the powder was dissolved in 100 ml of a 1:1 mixture of CH_2Cl_2 / n-hexane. The dichloromethane was allowed to evaporate within two weeks, resulting in 3.20 g (91 % yield) of a dark red solid.

IR (ATR) v/cm^{-1} : 1643 m, 1575 s, 1454 m, 1415 vs, 1373 m, 1340 m, 1243 s, 1072 w, 1041 w, 1007 w, 939 m, 888 w, 827 w, 654 m, 614 s

4.3.2.2 Synthesis of $[\text{Fe}_3\text{O}(\text{MA})_6(\text{MeOH})_3]\text{Cl} \cdot 0.5\text{CHCl}_3$ (8)

A dried crystalline sample of **3** (0.5 g, 0.6 mmol) was dissolved in CHCl_3 and 3 equivalents of methanol (82.3 μl , 1.8 mmol) were added to the solution. A color change to dark red was indicating the ligand substitution. After one hour of stirring the solution was filtered through a syringe filter and n-pentane was allowed to diffuse into the solution. After two days 0.10 g (21 % yield) crystals suitable for single crystal XRD were obtained.

IR (ATR) v/cm^{-1} : 1644 m, 1580 s, 1544 s, 1487 w, 1454 m, 1448 m, 1413 vs, 1371 m, 1243 s, 1219 w, 1153 w, 1071 w, 1040 w, 1006 w, 934 m, 893 w, 826 m, 758 w, 697 m, 664 w, 610 s

Anal. Calcd. (wt %): C 34.02 H 4.44 Cl 3.72

Found (wt %): C 35.09 H 4.12 Cl 6.11

4.3.2.3 Synthesis of $[\text{Fe}_3\text{O}(\text{MA})_6(\text{MeOH})_2(\text{H}_2\text{O})]\text{FeCl}_4 \cdot \text{CH}_2\text{Cl}_2$ (9)

Sodium methacrylate (4 g, 37 mmol) was added to an iron(III)chloride hexahydrate (5 g, 18.5 mmol) solution in 60 ml of methanol. The liquid turned dark red and a white precipitate was formed, which was removed by filtration. The solvent was removed and the resulting

powder was dissolved in 50 ml of CH₂Cl₂, which was removed again. Then the product was dissolved in a 1:1 mixture of CH₂Cl₂/ n-heptane. The dichloromethane was allowed to evaporate and within two weeks 3.42 g (76 % yield) crystals suitable for single crystal XRD could be obtained.

IR (ATR) v/cm⁻¹: 1641 w, 1561 s, 1500 w, 1455 m, 1415 vs, 1374 m, 1240 s, 1110 w, 1017 m, 1008 m, 961 m, 944 m, 823 s, 651 m, 616 s

Anal. Calcd. (wt %): C 29.64 H 3.83 Cl 13.46 Re 30.3

Found (wt %): C 30.04 H 3.81 Cl 14.63 Re 33.6

4.3.2.4 Synthesis of [Fe₃O(MA)₆(EtOH)₃]NO₃ · CH₂Cl₂ (10)

Method 1: **1** (0.5 g, 0.6 mmol) was suspended in 10 ml of CHCl₃ and 3 equivalents of ethanol (105 μl, 1.8 mmol) were added. The solid dissolved, accompanied by a color change to dark red. The solution was stirred for one hour, filtered through a syringe filter and n-pentane was allowed to diffuse into the solution. After one day, 0.45 g (83 % yield) big red crystals were obtained suitable for single crystal X-ray diffraction.

Method 2: Iron(III)nitrate nonahydrate (5 g, 12.4 mmol) was dissolved in 60 ml of ethanol and sodium methacrylate was added to the solution. The liquid turned to dark red and after a few minutes a white precipitate was formed which was removed by filtration. The solvent was removed *in vacuo* and the residue was dissolved in 50 ml of CH₂Cl₂. To remove last traces of ethanol, dichloromethane was added and removed twice, before the powder was dissolved in 100 ml of a 1:1 mixture of CH₂Cl₂/ n-hexane mixture. The dichloromethane was allowed to evaporate within two weeks, resulting in 2.83 g (77 % yield) small red crystals.

IR (ATR) v/cm⁻¹: 1644 m, 1577 s, 1454 m, 1415 vs, 1373 m, 1340 m, 1242 s, 1092 w, 1040 m, 1007 w, 939 m, 879 w, 853 w, 827 s, 654 m, 614 s

4.3.2.5 Synthesis of [Fe₃O(MA)₆(EtOH)₃]Cl (11)

A crystalline sample of **3** (0.5 g, 0.6 mmol) was dissolved in 20 ml of CHCl₃ and three equivalents of ethanol (103 μl, 1.8 mmol) were added to the solution. A color change to dark red was indicating the ligand substitution. After one hour of stirring n-pentane was allowed to diffuse into the solution and after two days 0.41 g (76 % yield) crystals suitable for single crystal XRD were obtained.

IR (ATR) v/cm⁻¹: 1642 w, 1570 s, 1508 w, 1454 m, 1415 vs, 1373 m, 1243 s, 1007 w, 943 m, 826 s, 657 m, 612 s

Anal. Calcd. (wt %): C 38.03 H 5.11 Cl 3.74 Re 25.28

Found (wt %): C 33.71 H 4.10 Cl 1.50 Re 27.9

4.3.2.6 Synthesis of $[\text{Fe}_3\text{O}(\text{MA})_6(\text{EtOH})_{2.5}(\text{H}_2\text{O})_{0.5}]\text{Cl} \cdot \text{HMA}$ (12)

Iron(III) chloride hexahydrate (5 g, 18.5 mmol) was dissolved in 60 ml of ethanol and 2 equivalents of sodium methacrylate (4 g, 37 mmol) were added to the solution. The white solid dissolved accompanied by a color change to dark red. After 15 minutes a white precipitate of NaCl was formed, which was removed by filtration. The solvent was removed *in vacuo* and 50 ml of CH_2Cl_2 were added and removed twice to get rid of the methanol. Finally, the obtained powder was dissolved in CHCl_3 , which was allowed to evaporate slowly, resulting in 4.39 g (85 % yield) crystals suitable for single crystal X-ray analysis.

IR (ATR) v/cm^{-1} : 1642 w, 1566 s, 1543 w, 1452 m, 1412 vs, 1373 m, 1240 s, 1081 w, 1029 m, 1007 w, 943 m, 876 w, 826 s, 807 w, 657 m, 613 s

Anal. Calcd. (wt %): C 37.32 H 4.97 Cl 3.80 Re 25.66

Found (wt %): C 34.72 H 4.69 Cl 13.92 Re 30.1

4.3.2.7 Synthesis of $[\text{Fe}_3\text{O}(\text{MA})_6(\text{EtOH})_2(\text{H}_2\text{O})]\text{FeCl}_4$ (13)

Iron(III) chloride hexahydrate (5 g, 18.5 mmol) was dissolved in 60 ml of ethanol and 2 equivalents of sodium methacrylate (4 g, 37 mmol) were added to the solution. The white solid dissolved accompanied by a color change to dark red and after 15 minutes a white precipitate of NaCl was formed, which was removed by filtration. The solvent was removed *in vacuo* and 50 ml of CH_2Cl_2 were added and removed twice to get rid of the methanol. Finally, the red solid was dissolved in a 1:1 CH_2Cl_2 / n-hexene mixture. The dichloromethane was allowed to evaporate and after one week 3.71 g (81 % yield) crystals, suitable for single crystal X-ray diffraction, were obtained.

IR (ATR) v/cm^{-1} : 1641 w, 1564 s, 1453 m, 1415 vs, 1373 m, 1240 s, 1081 w, 1030 m, 1007 w, 950 m, 877 w, 826 s, 654 m, 615 s

Anal. Calcd. (wt %): C 31.09 H 4.10 Cl 13.11 Re 29.53

Found (wt %): C 31.69 H 4.29 Cl 14.31 Re 32.90

4.3.3 Pyridine-Modified Clusters

4.3.3.1 Synthesis of $[\text{Fe}_3\text{O}(\text{MA})_6(\text{py})_3]\text{NO}_3$ (14)

1 g (1.2 mmol, 1 eq.) **1** was suspended in 20 ml of chloroform and 0.35 ml (4.3 mmol, 3.6 eq.) of pyridine were added to the suspension accompanied by a color change to dark green. After stirring for one hour, the solution was filtered through a syringe filter and n-pentane was allowed to diffuse into the solution. After one day, black crystals were obtained in quantitative yield.

IR (ATR) ν/cm^{-1} : 1643 m, 1604 w, 1572 vs, 1486 w, 1447 m, 1413 vs, 1371 m, 1342 w, 1288 w, 1241 s, 1218 m, 1154 w, 1071 m, 1041 m, 1012 m, 940 m, 853 w, 826 s, 761 m, 669 s, 661 w, 635 w, 609 s

^1H NMR (d^6 -acetone, 20 °C, 25 mg/ml) ppm: δ = 66.6 (NCH), 29.5 (NCHCH), 20.0 (CH_2), 8.4 (NCHCHCH), 7.1 (CH_3)

^{13}C $\{^1\text{H}\}$ NMR (d^6 -acetone, 20 °C, 25 mg/ml) ppm: δ = 890.7 (O_2C), 468.7 (NCH), 322.2 (NCHCH), 213.0 (CH_2), 212.3 (O_2CC), 125.1 (NCHCHCH), 72.7 (CH_3)

4.3.3.2 Synthesis of $[\text{Fe}_3\text{O}(\text{MA})_6(\text{py})_3]\text{Cl}$ (15)

1 g (1.3 mmol, 1 eq.) of **3** was dissolved in 20 ml chloroform and 0.35 ml (4.3 mmol, 3.3 eq.) of pyridine were added to the solution accompanied by a color change to dark green. After stirring for one hour, the solution was filtered through a syringe filter and n-pentane was allowed to diffuse into the solution. After one day 1.16 g (94 % yield) black crystals were obtained.

IR (ATR) ν/cm^{-1} : 1643 m, 1604 w, 1576 vs, 1488 w, 1449 m, 1415 vs, 1372 m, 1341 w, 1243 s, 1218 m, 1156 w, 1139 w, 1071 m, 1041 m, 1005 m, 937 m, 852 w, 827 s, 759 m, 698 s, 660 m, 635 w, 609 s

^1H NMR (d^6 -acetone, 20 °C, 25 mg/ml) ppm: δ = 66.5 (NCH), 29.8 (NCHCH), 20.0 (CH_2), 8.9 (NCHCHCH), 7.1 (CH_3)

^{13}C $\{^1\text{H}\}$ NMR (d^6 -acetone, 20 °C, 25 mg/ml) ppm: δ = 892.7 (O_2C), 469.2 (NCH), 322.9 (NCHCH), 213.4 (CH_2), 212.3 (O_2CC), 125.6 (NCHCHCH), 73.1 (CH_3)

4.3.3.3 Synthesis of $[\text{Fe}_3\text{O}(\text{MA})_6(\text{py})_3]\text{Br}$ (16)

0.5 g (1.2 mmol, 1 eq.) of **5** were suspended in 20 ml of chloroform and 0.35 ml (4.3 mmol, 3.6 eq.) of pyridine were added accompanied by a color change to dark green. After stirring for one hour, the solution was filtered through a syringe filter and n-pentane was allowed to diffuse into the solution. After one day, black crystals were obtained in quantitative yield.

IR (ATR) ν/cm^{-1} : 1642 m, 1604 w, 1574 vs, 1485 w, 1445 m, 1413 vs, 1372 m, 1341 w, 1241 s, 1217 m, 1145 w, 1070 m, 1041 m, 1012 m, 1005 sh, 937 m, 852 w, 825 s, 764 m, 751 sh, 701 s, 658 m, 634 w, 609 s

^1H NMR (CDCl_3 , 20 °C, 50 mg/ml) ppm: δ = 665.4 (NCH), 28.7 (NCHCH), 19.8 (CH_2), 8.2 (NCHCHCH), 7.1 (CH_3)

^{13}C $\{^1\text{H}\}$ NMR (CDCl_3 , 20 °C, 50 mg/ml) ppm: δ = 875.0 (O_2C), 459.9 (NCH), 318.8 (NCHCH), 212.7 (CH_2), 207.3 (O_2CC), 125.6 (NCHCHCH), 72.7 (CH_3)

4.3.3.4 Synthesis of $[\text{Fe}_3\text{O}(\text{MA})_6(\text{py})_3]\text{BF}_4$ (17)

1 g (1 mmol, 1 eq.) of **15** was dissolved in 20 ml of chloroform and 0.25 g (1.3 mmol, 1.3 eq.) of silver tetrafluoroborate were added. The suspension was stirred for 12 hours, filtered and n-pentane was allowed to diffuse into the solution resulting in quantitative yield of crystals after one day.

IR (ATR) ν/cm^{-1} : 1644 m, 1606 w, 1574 vs, 1488 w, 1447 m, 1415 vs, 1288 w, 1241 s, 1221 m, 1158 w, 1071 s, 1054 s, 1014 m, 1006 m, 960 m, 945 m, 828 s, 763 m, 702 s, 659 w, 637 w, 610 s

^1H NMR (d^6 -acetone, 20 °C, 25 mg/ml) ppm: δ = 66.6 (NCH), 29.4 (NCHCH), 19.9 (CH_2), 8.4 (NCHCHCH), 7.1 (CH_3)

^{13}C $\{^1\text{H}\}$ NMR (d^6 -acetone, 20 °C, 25 mg/ml) ppm: δ = 888.8 (O_2C), 467.9 (NCH), 321.9 (NCHCH), 212.8 (CH_2), 212.3 (O_2CC), 125.1 (NCHCHCH), 72.6 (CH_3)

4.3.3.5 Synthesis of $\text{Fe}_3\text{O}(\text{MA})_6(\text{py})_2(\text{MA}) \cdot \text{CHCl}_3$ (18)

The precipitated product **6** (0.5 g, 0.6 mmol) was suspended in CHCl_3 and 3 equivalents of pyridine (146 μl , 1.8 mmol) were added. The solid dissolved accompanied by a color change to black. n-Pentane was allowed to diffuse into the solution resulting in 0.48 g (86 % yield) big crystals after few days.

IR (ATR) ν/cm^{-1} : 1712 w, 1644 m, 1604 w, 1575 s, 1546 sh, 1487 w, 1448 m, 1414 vs, 1372 m, 1242 s, 1218 s, 1070 w, 1041 w, 1005 w, 937 m, 852 s, 759 m, 698 s, 660 m, 609 s

4.3.4 4-Vinylpyridine-Modified Clusters

4.3.4.1 Synthesis of $[\text{Fe}_3\text{O}(\text{MA})_6(4\text{-vpy})_3]\text{NO}_3$ (19)

1 g (1.2 mmol / 1 eq.) of dried $[\text{Fe}_3\text{O}(\text{MA})_6(\text{H}_2\text{O})_3]\text{NO}_3$ **1** was suspended in 20 ml of chloroform, and 0.4 ml of 4-vinylpyridine (3.7 mmol / 3.1 eq.) was added. This resulted in the solution of the cluster and a color change to dark green. The solution was stirred for one hour and then filtered by a syringe filter. Crystalline needles were obtained by diffusion of n-pentane into the chloroform solution after one day in quantitative yield.

IR (ATR) ν/cm^{-1} : 1643 m, 1616 m, 1571 s, 1548 w, 1504 w, 1454 m, 1414 vs, 1375 m, 1347 m, 1333 w, 1290 w, 1241 s, 1224 m, 1206 m, 1067 m, 1218 m, 1005 w, 991 w, 939 m, 842 m, 827 m, 802 m, 750 m, 660 w, 646 w, 612 s

^1H NMR (CDCl_3 , 20 °C, 0.1 g/ml) ppm: δ = 64.7 (NCH), 27.6 (NCHCH), 19.9 (CH_2), 7.1 (CH_3 , CHCH_2), 5.3 (CHCHH), 4.6 (CHCHH)

^{13}C $\{^1\text{H}\}$ NMR (CDCl_3 , 20 °C, 0.1 mg/ml) ppm: δ = 881.5 (O_2C), 461.3 (NCH), 324.0 (NCHCH), 219.7 (O_2CC), 212.4 (CH_2), 137.7 (CCHCH $_2$), 132.8 (NCHCHC), 127.7 (CCHCH $_2$), 72.6 (CH_3)

Anal. Calcd. (wt %): C 46.95 H 4.47 N 4.87

Found (wt %): C 47.23 H 4.57 N 4.86

4.4 Cluster-Co-Polymers

4.4.1 Solution Polymerization of Styrene and MMA in Pyridine

1 ml (12.5 mmol) of pyridine was placed in a Schlenk flask and 1 ml of the corresponding monomer was added. AIBN (0.005 g/ml, 0.015 g/ml, 0.03 g/ml, 0.045 g/ml) was then added. The reaction temperature was kept constant at 60 °C and 80 °C, respectively, for 17 hours. The pyridine was removed *in vacuo*. Afterwards, the product was dissolved in toluene and precipitated in n-pentane to remove residual monomer.

4.4.2 Solution Styrene-Co-Polymerization of $[\text{Fe}_3\text{O}(\text{MA})_6(\text{py})_3]\text{BF}_4$

An increasing cluster proportion (see Table 4.2) of carefully dried $[\text{Fe}_3\text{O}(\text{MA})_6(\text{py})_3]\text{BF}_4$ was placed in Schlenk flasks, and each dissolved in 1 ml (12.5 mmol) of pyridine. 4 ml of styrene were placed in another Schlenk flask and 12 mg / 18 mg (0.07 mmol / 0.11 mmol) of AIBN were dissolved in the monomer. 1 ml of this mixture was added to each of the pyridine solutions, which then were placed in an oil bath at 80 and 60 °C respectively. The reaction temperature was kept constant for 17 hours and then cooled to room temperature. The pyridine was removed *in vacuo*. Afterwards, the product was dissolved in toluene and precipitated in n-pentane to remove residual monomer.

Table 4.2: Proportion of $[\text{Fe}_3\text{O}(\text{MA})_6(\text{py})_3]\text{BF}_4$ **17** in the styrene co-polymer

Cluster Proportion [g/ml styrene]	Cluster Proportion [mol%]
0.02	0.22
0.05	0.56
0.075	0.83

IR (ATR) v/cm^{-1} (0.56 mol% $[\text{Fe}_3\text{O}(\text{MA})_6(\text{py})_3]\text{BF}_4$): 3082 w, 3059 w, 3025 m, 3002 w, 2921 m, 2849 w, 1601 w, 1583 w, 1493 m, 1452 m, 1417 w, 1370 w, 1244 w, 1220 w, 1181 w, 1154 w, 1069 w, 1028 w, 981 w, 964 w, 943 w, 906 w, 842 w, 755 s, 697 vs

4.4.3 Solution MMA-Co-Polymerization of $[\text{Fe}_3\text{O}(\text{MA})_6(\text{py})_3]\text{BF}_4$

0.02 g (0.02 mmol, 0.21 mol%) 0.05 g (0.05 mmol, 0.52 mol%) and 0.075 g (0.075 mmol, 0.82 mol%) of carefully dried $[\text{Fe}_3\text{O}(\text{MA})_6(\text{py})_3]\text{BF}_4$ were placed in Schlenk flasks and dissolved in 1 ml (12.5 mmol) of pyridine. 4 ml of MMA were placed in another Schlenk flask and 7 mg (0.04 mmol) of AIBN were dissolved in the monomer. 1 ml of this mixture was added to each of the pyridine solutions, which then were placed in an oil bath at 80 and 60 °C respectively. The reaction was heated for 17 hour, then cooled to room temperature, and the pyridine was removed *in vacuo*. The product was then dissolved in chloroform and precipitated in n-pentane to remove residual monomer. After drying the yields were around 100 %.

IR (ATR) v/cm^{-1} (0.52 mol% $[\text{Fe}_3\text{O}(\text{MA})_6(\text{py})_3]\text{BF}_4$): 2991 w, 2950 w, 2842 w, 1752 vs, 1600 br, 1481 m, 1446 m, 1434 m, 1386 w, 1268 m, 1292 s, 1190 s, 1145 vs, 1063 m, 987 m, 965 m, 911 w, 841 m, 827 w, 809 w, 750 m, 733 m, 697 m

4.4.4 Bulk Co-Polymerization of $[\text{Fe}_3\text{O}(\text{MA})_6(\text{vpy})_3]\text{NO}_3$

The cluster (see Table 4.3) was placed in a Schlenk flask equipped with a magnetic stirrer and repeatedly evacuated and purged with argon. In a second flask 4-vinylpyridine was mixed with 0.5 g/ml of AIBN under argon. 5 ml of this solution was then transferred under argon to dissolve the cluster. The solution was stirred for one minute and then placed in an oil bath at 50 °C for 17 hours. Then the temperature was stepwise increased to 80 °C (7 h), 120 °C (17 h) and finally to 150 °C (7 h) to finish the polymerization. The polymer was then allowed to cool to room temperature and in the end the flask was crashed to obtain the final material.

IR (ATR) v/cm^{-1} : 3032 w, 2924 m, 1596 vs, 1556 m, 1493 w, 1450 w, 1414 s, 1219 m, 1068 m, 993 s, 874 w, 818 s, 743 m, 669 w

Table 4.3: Proportion of $[\text{Fe}_3\text{O}(\text{MA})_6(4\text{-vpy})_3]\text{NO}_3$ **19** in the co-polymers

Cluster Proportion [mol%]	Cluster Proportion [g/5 ml]
0	0
0.05	0.026
0.10	0.053
0.25	0.132
0.49	0.263
0.98	0.526
1.47	0.789
2.45	1.315
3.43	1.841

4.5 Crystallographic Data

	1·10H₂O	2·CH₂Cl₂	3·4.5H₂O
Empirical formula	C ₄₈ H _{89.57} Fe ₆ N ₂ O _{46.79}	C ₂₅ H ₃₆ Cl ₂ Fe ₃ NO ₁₈	C ₅₂ H ₉₄ Cl ₂ Fe ₆ O ₄₂
Formula weight	1778.47	877.00	1797.27
Temperature /K	100	100	100
Crystal system	triclinic	orthorhombic	triclinic
Space group	<i>P</i> -1	<i>P</i> 2 ₁ 2 ₁ 2 ₁	<i>P</i> -1
Unit cell dimensions			
a /pm	1318.55(18)	1244.26(13)	1280.35(8)
b /pm	1744.4(3)	1381.11(15)	1766.18(14)
c /pm	1884.1(3)	214.18(2)	1889.81(13)
α /°	81.508(2)		87.353(2)
β /°	76.553(3)		77.903(2)
γ /°	68.520(3)		68.763(1)
Volume /pm ³ × 10 ⁶	3912.7(9)	3680.5(7)	3892.7(5)
Z	2	4	2
Calcd. density /g cm ⁻³	1.510	1.583	1.533
Absorption coeff. μ /mm ⁻¹	1.180	1.385	1.249
Crystal size /mm	0.30 × 0.25 × 0.20	0.20 × 0.15 × 0.10	0.20 × 0.15 × 0.10
θ range /°	2.23–24.99	2.20–28.32	2.21–27.50
Reflections collected/unique	20654/13585	25339/9150	25602/17562
Data/parameters	13585/1001	9150/460	17562/1030
GOF of <i>F</i> ²	1.037	0.951	1.015
R [<i>I</i> > 2σ(<i>I</i>)]	0.0805	0.0592	0.0519
ω <i>R</i> ²	0.2170	0.1032	0.1240
Largest diff. peak/hole / Å ⁻³	1.893/-0.703	0.713/-0.762	1.141/-0.954

	4 ·1.5H ₂ O·CH ₂ Cl ₂	5 ·2.75H ₂ O	6 ·1.5H ₂ O·MAH
Empirical formula	C ₅₀ H ₈₂ Cl ₆ Fe ₆ O ₃₅	C ₅₂ H ₇₆ Br ₂ Fe ₆ O _{38.50}	C ₆₄ H ₉₆ Fe ₆ O ₄₁
Formula weight	1790.96	1812.05	1856.51
Temperature /K	100	100	299
Crystal system	orthorhombic	triclinic	orthorhombic
Space group	<i>P b c n</i>	<i>P</i> -1	<i>P b c a</i>
Unit cell dimensions			
a /pm	2048.21(17)	1297.13(15)	1854.78(15)
b /pm	1731.36(15)	1761.1(2)	1925.04(15)
c /pm	2077.88(18)	1896.3(2)	2469.5(2)
α /°		86.992(2)	
β /°		77.785(2)	
γ /°		68.927(2)	
Volume /pm ³ × 10 ⁶	7368.6(11)	3949.2(8)	8817.3(12)
Z	4	2	4
Calcd. density /g cm ⁻³	1.614	1.524	1.399
Absorption coeff. μ /mm ⁻¹	1.453	2.169	1.047
Crystal size /mm	0.20 × 0.10 × 0.05	0.26 × 0.17 × 0.10	0.50 × 0.40 × 0.20
θ range /°	2.20–28.29	2.55–25.00	2.25–28.30
Reflections collected/unique	48817/9144	30805/13886	83371/10950
Data/parameters	9144/477	13886/971	10950/527
GOF of <i>F</i> ²	1.024	0.944	1.031
R [<i>I</i> >2σ(<i>I</i>)]	0.0683	0.0529	0.0548
ω <i>R</i> ²	0.1563	0.1478	0.1437
Largest diff. peak/hole / Å ⁻³	1.871/-0.727	3.066/-0.525	0.810/-0.556

	7 ·1.5CH ₂ Cl ₂	8 ·0.5CHCl ₃	9 ·CH ₂ Cl ₂
Empirical formula	C _{28.50} H ₄₅ Cl ₃ Fe ₃ NO ₁₉	C _{27.50} H _{42.50} Cl _{2.50} Fe ₃ O ₁₆	C ₂₆ H ₄₀ Cl ₆ Fe ₄ O ₁₆
Formula weight	979.55	885.29	1044.68
Temperature /K	100	100	100
Crystal system	orthorhombic	monoclinic	orthorhombic
Space group	<i>P</i> b c a	<i>P</i> 2 ₁ /m	<i>P</i> 2 ₁ 2 ₁ 2 ₁
Unit cell dimensions			
a /pm	1901.3(5)	1055.3(3)	1324.0(2)
b /pm	2111.4(5)	2113.0(6)	1390.1(3)
c /pm	2180.5(6)	1056.7(3)	2217.8(4)
α /°			
β /°		119.539(5)	
γ /°			
Volume /pm ³ × 10 ⁶	8754(4)	2050.0(9)	4082.1(13)
Z	8	2	4
Calcd. density /g cm ⁻³	1.487	1.434	1.700
Absorption coeff. μ /mm ⁻¹	1.234	1.271	1.849
Crystal size /mm	0.30 × 0.20 × 0.20	0.35 × 0.23 × 0.10	0.30 × 0.30 × 0.10
θ range /°	2.35–25.00	2.42–25.00	2.31–28.31
Reflections collected/unique	34796/7698	5877/3525	53725/10140
Data/parameters	7698/590	3525/273	10140/530
GOF of <i>F</i> ²	1.027	1.126	1.115
R [<i>I</i> > 2σ(<i>I</i>)]	0.0723	0.1600	0.0517
ω <i>R</i> ²	0.2043	0.3752	0.1555
Largest diff. peak/hole / Å ⁻³	1.519/-0.728	2.610/-3.424	1.466/-1.884

	10 ·CH ₂ Cl ₂	11	12 ·HMA
Empirical formula	C ₃₁ H ₅₀ Cl ₂ Fe ₃ NO ₁₉	C ₃₀ H ₄₈ ClFe ₃ O ₁₆	C ₆₂ H ₉₈ Cl ₂ Fe ₆ O ₃₄
Formula weight	979.17	867.68	1793.4
Temperature /K	100	296	296
Crystal system	Monoclinic	Monoclinic	Monoclinic
Space group	<i>P</i> 2 ₁ /c	<i>P</i> 2 ₁ /c	<i>P</i> 2 ₁
Unit cell dimensions			
a /pm	1099.46(13)	1104.63(13)	1089.63(5)
b /pm	1874.2(2)	1800.0(2)	2114.50(10)
c /pm	2159.6(2)	2163.7(3)	1924.65(9)
α /°			
β /°	102.810(2)	101.332(5)	91.636(1)
γ /°			
Volume /pm ³ × 10 ⁶	4339.3(8)	4218.4(9)	4432.6(4)
Z	4	4	2
Calcd. density /g cm ⁻³	1.499	1.366	1.344
Absorption coeff. μ /mm ⁻¹	1.185	1.142	1.091
Crystal size /mm	0.40 × 0.30 × 0.25	0.90 × 0.60 × 0.10	0.40 × 0.35 × 0.15
θ range /°	1.90–27.50	2.23–23.05	2.68–25.00
Reflections collected/unique	26554/9951	26053/5566	31178/12189
Data/parameters	9951/579	5566/521	15189/1084
GOF of <i>F</i> ²	1.064	1.074	1.000
R [<i>I</i> > 2σ(<i>I</i>)]	0.0705	0.0947	0.0378
ωR ₂	0.2006	0.2318	0.904
Largest diff. peak/hole / Å ⁻³	1.476/-2.132	0.654/-0.520	0.368/-0.211

	13	18·CHCl₃
Empirical formula	C ₂₈ H ₄₄ Cl ₄ Fe ₄ O ₁₆	C ₃₉ H ₄₆ Cl ₃ Fe ₃ N ₂ O ₁₅
Formula weight	1001.83	1056.68
Temperature /K	300	296
Crystal system	Triclinic	Monoclinic
Space group	<i>P</i> -1	<i>P</i> 2 ₁ /n
Unit cell dimensions		
a /pm	1206.21(17)	1271.7(7)
b /pm	1350.9(2)	1514.1(8)
c /pm	1421.2(2)	2829.6(16)
α /°	85.078(3)	
β /°	69.637(2)	98.126(7)
γ /°	83.423(3)	
Volume /pm ³ × 10 ⁶	2154.3(5)	5394(5)
Z	2	4
Calcd. density /g cm ⁻³	1.544	1.301
Absorption coeff. μ /mm ⁻¹	1.629	1.002
Crystal size /mm	0.55 × 0.40 × 0.20	0.50 × 0.50 × 0.30
θ range /°	2.25–28.32	2.53–25.00
Reflections collected/unique	14542/10315	36772/9467
Data/parameters	10315/568	9467/565
GOF of <i>F</i> ²	1.016	1.077
R [<i>I</i> > 2σ(<i>I</i>)]	0.0591	0.1025
ω <i>R</i> ²	0.167	0.297
Largest diff. peak/hole / Å ⁻³	3.168/-1.159	1.041/-0.836

5 References

- ¹ Kickelbick G., Hybrid Materials, Wiley-VCH, Weinheim, **2006**
- ² Schindler A. and Williams J. L., *Polym. Prepr., Amer. Chem. Soc., Div. Polym. Chem.* **1969**, *10*, 832.
- ³ Quentin J. P., Ger. Offen. 2, 50, 965.
- ⁴ Grosmaning J. and Peyrot J., Ger. Offen. 2, 56, 76.
- ⁵ Mastrorilli P. and Nobile C. F., *Coord. Chem. Rev.* **2004**, *248*, 377-395.
- ⁶ Pardey A. J., Rojas A. D., Yanez J. E., Betancourt P., Scott C. China C., Urbina C., Moronta D. and Longo C., *Polyhedron* **2005**, *24*, 511-519.
- ⁷ Dzhardimalieva G. I., Pomogailo A. D. and Volpert V. A., *J. Inorg. Organomet. Poly.* **2002**, *12*, 1-21.
- ⁸ Forster R. J. and Vos J. G., *Macromolecules* **1990**, *23*, 4372-4377.
- ⁹ McCurdie M. P. and Belfiore L. A., *Polymer* **1999**, *40*, 2889-2902.
- ¹⁰ Khairou S. K., *Polym. Deg. Stab.* **1994**, *46*, 315-318.
- ¹¹ Kickelbick G. *Prog. Polym. Sci.* **2003**, *28*, 83-114.
- ¹² Nagata K., Kodarna S., Kawasaki H., Keki S. and Mizuhata M., *J. Appl. Polym. Sci.* **1995**, *56*, 1313-1321.
- ¹³ Smith T. W. and Wychick D., *J. Phys. Chem.* **1980**, *84*, 1621-1629.
- ¹⁴ Feichtenschlager B., *Diploma Thesis*, Vienna University of Technology (Vienna, Austria) **2008**.
- ¹⁵ Kanatudis M. G., Wu C. G., Macy H. O. and Kannewurf C. R., *J. Am. Chem. Soc.* **1989**, *111*, 4139-4141.
- ¹⁶ Bissessur R., DeGroot D., Schindler J., Kannewurf C. and Kanatzis M., *Chem Comm.* **1993**, *8*, 687-689.
- ¹⁷ Cotton F. A., *Acc. Chem. Res.* **1969**, *2*, 240.
- ¹⁸ Kogler F. R. and Schubert U., *Polymer* **2007**, *48*, 4990-4995.
- ¹⁹ Liu H., Kondo S., Takeda N. and Unno M., *Eur. J. Inorg. Chem.* **2009**, *18*, 1317-1319.
- ²⁰ Liu H., Kondo S., Takeda N. and Unno M., *J. Am. Chem. Soc.* **2008**, *130*, 10074-10075.
- ²¹ Rozes L., Steunou N., Fornasieri G. and Sanchez C., *Monatsh. Chem.* **2006**, *137*, 501-528.
- ²² Gao Y., Kogler F. R., Peterlik H. and Schubert U., *J. Mater. Chem.* **2006**, *16*, 3268-3276.
- ²³ Kickelbick G., Holzinger D., Brick C., Trimmel G. and Moons E., *Chem. Mater.* **2002**, *14*, 4382.
- ²⁴ Ivanovici S., Peterlik H., Feldgitscher C., Puchberger M. and Kickelbick G., *Macromolecules* **2008**, *41*, 1131-1139.
- ²⁵ Gross S., Di Noto V., Kickelbick G. and Schubert U., *Mat. Res. Soc. Sym. Proc.* **2002**, *726*, 47-55.

- ²⁶ Torma V., Hüsing N., Peterlik H. and Schubert U., *C. R. Chimie* **2004**, *7*, 495-502.
- ²⁷ Kogler F. R., Koch T., Peterlik H., Seidler S. and Schubert U. *J. Polym. Sci. B* **2007**, *45*, 2215-2231.
- ²⁸ Koch T., Kogler F. R., Schubert U. and Seidler S., *Monatsh. Chem.* **2007**, *138*, 293-299
- ²⁹ Gao Y., Kogler F. R. and Schubert U., *J. Polym. Sci. A* **2005**, *43*, 6586-6591.
- ³⁰ Nyden M. R., Forney G. P. and Brown J. E., *Macromolecules* **1992**, *25*, 1658-1666.
- ³¹ Kogler F. R. and Schubert U., *Polymer* **2007**, *48*, 4990-4995.
- ³² Dragan D. S., Kogler F. R. and Schubert U. *Polymer* **2008**, *49*, 378-385.
- ³³ Palacio F., Oliete P., Schubert U. Mijatovic I. Hüsing N. and Peterlik H., *J. Mater. Chem.* **2004**, *14*, 1873-1878.
- ³⁴ Bendova M., Puchberger M., Pabisch S., Peterlik H. and Schubert U. *Eur. J. Inorg. Chem.* **2010**, *15*, 2266-2275.
- ³⁵ Wieghardt K., Pohl K., Jibril I. and Hutter G., *Angew. Chem.* **1984**, *96*, 66-67.
- ³⁶ Rodriguez E., Gich., Roig A., Molins E., Nedelko N., Slawska-Waniewska A. and Szewczyk A., *Polyhedron* **2006**, *25*, 113-118.
- ³⁷ Weinland R. and Dinkelacher P., *Ber. deutsch. chem. Ges.* **1910**, *42*, 3881-3894.
- ³⁸ Weinland R., Kessler K., and Bayerl A., *Z. allg. anorg. Chem.* **1924**, *132*, 209-225.
- ³⁹ Weinland R. and Loebich O., *Z. all. u. anorg. Chem.* **1926**, *151*, 271-288.
- ⁴⁰ Weinland R. and Herz A., *Ber. deutsch. chem. Ges.* **1913**, *45*, 2662-2680.
- ⁴¹ Weinland R. and Gussmann E., *Ber. deutsch. chem. Ges.* **1910**, *43*, 2144-2149.
- ⁴² Anzenhofer K. and De Boer J. J., *Recueil* **1969**, *88*, 286-288.
- ⁴³ Kiskin M. A., Fomina I. G., Sidorov A. A., Aleksandrov G. G., Proshenkina O.Y., Dobrokotova Z. V., Ikorskii V. N., Shvedenkov Y. G., Novotortsev V. M., Eremenko I. L. and Moiseev I. I., *Russ. Chem. Bull., Int. Ed.* **2004**, *53*, 2508-2518.
- ⁴⁴ Bond A. M., Clark R. J. H., Humphrey D. G., Panayiotopoulos P., Skelton B. W. and White A., *J. Chem. Soc., Dalton Trans.* **1998**, *11*, 1845-1852.
- ⁴⁵ Anson C. E., Bourke J. P., Cannon R. D., Jayasooriya U. A., Molinier M. and Powell A. K., *Inorg. Chem.* **1997**, *36*, 1265-1267.
- ⁴⁶ Earnshaw A., Figgis B. N. and Lewis J., *J. Chem. Soc. (A)* **1966**, *12*, 1656-1663.
- ⁴⁷ Duncan J. F., Kanekar C. R. and Mok K. F., *J. Chem. Soc. (A)* **1969**, *3*, 480-482.
- ⁴⁸ Long G. J, Robinson W. T., Tappmeyer W. P. and Bridges D. L., *J. Chem. Soc. Dalton Trans.* **1973**, *6*, 573-579.
- ⁴⁹ Jones D. H., Sams J. R. and Thompson R. C., *J. Chem. Phys.* **1984**, *81*, 440-447.
- ⁵⁰ Murao T., *Phys. Lett.* **1974**, *49A*, 33-35.
- ⁵¹ Rakitin Y. V., Kalinnikov V. T. and Novotortsev V. M., *Russ. Chem. Bull.* **2004**, *53*, 2478-2484.
- ⁵² Overgaard J., Rentschler E., Timco G. A., Gerbeleu N. V., Arion V., Bousseksou A., Tuchagues J. P. and Larsen F. K., *J. Chem. Soc., Dalton Trans.* **2002**, *15*, 2981-2986.
- ⁵³ Nakamoto T., Hanaya M., Katada M., Endo K., Kitagawa S. and Sano H., *Inorg. Chem.* **1997**, *36*, 4347-4359.

- ⁵⁴ Oh S. M., Hendrickson D. N., Hassett K. L. and Davis R. E., *J. Am. Chem. Soc.* **1984**, *106*, 7984-7985.
- ⁵⁵ Oh S. M., Kambara T., Hendrickson D. N., Sorai M., Kaji K., Woehler S. E. and Wittebort R. J., *J. Am. Chem. Soc.* **1985**, *107*, 5540-5541.
- ⁵⁶ Oh S. M., Wilson S. R., Hendrickson D. N., Woehler S. E., Wittebort R. J., Inniss D. and Strouse C. E., *J. Am. Chem. Soc.* **1987**, *109*, 1073-1090.
- ⁵⁷ Sowrey F. E., Tilford C., Wocadlo S. Anson C. E., Powell A. K., Bennington S. M., Montfrooij W., Jayasooriya U. A. and Cannon R. D., *J. Chem. Soc., Dalton Trans.* **2001**, *6*, 862-866.
- ⁵⁸ Filoti G., Bartolome J., Dickson D. P. E., Rillo C., Prisecaru I., Jovmir T., Kuncser V. and Turta C., *J. Mag. Mag. Mater.* **1999**, *196-197*, 561-563.
- ⁵⁹ Sowrey F. E., MacDonald C. J. and Cannon R. D., *J. Chem. Soc., Faraday Trans.* **1998**, *94*, 1571-1574.
- ⁶⁰ Jary W., Poechlauer P., Neuwirth N., Nagl M. and Schmid W., *PTC Int. Appl.* WO2005063385 2005, [Chem. Abstr. **2005**, *143*, 133822].
- ⁶¹ Trettenhahn G., Nagl M., Neuwirth N., Arion V. B., Jary W., Pöchlauer P. and Schmid W., *Angew. Chem. Int. Ed.* **2006**, *45*, 2794-2798.
- ⁶² Smith A. A., Coxall R. A., Harrison A., Helliwell M., Parsons S. and Winpenny R. E. P., *Polyhedron* **2004**, *23*, 1557-1565.
- ⁶³ Yao H.-C., Li Y.-Z., Zheng L.-M. and Xin X.-Q., *Inorg. Chim. Acta* **2005**, *358*, 2512-2529.
- ⁶⁴ Khanra S., Konar S., Clearfield A., Helliwell M., McInnes E. J. L., Tolis E., Tuna F. and Winpenny R. E. P., *Inorg Chem.* **2009**, *48*, 5338-5349.
- ⁶⁵ K. L. Taft, C. D. Delfs, G. C. Papaefthmiou, S. Foner, D. Gatteschi, S. J. Lippard, *J. Am. Chem. Soc.* **1994**, *116*, 823-832.
- ⁶⁶ Stamatatos T. C., Christou A. G., Mukherjee S., Poole K. M., Lampropoulos C., Abbound K. A., O'Brien T. and Christou G., *Inorg. Chem.* **2008**, *47*, 9021-9034.
- ⁶⁷ Alboores P. and Rentschler E., *Eur. J. Inorg. Chem.* **2008**, *25*, 4004-4011.
- ⁶⁸ Trif M., Troiani F., Stepanenko D. and Loss D., *Phys. Rev. Lett.* **2008**, *101*, 217201.
- ⁶⁹ Choi K.-Y., Matsuda Y. H. and Nojiri H. *Phys. Rev. Lett.* **2006**, *96*, 107202.
- ⁷⁰ Palacio F., personal response.
- ⁷¹ Serre C., Millange F., Surble S. and Ferey G., *Angew. Chem. Int. Ed.* **2004**, *43*, 6286-6289.
- ⁷² Sudik A. C., Cote A. P. and Yaghi O. M., *Inorg. Chem.* **2005**, *44*, 2998-3000.
- ⁷³ Zhang K.-L., Shi Y.-J., You X.-Z. and Yu K.-B., *J. Mol. Struct.* **2005**, *743*, 73-77.
- ⁷⁴ Losada G., Mendilola M. A. and Sevilla M. T., *Inorg. Chim. Acta* **1997**, *255*, 125-131.
- ⁷⁵ Long D.-L., Kögerler P., Farrugia L. J. and Cronin L., *Chem. Asian J.* **2006**, *1*, 352-357.
- ⁷⁶ Walther P., Puchberger M., Kogler F. R., Schwarz K. and Schubert U., *Phys. Chem. Chem. Phys.* **2009**, *11*, 3640-3647.

- ⁷⁷ Puchberger M., Kogler F. R., Myhedin J., Gross S., Fric H., Kickelbick G. and Schubert U., *Eur. J. Inorg. Chem.* **2006**, *16*, 3283-3293.
- ⁷⁸ Asamaki K., Tadaihiro T., Kawata S., Sano H., Katada M. and Endo K., *Inorg. Chim. Acta* **1995**, *236*, 155-161.
- ⁷⁹ Overgaard J., Larsen F. K., Schiott B. and Iversen B. B., *J. Am. Chem. Soc.* **2003**, *125*, 11088-11099.
- ⁸⁰ Johnson M. K., Powell D. B. and Cannon R. D. *Spectrochimica Acta* **1981**, *37A*, 995-1006.
- ⁸¹ Deacon G. E., Phillips R. J., *Coord. Chem. Rev.* **1980**, *33*, 227-250.
- ⁸² Riedel E., *Anorganische Chemie* 3. Auflage, de Gruyter, Berlin-New York, **1994**, 813.
- ⁸³ Suprinya S. and Das S. K., *New J. Chem.* **2003**, *27*, 1568-1574.
- ⁸⁴ Suprinya S., Manikumari S., Raghavaiah P. and Das S. K., *New J. Chem.* **2003**, *27*, 218-220
- ⁸⁵ Suprinya S., Latha S. K. and Das S. K., *Eur. J. Inorg. Chem.* **2005**, *2*, 357-363.
- ⁸⁶ Data from the Spectral Database of Organic Compounds, SDDBS No. 1300.
- ⁸⁷ Blake A. B. and Fraser L. R., *J. Chem. Soc., Dalton Trans.* **1975**, *3*, 193-197.
- ⁸⁸ Montri L. and Cannon R. D., *Spectrochimica Acta* **1985**, *41A*, 643-646.
- ⁸⁹ Roda J., *Makromol. Chem.* **1977**, *178*, 203-210.
- ⁹⁰ Novitchi G., Riblet F., Scopelliti R., Helm L., Gulea A. and Merbach A. E., *Inorg. Chem.* **2008**, *47*, 10587-10599.
- ⁹¹ Ghosh P. and Mukhopadhyay G., *J. Polym. Sci.* **1979**, *17*, 583-593.
- ⁹² Ghosh P. and Mukhopadhyay G., *Macromol. Chem.* **1979**, *180*, 2253-2256.
- ⁹³ Hamza F. unpublished results.
- ⁹⁴ Oliver W. C., Pharr G. M., *J. Mater. Res.* **1992**, *7*, 1564.

CURRICULUM VITAE – ROBERT POTZMANN

General information

Name DI Robert Potzmann
Address Dommessgasse 9–15/8/11, 1110 Wien
E-Mail robert.potzmann@gmx.at
Nationality Austria
Date/ Place of birth 11. February 1983 in Vienna

Professional experience

since 09/2010 Group Leader – Water-Borne Acrylic Coating Resins
Cytec Austria Gmb, Leechgasse 21, 8010 Graz
Research activities in the field of acrylic based organic-organic and organic-inorganic hybrid liquid coating resins

01/2007 – 06/2010 Project Assistant
Institute of Materials Chemistry, **Vienna University of Technology**, Getreidemarkt 9/165 AC, 1060 Vienna
Research and teaching activities in the field of applied inorganic and materials chemistry

Education

since 03/2007 **PhD studies on technical sciences** in the field of applied inorganic and materials chemistry
Dissertation on the provisional topic „Synthesis and Characterization of Iron(III)oxo Clusters and their use as Building Blocks for Cluster Reinforced Polymers“
Institute of Materials Chemistry, Technical University Vienna, Getreidemarkt 9/165 AC, 1060 Vienna
Receive a **scholarship** for the scientific project (FWF)

09/2009 One month abidance at the CSIC in Saragossa/Spain with financial support of the ÖAD to gain knowledge about magnetism and SQUID measurements

10/2001 – 11/2006 **Diploma program in technical chemistry** – completed with honour and the academic degree „Diplom Ingenieur“-comparable to „Master of Science“
Education emphasis: Applied synthetic chemistry
Specialisation: Element organic and complex chemistry
Topic of the Diploma thesis „Herstellung und Analyse hierarchisch strukturierter Monolithen aus Bis-Silyl Verbindungen“ („Synthesis and Characterisation of Hierarchical Structured Monoliths based on Bis-Silyl Compounds“)
The practical work was done at the Ulm University, Institute of Inorganic Chemistry I, Albert Einstein Allee 11, 89081 Ulm/Germany
Diploma examination at the Technical University Vienna, Faculty for Technical Chemistry, Karlsplatz 13, 1040 Vienna

09/1993 – 06/2001 **Grammar school** – with A-Level examination completed
Bundesgymnasium Vienna XI, Geringergasse 2 (until 1997 Gottschalkgasse 21), 1110 Vienna
Class representative during the school year 2000/2001
Participance: “Chemie Olympiade“, “Mathematik Olympiade“ and “politische Bildung Olympiade“